FINITE ELEMENT MODELLING OF WIRE-ARC-ADDITIVE-MANUFACTURING PROCESS (WAAM)

SHIHAO SUN

RESEARCH PROJECT SUBMITTED IN PARTIAL FULFILMENT OF THE REQUIREMENTS FOR THE DEGREE OF MASTER OF MECHANICAL ENGINEERING

FACULTY OF ENGINEERING
UNIVERSITY OF MALAYA
KUALA LUMPUR

2022

UNIVERSITY OF MALAYA

ORIGINAL LITERARY WORK DECLARATION

Name of Candidate: SHIHAO SUN

Matric No: S2022085/1

Name of Degree: Master of Mechanical Engineering

Title of Project Paper/Research Report/Dissertation/Thesis ("this Work"):

Finite Element Modelling of Wire-Arc-Additive-Manufacturing Process (WAAM)

Field of Study: Additive Manufacturing

I do solemnly and sincerely declare that:

(1) I am the sole author/writer of this Work;
(2) This Work is original;
(3) Any use of any work in which copyright exists was done by way of fair dealing and for permitted purposes and any excerpt or extract from, or reference to or reproduction of any copyright work has been disclosed expressly and sufficiently and the title of the Work and its authorship have been acknowledged in this Work;
(4) I do not have any actual knowledge nor do I ought reasonably to know that the making of this work constitutes an infringement of any copyright work;
(5) I hereby assign all and every rights in the copyright to this Work to the University of Malaya ("UM"), who henceforth shall be owner of the copyright in this Work and that any reproduction or use in any form or by any means whatsoever is prohibited without the written consent of UM having been first had and obtained;
(6) I am fully aware that if in the course of making this Work I have infringed any copyright whether intentionally or otherwise, I may be subject to legal action or any other action as may be determined by UM.

Candidate's Signature Date: 21/1/22

Subscribed and solemnly declared before,

Witness's Signature Date: 21/1/22

Name: Dr. Farazila Binti Yusof

Designation: Assoc. Prof. Dr.

ABSTRACT

There are many advantages to using Wire-Arc-Additive-Manufacturing technology, including lower costs, shorter construction cycles, and freedom from workpiece size constraints. This paper chooses to use a numerical simulation technique to study the additive manufacturing of stainless steel 316 material based on ANSYS WORKBENCH.

In this study, the Gaussian heat source and Goldak double ellipsoid heat source models are analyzed in detail. Using 3D finite element meshing technology, the workpiece is meshed, and the mesh self-adaptive technology is used to automatically refine and generate meshes for the weld metal, which creates conditions for shortening the numerical simulation time of the welding process. The results show that the higher the welding power and initial temperature, the higher the temperature of the temperature field, the higher the welding speed, the lower the average temperature. The higher the welding power and speed, the higher the tension; the lower the stress, the higher the starting temperature. At the end of the study, the group 6 has been selected as the optimized group (300 w, 0.4 mm/s, 300 °C).

Keywords: Casting, WAAM, Thermal Analysis, Stress Analysis, Ansys

ABSTRAK

Terdapat banyak kelebihan menggunakan teknologi Wire-Arc-Additive-Pembuatan, termasuk kos yang lebih rendah, kitaran pembinaan yang lebih pendek dan kebebasan daripada kekangan saiz bahan kerja. Kertas kerja ini menggunakan teknik simulasi berangka untuk mengkaji pembuatan bahan tambahan bagi bahan keluli tahan karat 316 berasaskan ANSYS WORKBENCH.

Dalam kajian ini, model sumber haba Gaussian dan Goldak double ellipsoid dianalisis secara terperinci. Menggunakan teknologi jejaring unsur terhingga 3D, bahan kerja dirangkai, dan teknologi penyesuaian diri jejaring digunakan untuk menapis dan menjana jerat secara automatik untuk logam kimpalan, yang mewujudkan keadaan untuk memendekkan masa simulasi berangka bagi proses kimpalan. Keputusan menunjukkan bahawa semakin tinggi kuasa kimpalan dan suhu awal, semakin tinggi suhu medan suhu, semakin tinggi kelajuan kimpalan, semakin rendah suhu purata. Semakin tinggi kuasa dan kelajuan kimpalan, semakin tinggi ketegangan; semakin rendah tekanan, semakin tinggi suhu permulaan. Pada akhir kajian, kumpulan 6 telah dipilih sebagai kumpulan yang dioptimumkan (300 w, 0.4 mm/s, 300 °C).

Kata Kunci: Casting, WAAM, Analisis Terma, Analisis Tekanan, Ansys

ACKNOWLEDGEMENTS

The time of postgraduates is in the blink of an eye, and now it is nearing its end. It has been a long time since I received the project topic and completed the graduation project and thesis. My heart is full of gratitude when I finish this article.

I would like to thank the University of Malaya for providing me with the opportunity to study here. Under the careful guidance of my supervisor, Dr. Farazila Binti Yusof, my research report can be completed from topic selection to completion. The professor's guidance on theoretical knowledge, experimental methods and thesis writing has benefited me a lot during these two semesters. My supervisor 's profound professional knowledge background, rigorous and realistic scientific attitude and approachable personality had a profound impact on me, and also made me firmer in my professional interest and direction. During this period, I learned the knowledge related to the thesis, from knowing little at first, to consulting relevant materials step by step, to being able to simulate the temperature field and stress field, to writing code to implement functions, all of which make the I have benefited a lot.

I also need to thank my supervisor for patiently answering any questions that arise during my thesis and design process. She also carefully guide me on how to write the outline, content and framework of the thesis, so that my article can be gradually improved until now. Many times I encountered technical difficulties and my supervisor were very attentive to give me a solution, and then I solved the problem. I would also like to thank the teachers in the computer lab of the school for giving me the opportunity to use the computers, which saved me a lot of time in simulations. I would also like to thank my classmates. It was the comfort of my classmates that gave me the confidence to complete my research project. Thank you to all the excellent teachers who have taught me, it is the

knowledge you have imparted to me that has given me the motivation to complete studying.

In the process of writing this paper, despite the efforts of time and energy, I deeply feel that my professional knowledge is very lacking. Life is a process of continuous learning, so I hope that I will maintain a research enthusiasm and a diligent attitude towards life in my future life and work.

In the end, I would like to thank my alma mater again for giving me the opportunity to study and hope that my alma mater will get better and better!

TABLE OF CONTENTS

LIST OF FIGURES

LIST OF TABLES

LIST OF SYMBOLS AND ABBREVIATIONS

%	:	Percent
°C	:	Degree Celsius
Al	:	Aluminium
Ar	:	Argon
af, f1	:	Enerfy distribution factor
ar, f2	:	Enerfy distribution factor
AM	:	Additive Manufacturing
WAAM	:	Wire-Arc-Additive-Manufacturing
GMAW	:	Gas metal arc welding
SS 316	:	Material stainless steel
Q	:	Heat input power
mm	:	Millimeter
V	:	Welding Speed
b	:	Width of heat source
c	:	Depth of heat source

LIST OF APPENDICES

CHAPTER 1: INTRODUCTION

The goal of chapter 1 is to give a general overview. of research and to discuss it. This section contains information on the research's history, problem statement, goal, objectives, and scope of the study. In addition, the thesis framework is provided in this chapter.

1.1 Background

Additive Manufacturing (AM) technology, also known as 3D printing, is based on the idea of terrain-forming technology developed in the United States in the last century and only gradually developed in the late 1980s(Yap et al., 2014). Due to the increase of material manufacturing technology, the "freedom" of manufacturing can be realized, and parts of any complex shape can be produced on one piece of equipment. Compared with traditional processing methods, the processing steps of parts are greatly reduced, the processing cycle is shortened, and the parts are improved. utilization rate. Therefore, in the past 30 years, a variety of material manufacturing technologies have emerged and have begun to be widely used in the market. Anyway, additive manufacturing is the concept of the last century, the technology of the last century, and the market of this century. Among many forming technologies, metal additive manufacturing technology is more difficult to research, and it is also an important part of industrial applications. Especially with the increasing maturity of topology optimization technology, metal additive manufacturing technology is widely used in aerospace, vehicles, ships, medical equipment(Yue Chen et al., 2013). Contour - the demand in the terminal manufacturing field is more urgent. Since 2009, the United States has begun to attach importance to additive manufacturing technology and invested a lot of money in related basic technology research. In 2012, it further increased its support for the research on key

technologies of additive manufacturing, established the first national material manufacturing innovation center, and took the lead in promoting the development and industrialization of additive manufacturing technology at the national level. With more and more attention, driven by universities and research institutions, my country's metal additive manufacturing technology has reached the international leading level and is gradually applied in aerospace, weaponry, and other fields. However, additive manufacturing technology still needs to improve in terms of molding materials, process control, process monitoring, quality control, etc. Taking process control as an example, some current researches still mainly rely on experience and multiple experimental verifications, while better methods tend to be more theoretically based research. Therefore, it is far from enough to achieve "control" in metal additive manufacturing technology, and more basic theoretical research is needed to achieve "control".

WAAM uses an electric arc as an energy beam to build metal parts layer by layer. At present, the types of arcs used by WAAM mainly include gas metal arc welding (GMAW) (Chunming Xu *et al*., 2019). Such thermal heat sources Due to the large heating radius and high heat source intensity, the molding speed is fast and the efficiency is high, which is suitable for the molding of large-sized parts. Second, arc generators are a relatively inexpensive and more traditional type of heat source relative to laser, electron beam, etc. types of heat sources.

The welding heat process depends on the distribution form of the external heating source, the thermophysical properties of the material, and the heat exchange between the material and its surroundings. The classic Rekalin formula simulates various welding heat sources by distributing heat sources on points, lines and surfaces, but it has certain limitations. The research on numerical simulation of welding process has stayed at the two-dimensional level in the early stage. In recent years, as a result of the advancement of computer and finite element technology, the research on 3D numerically simulating of

welding process has become a research frontier in this field. However, due to the complexity of the welding process, the 3D numerically simulating of the weld procedure still only takes typical joints as the research object, and there are still great limitations in practical applications. The main reason that the numerical simulation technology cannot be applied in actual production is that duration of computing period is too lengthy or calculation accuracy is not high, that is mainly made by these three reasons: First. The number of degrees of freedom in the 3D model of welding structure is huge; Second. Serious The material nonlinearity of , leads to the difficulty of convergence of the solution process; Third. The existence of high temperature region makes it difficult to control the accuracy and stability of numerical simulation.

1.2 Problem statement

At present, there is a research gap on the parameter optimization of the welding process of SS316 material in WAAM process. The current research on the temperature and stress field of additive manufacturing at domestic and abroad mainly focus on additive manufacturing based on laser welding rather than WAAM.

Although the WAAM process has proven its ability to produce medium to large-scale components, the problems are that it cannot be able to apply as fully-fledged in the industry due to unmatched mechanical properties, huge internal stress, and it requires post-deposition procedure for the functional part model. There are many defects associated with the process including delamination, warping, porosity, crack and etc.

To cope with the above shortcomings, this research needs the temperature field and stress field distribution during WAAM to select the best setting of parameters.

1.3 Objectives

Since deformation and residual stress are connected to the non-uniform distribution of the temperature field and the variation of the temperature field with time during WAAM

production, it is first necessary to determine the temperature distribution over time during part production. Because most metal materials have the property of thermal expansion and contraction, large stresses and strains are generated at high temperatures. After knowing the temperature distribution, it is possible to improve the temperature distribution by adjusting the parameters in the production process, such as speed or power.

Therefore, the goals of this study are as follows.

1, to determine the temperature distribution in the WAAM process.

2, to propose the optimized parameters in the WAAM process based on temperature distribution.

This simulation is using the numerical approach. Due to the epidemic, the laboratory was closed, making it impossible to use the experimental approach.

For the first objective of how to determine the temperature distribution, this study set up 9 temperature sensors on the surface of one side of the substrate to display the temperature at specific locations. Because the left and right are symmetrical, the 9 temperature sensors are placed on the same side. At the same time, the relative temperature of each location can also be observed directly through the color. A temperature sensor is also set up where the weld bead contacts the substrate to measure whether the melting point is met.

1.4 Scope of Research

Recently, wire arc additive manufacturing (WAAM) has increased in demand from the industrial manufacturing sector due to its capability to produce large metal components with a high deposition rate (A R Kohandehghan, 2010). The application of WAAM can be applied to replace a conventional method of producing large structures. Thus, this research is intended to investigate the effect of temperature distribution during the fabrication of the WAAM samples (Dong-Gyu Ahn, 2021). The information from temperature distribution could be used to improve the quality of the final product.

The focus of this study is to use ANSYS WORKBENCH to simulate the temperature field distribution over time during WAAM. Additive manufacturing is getting many attention right now. In fact, many studies have proven that they are a really useful method for producing large metal parts, and very quickly. However, large residual stresses and deformations arise from current production methods. Therefore, the focus of this study is to find suitable parameters to improve the distribution of the temperature field. Furthermore, in order to find suitable parameters, the temperature fields must be compared between different parameters. The flow chart of the experiments covered in this study is shown in Fig1.1.

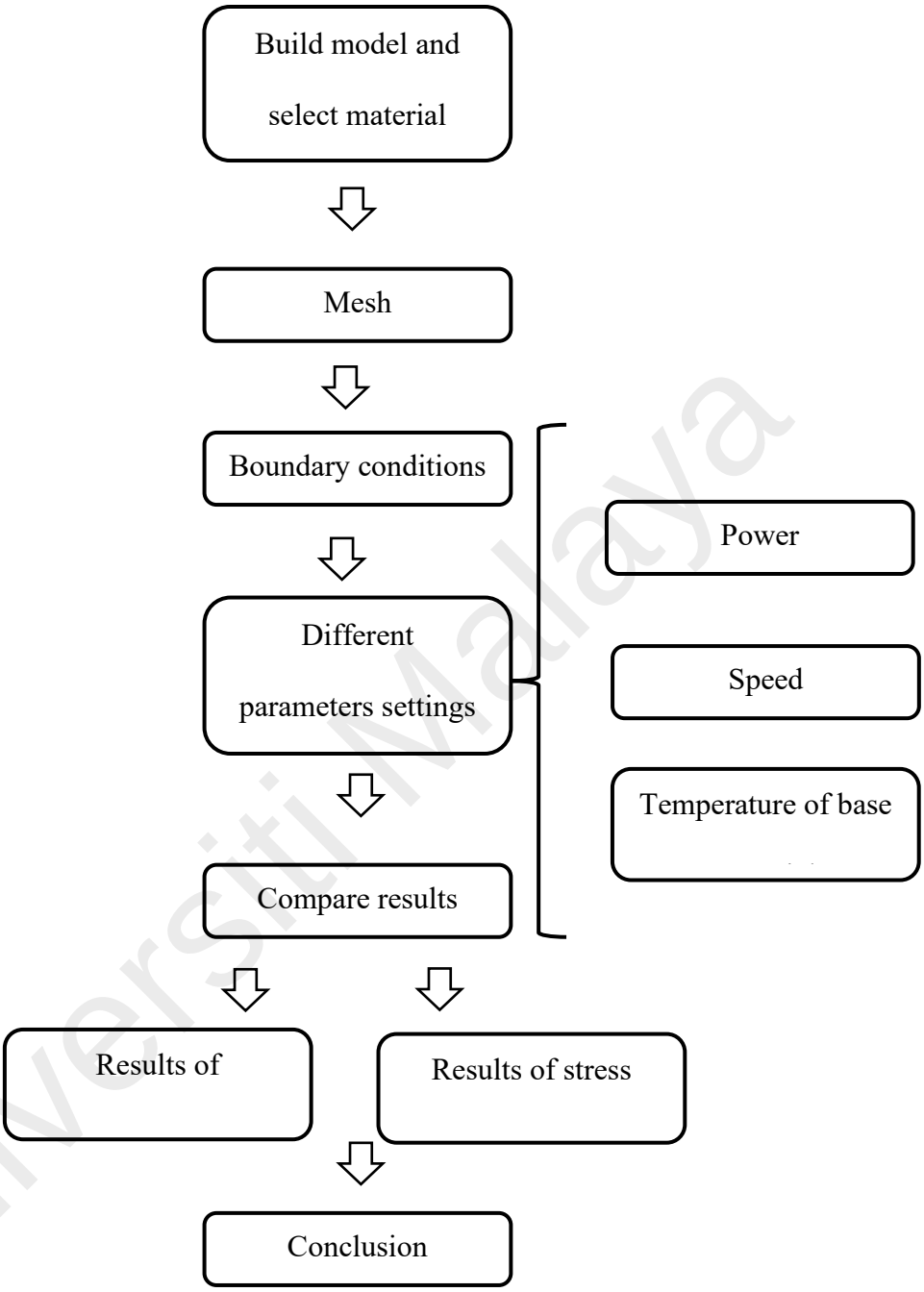

Figure 1.1: The flowchart of the experiment.

1.5 Thesis Structure

A total of five chapters makes up this report. Introduction, Literature Review, Methodology, Results and Discussion, and Conclusions are sections of the paper. Each chapter will cover a different area of this investigation in detail. This section provides a succinct summary of the content of this research.

Chapter One

A general overview and an overview of the investigation are provided in this chapter, which includes a description of the issue, the objective of the investigation, and the scope of the inquiry. This section contains additional information to help understand the chosen title. It is important to note that the stated objectives and goals are references to what should be accomplished during the study process. This chapter also contains a description of the dissertation's organisational framework.

Chapters two

The purpose of this chapter is to review the literature that is relevant to the present survey. A brief history of determining welding temperature fields using finite element numerical simulation techniques is presented along with the categorization of additive manufacturing technologies. In addition, the factors of the manufacturing process and their impact on the temperature field distribution are discussed in detail in this chapter. In addition, this chapter identifies research needs in the areas of 3D printing and manufacturing.

Chapter three

The methodology of this study is explained in detail in Chapter 3. The approach of controlling variables is the most often used research method. It is discussed in detail in this chapter how the experimental design of this investigation was carried out. This includes model design, meshing, boundary condition setup, and coding of heat sources.

Chapter four

Specifically, the findings and discussion of the present investigation are covered in Chapter 4. The findings are primarily concerned with the effect of the parameters utilised in additive manufacturing. The research tested the influence of several parameters on thermal field as well as the cycle temperature map at various times during the experiment. A review of anticipated findings from prior research follows, and the chapter finishes with a discussion of appropriate parameter values for reference in real additive manufacturing procedures.

Chapter Five

This chapter presents a comprehensive summary of all of the results from this study endeavour. The limitations that were discovered throughout the study are also discussed in detail in order to generate fresh ideas and strategies for overcoming them in the future. Because of this, to increase the quality of the research, this chapter includes recommendations for further research.

CHAPTER 2: LITERATURE REVIEW

2.1 History of AM

Additive Manufacturing (AM) technology, also named as 3D printing technology, is a kind of additive manufacturing. Its concepts are derived on geomorphological technology research conducted in the United States throughout the previous century. However, it was not until the latter part of the 1980s that the technology began to progress. Because additive manufacturing technology may accomplish "freedom of production," that is, pieces of any complicated form can be made on a single piece of equipment, this technology is becoming more popular among manufacturers. When compared to the old processing approach, the processing procedure is much shorter, and the processing cycle is significantly shorter. Due to advancements in material use, many additive manufacturing methods have evolved and begun to be extensively employed in the market during the last 30 years, according to the National Institute of Standards and Technology. Additive manufacturing technology, in its simplest form, may be stated as the thinking of the twentieth century, the technology of the 20th century, and market of the 21st century Metal additive manufacturing technique is one of several forming technologies that is more difficult to learn, but it is also a significant aspect of industrial applications due to its complexity. The need for metal additive manufacturing technology in high-end manufacturing areas like as aircraft, cars, ships, and medical equipment is becoming more urgent, especially as topology optimization technology matures. Since 2009, the United States has been paying close attention to additive manufacturing technology and has made significant investments in fundamental technology research in this area. Additionally, it strengthened its funding for research into critical additive manufacturing technologies in 2012, and it launched the first national additive manufacturing innovation centre the following year, 2013. China was a little later than other countries in promoting the development of additive manufacturing technology and the industrialization process at

the national level; however, in recent years, it has received an increasing amount of attention because of the promotion of major universities and research institutes. According to research institutes, metal additive manufacturing technology has achieved a very high degree of application and has been steadily used in a variety of disciplines, including aerospace, weapons, and other industries. However, there is need for improvement in additive manufacturing technology in terms of moulding materials, process control, process monitoring, and quality control procedures.

The WAAM method is, at its core, a surface preparation procedure. In the course of the forming process for metal components, the parts go through a complicated heat cycle, with the temperature field distribution being exceedingly uneven. The uneven temperature field distribution causes residual tension to build up within the moulded object as a consequence of this. Excessive residual stress will result in microcracks and warping deformation of the components, resulting in a huge falling in the overall properties of parts. This event is accompanied by a number of responses, including, on the one hand, passive detection of the internal residual tension of the moulded component, which helps to assure the quality of the moulded part. The quality matches the needs of the intended audience. However, by actively evaluating the evolution law impacting the temperature field and stress field of a formed part, as well as by enhancing different welding process parameters that influence the residually generated stresses of parts, the residual stress of formed part may be minimised. In the traditional welding process research, the experimental method is primarily used, which consists in simulating the thermal process in the welding process with a simulation testing machine, observing the metallographic structure of the sample, measuring the mechanical properties, and inferring the welding process's performance based on these measurements. This approach necessitates a large amount of experimental data and necessitates a large amount of human and material resources. The use of numerical simulation approaches to the welding

process gained momentum as a result of the attention of researchers. The first attempts at numerical modelling of welding heat processes were made in the 1970s. It has taken many years to successfully incorporate the finite difference approach and the finite element method into the field of welding analysis (J.T. Hofman, 2011). Employing the finite element approach, Paley and Hibbert published a research article in 1975 that demonstrated the viability of using the finite element numerical simulation method to determine the welding temperature field using the nonlinear heat conduction mechanism of welding (Fang Hongyuan, 2005). Cruz of America wrote his PhD dissertation on the heat cycle of welding the next year in the United States. There are many aspects to consider, including not just dynamic thermal conductivity and specific heat capacity but also latent heat of phase transition, radiation, convection, and other contributing factors. The numerical simulation technique of the welding temperature field was used to create a working prototype.

Due to a mismatch between the "blackbody" absorption effect generated by the gaps between the powder particles and the energy acceptance of the particles, an uneven heating of the powder layer by laser irradiation occurs during the formation process, which is the cause of this phenomenon. Mazumder and colleagues from the University of Michigan in the United States were responsible for the commercialization and industrialisation of laser additive manufacturing technology in the United States market. For the Direct Metal Deposition (DMD) system, they combined lasers with CNC platforms, image and temperature sensors, 3D modelling, and other components. Because it is capable of implementing real-time monitoring and intelligent control, this system significantly enhances the accuracy with which structural pieces are formed. When the laser additive manufacturing technology was used to create cracks in two distinct materials, Chen Jing and colleagues investigated the mechanism of fracture formation. Ni-based alloy powder was used for one of the cladding materials; stainless steel powder

(316L) was used for the other. The experiment revealed that cold fractures formed in Ni-based alloy powders during multilayer cladding, while hot cracks appeared in 316L stainless steel powders during cladding, as noted in the literature. According to the results of the investigation, cold cracks appear because of the low ductility of Ni-based alloys and the residual thermal stress after cladding, whereas hot cracks in the cladding layer of 316L stainless steel appear as a result of the residual liquid phase at the grain boundary within the solidification temperature range being affected by the cladding layer, according to the findings. In Germany, the findings of liquid film separation produced by heat stress were seen. T-6AI4V titanium alloy bulk created by wire feeding laser additive manufacturing was investigated by Erhard Brand and colleagues in terms of its shape, microstructure, chemical content, and hardness. Three different heat treatment methods were used in the experiment, with two different welding parameters and three different heat treatment methods being considered. The results of the experiment revealed the fundamental characteristics of laser additively manufactured titanium alloys under various welding parameters and heat treatment conditions. K. Kempenl examined the mechanical characteristics of additively manufactured AISi10Mg by selective laser cladding, which was created by selective laser cladding. As part of this experiment, the researchers examined the properties of the moulded parts and compared them to the properties of the standard cast AISi10Mg components. The results of this experiment are published in Advanced Materials and Structures. In accordance with the experimental findings, the mechanical qualities of the additively made AISiIOMg components are equal to those of the cast components, and in certain cases, they significantly outperform the mechanical properties of the cast components. Dr. Eric Wycisk investigated the influence of flaws on the fatigue characteristics for titanium alloys Ti-6AL-4V that were manufactured utilizing additive manufacturing techniques. The flaws that are discussed in this work are mostly porosity and surface roughness, to name a few. Crack

development rate and surface roughness are used to determine the fatigue strength of a material. The experimental results reveal that the Ti-6AL-4V titanium alloy synthesised by laser additive has excellent fatigue strength under the stress condition of 500MPa, this is in accordance with prior studies. The titanium alloy Ti-6AL-4V was studied utilising electron beam welding methods by Suo Hongbo and his colleagues. In the findings, it is shown that the usual microstructure of the deposition layer is epitaxially developed columnar B grain nuclei along its height direction, and that bands of light and dark texture alternate between tracks and layers in a way that is similar to that of the deposition layer. During the deposition process, the components were constantly annealed by consecutive deposition layers, which resulted in a more durable component. As an electron beam additive manufacturing material, the T-45AL-7Nb-0.3W titanium-aluminum alloy was employed in the experiment. It was discovered that raising the preheating temperature and post-heating treatment after forming could successfully minimise residual stress. 3. Plasma additive manufacturing technology is being developed. In his PhD dissertation, Xu Fujia investigated the microstructure management and process optimization of Inconel625 alloy plasma arc fast prototyping in order to improve its efficiency. Specifically, the research object in this work is the pulsed plasma arc fast prototyping technique, with the Incone1625 alloy serving as the forming material. F Martinal and colleagues investigated the forming process of Ti6A14V alloy used in cold filled wire plasma arc additive manufacturing. The factorial experiment was utilised to carry out the experimental design in the experimental procedure, and the effects of the three influencing elements of welding current, deposition velocity, and wire velocity on effective wall thickness and surface fluctuation was investigated. The alteration of the microstructure of the cladding layer between various layers was investigated. It is argued that the varied architectures of distinct deposition layers are caused by the different thermal cycles, which contradicts the generally held belief that the cooling rate varies

from one deposition layer to the next. A study done by Hu Xiaodong and colleagues investigated pulsed plasma additive manufacturing, with the filler wire being 0.4mm 304 stainless steel wire. One research was conducted for determining the influence of peak welding current, weld velocity, and wire's feeding angle on forming width. It should be noted that the filling table is positioned in the water tank with the filling end facing about 3mm-5mm away from the water surface to avoid being overheated and oxidated of weld surface during the filling operation. It was discovered that adjusting the welding conditions might result in varied aspect ratios of distinct weld cross-sections in the experiment. When the austenitic stainless steel HOOCr20Nil0 was used for experimental verification, it was discovered that the surface quality of the formed components produced with a large aspect ratio was superior, and the microstructure was denser. This was confirmed in the literature.

British I.A.Robert carried out finite element simulation of three-dimensional temperature field of laser cladding metal powder(Jiajing Pan *et al*., 2015). The temperature field and stress field of cladding 5 layers of Ti6AL4V alloy powder are simulated by ANSYS software and life-death element technology, and the thickness of each layer is 30um. The research results show that the heated area undergoes a rapid thermal cycle, and the cycle period is the same as that of thermal stress: during continuous cladding, the peak temperature of a certain cladding layer is generated when the next layer is clad, The net effect is that as the cladding layer increases, the temperature remains constant in the layers below.

Panagiotis Michaleris of the United States conducted a study on the processing of cells in the additive manufacturing simulation process (Michaleris *et al*., 1997). In this paper, according to the method of life and death units, the simulation idea of parallel between static units and life and death units is improved. Compared with the traditional simulation method, the calculation results are closer to reality and save a lot of calculation time.

A finite element simulation of the temperature field was conducted in the process of laser cladding AISi10Mg alloy powder and the effects of laser's energy and moving velocity on the temperature field were studied (Hao Lv *et al*., 2021). The research results show that increasing the sweep second speed has a more significant influence on the cooling rate of the molten pool than increasing the laser power. The study also found that the laser power and sweep second speed also have significant differences in the thermal field of the molting pools in the depth direction.

The residual stress generated in the laser additive manufacturing process was studied, and the residual stress under different additive manufacturing paths was compared (Xushan Zhao *et al*., 2021).

Because TIG additive manufacturing employs non-meltable tungsten electrodes, it is required to have a separate wire feeding system in order to melt the filler material in order to perform layer-by-layer manufacture. According to the forming method, the welding wire is uniformly sent between the tungsten argon arc and the substrate through an external wire feeding system, where it melts to form a dense welding seam, which is then stacked layer by layer in the desired forming structural parts according to the planned path. Experimental work was done by Huijun Wang on the AM method of 4043 aluminium alloy using variable-polarity Argon-Tungsten-Arc technology (VP-GTAW). It is the primary focus of this paper to investigate the morphology of single-pass multi-layer moulding under various welding currents, cladding speeds, and wire feeding speeds: the moulding comparison between different cladding layers, the moulding manufacturing process, and the microstructure analysis of cylindrical parts. The connection model between process parameters and single-layer forming is constructed, and the microstructure changes of simplified sections along the deposition direction are investigated. On the other hand, it is pointed out that the difference in microstructure transformation is caused by a rise in height, more severe heat dissipation conditions, and

the speed with which microstructure diffusion occurs along the heat flow. The inclination to develop in the quickest direction grows greater; The result is a simple-shaped aluminium alloy rotating body with a simple form.

Fude Wang *et al.*(2020) conducted additive manufacturing research using a DC pulsed tungsten argon arc. The cladding material utilised in the experiment was a Ti6A14V alloy, which was chosen by the researchers. The microstructure, as well as the transverse and longitudinal tensile characteristics of the straight-walled sections that have been created, are the primary focus of this research. In addition, the transverse and longitudinal fatigue resistance qualities are investigated, as well as the potential reasons of fatigue fracture, which are discussed. Organizational change takes place at several levels. The fatigue resistance test reveals that, with the exception of individual layers, the fatigue resistance of other layers is improved when compared to the fatigue resistance of rolled base metal, and that the cause of fatigue fracture is all pores. The microstructure analysis of the straight-walled parts reveals that epitaxially grown B primary crystals appear in each layer, with the growth method being epitaxial growth along the interface of the upper B primary crystals. The straight-walled parts have a crystalline structure with a straight wall. Straight-walled pieces exhibit anisotropic strength and ductility, according to the results of strength performance testing. Fude Wang attempted to improve the main crystal of B on the basis of the aforementioned study by boosting the stirring impact of the current on the molten pool during the formation process by adding pulse current and increasing welding current. The experimental findings demonstrate that the pulse current cannot refine the primary crystal of B, and the analysis demonstrates that the pulse stirring can only break the dendrites, but the titanium alloy solidifies mostly into planar cell crystals. When it comes to properly creating huge welding currents, fast wire feed rates are essential. According to the findings of the research, the grains were greatly refined when fed at a high wire feeding speed. According to the results of the investigation, the greater

the wire feeding speed, the more filler metal is present in the molten pool, and the more heterogeneous cores that may be employed for nucleation, resulting in the refinement of the grains. Figure depicts the microstructure of the wire feed at various wire feed rates.

2.2 Types of AM

Additive Manufacture (AM), also known as 3D printing(G. Posch, 2014), is based on the principle of discrete stacking, and is a processing technology that integrates the manufacture of parts driven by the 3D model data of the part. According to the processing material, it can be divided into metal 3D printing and non-metal 3D printing. Metal 3D printing technologies mainly include: Although these three are all metal 3D printing technologies, each has its own characteristics, and their processing quality is also very different.

2.2.1 SLM-slective laser melting

The working principles of SLS and SLM technology are basically the same. As shown in Figures 2.1 and 2.2, the powder of each layer is sintered or melted by the laser to obtain a single-layer part, and then the molding chamber is lowered by one layer thickness, the scraper is used to spread the powder, and the laser The powder is reprocessed and this is repeated to obtain the final part. SLS technology developed earlier. It sinters powder materials through lasers and cannot completely melt the powder. There are both liquid and solid states. It was only used for processing non-metallic materials at first, and now it is also used for processing metal materials, but the performance and quality of metal

products are not good. SLM technology is a processing technology developed on the basis of SLS technology for direct metal forming manufacturing. Compared with SLS technology, SLM technology uses a higher laser power (150W-500W), which can

completely melt the powder into a liquid state when the laser scans the powder, shorten

the processing time, and improve the precision and mechanical properties of the molded parts.

A major distinction between EBM technology and the other two types of laser processing is that it employs electron beams as its energy source and processes components in a vacuum environment.

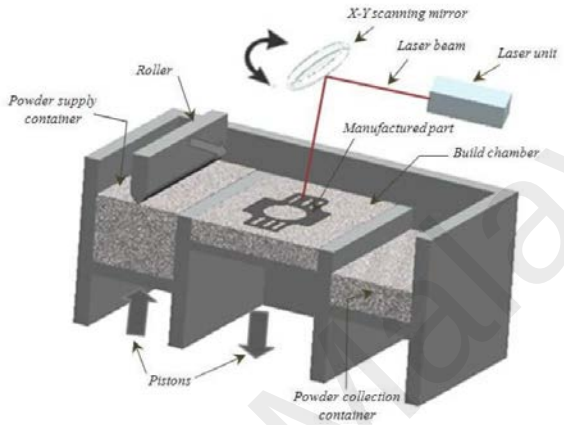

Figure 2.1: Working principles of SLM (Rachel Gordon, 2016).

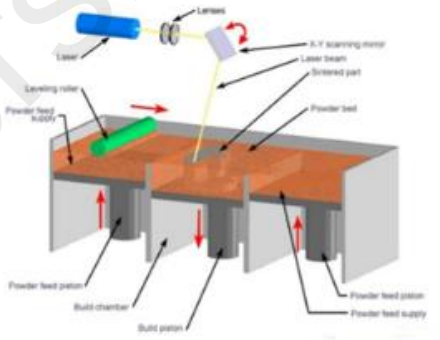

Figure 2.2: Working principles of SLS (Tan C *et al*., 2017)

Because it is necessary to process in a vacuum environment, specific equipment and maintenance are needed, which not only raises the expense of this technology, but also makes it unsuitable for processing bigger components due to its limited processing capacity.

The following are some of the advantages of SLM technology:

1. It can process a wide range of complicated components. In contrast to the typical metal cutting processing technique, SLM processing does not need the use of tools, moulds, or other similar devices, and the components are treated layer by layer by the laser rather than all at once. No matter how sophisticated the components are, they are only a layer of plane data for SLM equipment, and they only need to be modified in accordance with the plane data. Each layer may be formed by the laser processing location alone, without the need to take into consideration the needed processing procedures, as is the case with conventional processing. Processes such as SLM can handle not just complicated curved surfaces, but also porous structures, thin-walled components, and other materials as well.

2. The rate of use of raw resources is quite high. Except for a little amount of smoke and dust, no additional contaminants are created throughout the SLM production process, and materials are used almost entirely to their full potential. The leftover powder left over after processing will be recovered for use in further processing, allowing for a high rate of reuse rather than being rendered worthless, as is the case with iron filings created in conventional processing, which significantly decreases waste of raw materials.

3. Extremely high machining precision. The form accuracy of SLM direct moulding components may be as high as 0.1mm, and the surface roughness can be as high as Ra6.3, allowing them to be employed as structural parts right away.

4. Reduce the amount of time spent on product development. SLM technology allows for direct product formation during product development because it does not require the use of moulds for processing, which reduces product development time and costs. SLM technology is particularly well suited for the processing of single-piece and small-batch products and is becoming increasingly popular.

5. The protection of the environment and the preservation of the environment. Because SLM equipment does not need cutting fluid during processing and does not create iron

filings or other waste materials, the processing procedure is more ecologically friendly than traditional methods. This is a distinct benefit of SLM technology that cannot be replicated by conventional processing or even certain 3D printing processes. While SLM technology has advanced rapidly in recent years, it continues to be highly regarded by businesses, academics, and even national governments. Nevertheless, it is apparent that the technology has its own drawbacks, which are as follows:

1. There are just a handful different sorts of materials. At the moment, the reasonably mature processing materials for SLM technology include: Ti6Al4V, die steel, stainless steel, AlSi10Mg, and others. Ti6Al4V, die steel, stainless steel, and others. Because there are so few varieties, they are distant from the materials necessary for industrial applications, which is unfortunate.

2. There is a limit to the amount of data that can be processed. The processing size of the present SLM equipment is typically less than 500mm × 500mm in dimension. It is very difficult to integrally process pieces that are larger than this, and the processing is subject to a number of constraints as a result. As a result, while developing the pieces, the designer must also take the equipment into consideration. the size of the processing

3. Processing efficiency is insufficient. There is a significant inefficiency in the processing efficiency of the present SLM equipment. When working with bigger parts, it is typical to spend 10 hours or more on each one.

4. Restrictions on the design. Despite the fact that the advancement of SLM technology has significantly increased the creative flexibility of designers, there are still certain restrictions. Consider the length of the cantilever structure, its inclination angle with the horizontal plane, and the size of the aperture. If these factors are not considered, substantial deformation will occur, impairing the processing and even resulting in processing failure, as shown in the example above.

2.2.2 Introduction of WAAM,

WAAM, which uses an arc as a heat source, offers simple forming equipment, cheap equipment costs, a high material utilisation rate, and high forming process deposition efficiency, and is ideal for fast prototyping of large-scale components. The arc additive forming path deposits molten metal on the base plate along a predefined forming route, layer by layer, in a principle and method similar to surface welding, to produce a metal component with a predetermined shape and structure. WAAM technology enables low-cost, high-efficiency research and design for direct metal component production(Xiong Jun *et al*., 2015)(Dang Xiaoling & Wang Jing, 2020).

Arc additive manufacturing technology is a method of producing finished structural parts by melting filler metal and stacking it layer by layer along a pre-planned path. It is a sort of AM technology using arc heat to melt filler metal and stack it layer by layer along a pre-planned path. When compared to typical forging components, the produced parts have a more consistent chemical composition, a higher density, greater strength, and superior toughness. The heating and quenching of each cladding layer have been repeated numerous times throughout the layer-by-layer accumulation process, which is equal to multiple short-term tempering and quenching cycles. There will be no macro-segregation in conventional forging and casting, nor will there be any problem in hardening, nor will there be any length or diameter limitations.

Comparing arc additive manufacturing to high-energy beam additive manufacturing, arc additive manufacturing offers the benefits of cheaper cost and a faster moulding cycle.

MIG welding is referred to as MIG welding, but MAG welding is referred to as MIG active gas protection (MAG). In additive manufacturing, fusible welding wire is utilised as the filler material, and the melting point is determined by the arc created between the uniformly supplied weld wires and the basic material throughout production process. It is created by heating welding wire and base metal surface to generate a molten pool, which

is then quickly solidified into a cladding layer by applying heat to the source. Its characteristics are as follows: it has high versatility, as almost all metals can be welded by MIG/MAG; it can be welded with high current, with rapid cladding speed, and with high production efficiency; it can be welded with high current, with rapid cladding speed, and with high production efficiency. Three-dimensional rapid prototyping (Three-Dimensional Welding Shaping) was initially suggested by J.D. Spencerl26 and colleagues in 1993, when they used a robot to weld fast prototyping metal moulds. This considerably increased the manufacturing efficiency of moulds, which was previously quite low. Researchers Panagiotis Kazanas1277 and colleagues investigated the formation of straight-walled structural elements under a variety of welding angles by using cold metal transfer technology (CMT). It is necessary to employ a staggered and continuous stacking strategy, as seen in the image below. The effective thickness (EWT) and the surface fluctuation (SW) were utilised in the analysis of the experimental data. The effective thickness (EWT) is a characterisation quantity of the moulding state, and its definition is presented in the figure below. The findings of the study demonstrate that CMT may be used for all-position and arbitrary-angle moulding, and that it is capable of moulding structural pieces of any shape. In addition, it is pointed out that this technology may be employed for additive manufacturing without the usage of a displacement device in certain cases.

Because TIG additive manufacturing employs non-meltable tungsten electrodes, it is required to have a separate wire feeding system in order to melt the filler material in order to perform layer-by-layer manufacture. According to the forming method, the welding wire is uniformly sent between the tungsten argon arc and the substrate through an external wire feeding system, where it melts to form a dense welding seam, which is then stacked layer by layer in the desired forming structural parts according to the planned path.

Experimental work by Huijun Wang was carried out on the additive manufacturing technique for 4043 aluminium alloy, which relied on variable-polarity argon-tungsten arcs (VP-GTAW). It is the primary focus of this paper to investigate the morphology of single-pass multi-layer moulding under various welding currents, cladding speeds, and wire feeding speeds: the moulding comparison between different cladding layers, the moulding manufacturing process, and the microstructure analysis of cylindrical parts. The connection model between process parameters and single-layer forming is constructed, and the microstructure changes of simplified sections along the deposition direction are investigated. On the other hand, it is pointed out that the difference in microstructure transformation is caused by a rise in height, more severe heat dissipation conditions, and the speed with which microstructure diffusion occurs along the heat flow. Because of the increasing inclination to expand in the quickest direction, the resultant cylindrical aluminium alloy spinning body is shown in this illustration.

2.3 Parameters that Influencing the temperature distribution of sample

It is vital to investigate the link between these process parameters and the temperature field distribution in order to increase the precision of Arc Additive Manufacturing of manufactured items. The following process factors have the greatest impact on temperature field distribution: welding speed, wire feeding speed, arc voltage, wire extension length, shielding gas type and flow, substrate material and thickness, wire type and diameter, and wire type and diameter distribution. As a result, the primary objectives of this part are to determine how to completely analyse the effect of various parameters on the temperature field and to identify the components that have the most influence and are the easiest to regulate(Yan, 2013)(Xia Ranfei, 2016).

The temperature field distribution is a critical aspect in the additive manufacturing process because it has a significant impact on the moulding effect. The following are the most common forming effects: forming accuracy, welding faults, and etc (Yu Lu, 2017).

Forming precision is a critical need for additive manufacturing since it is so difficult to achieve. Because of poor forming accuracy, the time and money necessary for further processing will be significantly increased, and in severe circumstances, the manufacturing process may fail entirely. Because of the limited capability of the arc as one heating core, width of the melted channel is rather broad and unpredictably unstable. The arc additive manufacturing process is mostly responsible for the welding flaws. In essence, droplet welding is used in the construction of this technology. The droplet welding method will not be able to be welded or will be welded excessively if the process parameters are not acceptable. This will result in stress concentration or possibly cracking. Obtaining suitable process parameters via trials may be used to manage manufacturing failures, forming accuracy, and welding faults. For fully understanding the effects of various process parameters on forming effect of arc additive manufacturing structural components, it is essential to do extensive research.

In most cases, heat input, manufacturing speed, and arc length are the most important factors influencing the temperature field distribution of arc additively built structural elements. According to Yu Lu (2017), the effects of heat source on the formation effect of aluminium alloy manufacturing structural components was investigated, with the major focus on pulse frequency and alternating current. Consequently, since these two parameters are those that have the most direct impact on the heat input, they are also the two ones that have the greatest influence on the moulding effect.

Many elements, such as additive voltage, additive current, additive layers, welding speed, and so on, have an impact on how well the WAAM process works. Xing Tianhang (2018) investigated the link between these parameters and the WAAM thermal field using a single variable technique to identify the association between these factors and the thermal field. The variables that have the greatest influence on the thermal field are those that are chosen for quantitative investigation. Finally, the simulation of complicated components

is carried out, and the solid model is printed, using an appropriate parameter combination.

2.3.1 Influence of additive voltage on stress field

A schematic representation of the centre area of the weld bead, looking in the direction of the WAAM, is put in Figure 2.3. To investigate influence of various variables on the thermal field, this area is the one that is selected for investigation. It should be noted that the middle line of the fourth layer surface is represented by the point MN, the middle line of the second layer surface is represented by the point EF, the centre point of the middle line of the first layer is represented by the point G, and the first layer is represented by the point H. There is a single layer of midline terminals present.

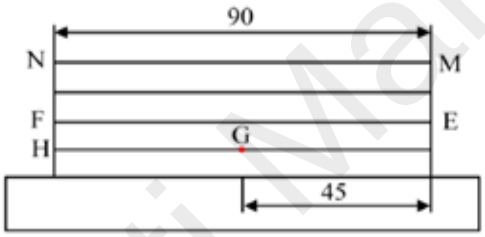

Figure 2.3: Schematic cross-section along the additive direction (Xing Tianhang, 2018).

Figure 2.4 depicts the cloud diagram of the equivalent residual stress distribution of the model when various additive voltages are used to generate the stress distribution. The results of the investigation reveal that when the additive voltage is altered, the equivalent residual stress of the weld metal does not vary much. In fact, the metal wire melts and the metal in the weld bead transforms from liquid to solid under the additive voltages. However, the peak temperature above the melting point is different for each additive voltage, and the equivalent residual stress is also different when the WAAM material is different.

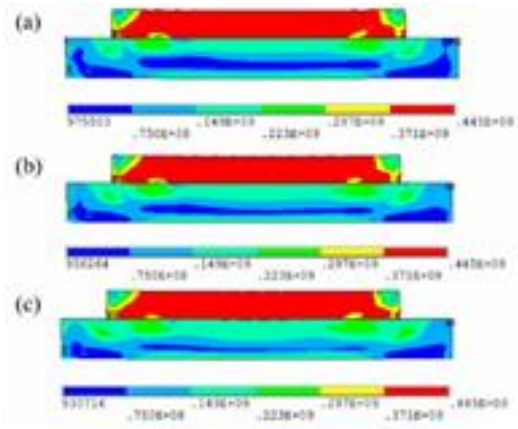

Figure 2.4: Residual stress distribution cloud diagram under different voltages (a) 21V (b) 23V (c) 25V (Xing Tianhang, 2018).

2.3.2 Effect of welding speed on stress field

Figure 2.5 depicts the equivalent residual stress distribution cloud diagram obtained from the model when various welding rates are used. The results of the study demonstrate that the welding speed has only a little effect on the metal temperature field of the weld bead metal, and that it has no effect on the equivalent residual stress field of the weld bead metal, as previously thought. The equivalent residual stress field of the weld bead is virtually the same for all three welding rates, and it is 445MPa, which is not more than the tensile strength of ER2209 duplex stainless steel, which is 700MPa.

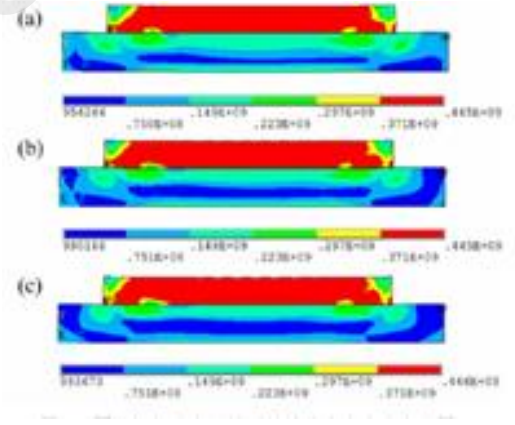

Figure 2.5: Residual stress diagram for different welding speeds (a) 200mm/min (b) 250mm/min (c) 300mm/min (Xing Tianhang, 2018).

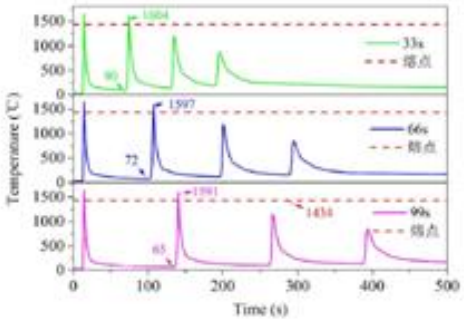

Figure 2.6: Cloud map of temperature change at point G under different cooling time (Xing Tianhang, 2018).

2.3.3 Influence of interlayer cooling time on thermal field

Figure 2.6 depicts the temperature change curve of point G as a function of the time spent cooling between layers as shown in the figure. According to the results of the investigation, increasing the cooling time between layers has a less significant influence on the maximum temperature of the heat source, but has a bigger impact on the cooling temperature after welding and vice versa. By increasing the interlayer cooling time by a factor of two, the maximum temperature during the additive process is decreased by one percent, and the cooling temperature after welding is reduced by forty percent. It is thus not recommended to lower the temperature of arc additive multi-layer components by extending the cooling time between layers when such parts are employed.

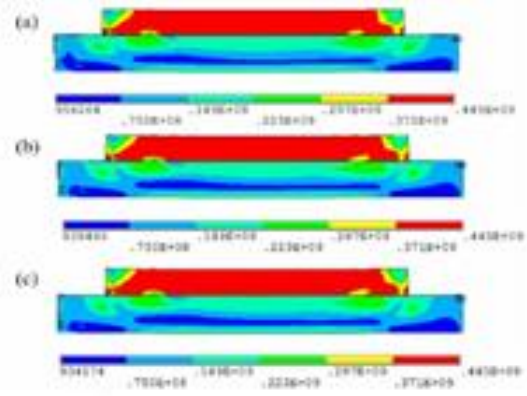

Figure 2.7: Equivalent residual stress nephogram for different cooling time (a) 33s (b) 66s (c) 99s (Xing Tianhang, 2018).

Using a variety of interlayer cooling times, the corresponding residual stress distribution cloud diagram of model is put in Figure 2.7. As a result of this analysis, it is determined

that there is no relationship between the difference between layers and cooling time on equivalent residual stress of the weld metal, and that the maximum equivalent residual stress of 445MPa does not exceed the tensile strength of ER2209 duplex stainless steel, which is 700MPa (Junzhou Huo, 2017).

2.3.4 The effect of additive orientation on the thermal field

As shown in Figure 2.8, the heat cycle curves experienced by point H under various additive directions are shown. Observed by means of the study is the fact that, as a result of the impact of temporal accumulation, the peak temperature of the H point of same-direction additive manufacturing is 134 degrees Celsius greater than the peak temperature of the H point of reverse additive manufacturing. The reverse additive approach is thus used in the WAAM process to prevent the formation of a welding layer, as previously stated. One of the ends has collapsed.

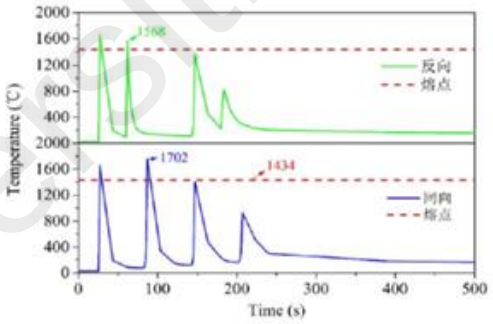

Figure 2.8: Curve of temperature change at point H in different additive directions (Xing Tianhang, 2018).

The cloud diagram of the equivalent residual stress distribution of the model with varied additive directions is seen in Figure 2.9. Because the equivalent residual stress of the welding bead metal is almost same in all additive directions, the maximum equivalent residual stress of 445MPa is less than the tensile strength of the material, which is 700MPa, according to the results of the study.

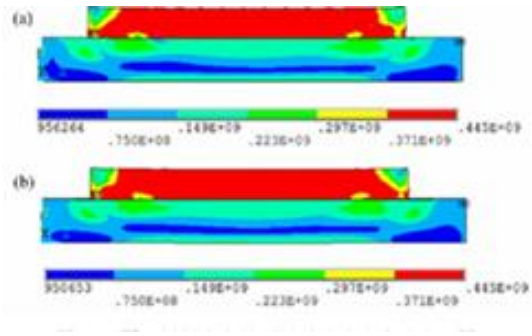

Figure 2.9: Equivalent residual stress nephogram in different additive directions

(a) Opposite (b) Same direction (Xing Tianhang, 2018).

2.3.5 The effect of the number of additive layers on the thermal field

The temperature curves of the respective layers as a function of distance when the heat source is at the end of the fourth layer, the end of the sixth layer, and the end of the tenth layer when the heat source is at the end of the fourth layer(Daniela Fátima Giarollo et al., 2021). This study demonstrates that as the number of additive layers grows, the temperature accumulates fast(A N Jinoop *et al*., 2021). The temperature close to the heat source climbs from 2200c to 2500c whereas the temperature distant from the heat source rises between 500°C and 1100 degrees centigrade (or 1100 degrees centigrade). The rise in metal temperature of a weld bead throughout the WAAM process is thus primarily driven by the increase in the number of additive layers applied to the weld bead.

Figure 2.10 and Figure 2.11 depicts a cloud map of the equivalent residual stress distribution during additive manufacturing of four, six, and ten layers, respectively, during additive manufacturing. In accordance with the results of the analysis, as the number of additive manufacturing layers increases, the equivalent residual stress distribution of the weld metal becomes increasingly unequal, the proportion of high stress areas decreases, and the maximum equivalent residual stress is less than the tensile strength of the material (liang tian *et al*., 2021) (Yeye Cheng & Hehui Wang, 2021).

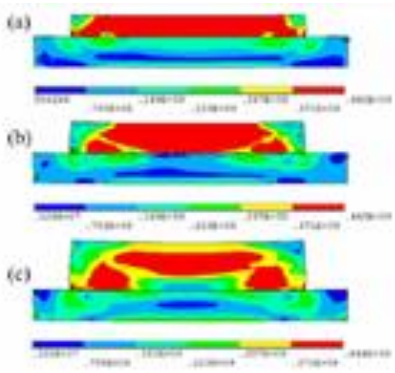

Figure 2.10: Equivalent stress distribution cloud map of different additive layers

(a) 4 (b) 6 (c) 10 (Xing Tianhang, 2018).

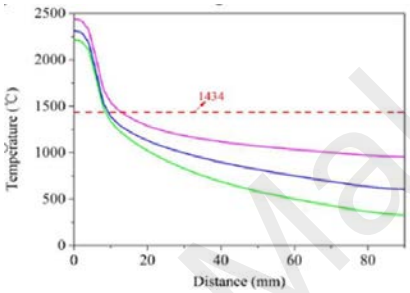

Figure 2.11: Graph of temperature versus distance for different additive layers (Xing Tianhang, 2018).

2.3.6 Influence of cooling method on thermal field

Figure 2.12 depicts a cloud diagram of the equivalent residual stress distribution of the section under various cooling techniques, as shown in the previous figure. Following the analysis, it is discovered that the maximum equivalent residual stress in the water-cooled state is 5MPa greater than the maximum equivalent residual stress in the air-cooled state, that the stress distribution is identical in both states.

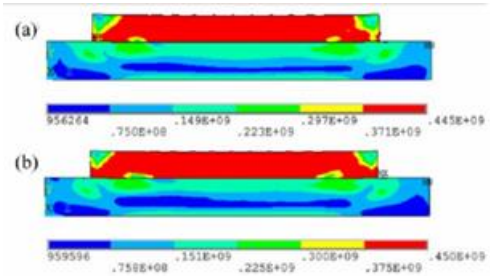

Figure 2.12: Equivalent residual stress distribution cloud diagram of section with different cooling methods

(a) Air cooled (b) Water cooled (Xing Tianhang, 2018).

2.4 Summary

Because Xing Tianhang (2018) used constant power, the current also changed when the voltage was changed. The constant power is equivalent to the constant rate of heat input, so the stress distribution hardly changes at the same power. One of the research gaps completed in this study was to investigate the effect of increasing and decreasing power on the residual stress field.

Although Xing Tianhang (2018) used different welding speeds to simulate the results of the stress field, the residual stress hardly changed because the gap between the welding speeds was not large enough. One of the research gaps completed in this study was to investigate the effect of increasing and decreasing the welding speed on the residual stress field with a sufficiently large change. A sufficient change in welding speed means that a significant change in the stress field will appear.

The automobile and aircraft sectors are moving away from conventional subtractive manufacturing processes and toward additive manufacturing techniques based on welding arcs, which allow to produce multi-faceted product structures. The variety of micromechanical characteristics of WAAM components/parts is a significant issue owing to residual stress, the step effect, solidification cracking, and porosity (Liuping Qiao, 2013)(Sagar Singh *et al*., 2021). As of right now, WAAM for many metals is still in its infancy; Nevertheless, some researchers believe that as technology evolves and hardware develops, WAAM will be the most promising technique in the near future (Rodrigues *et al*., 2019). Even while faster deposition rates are a significant benefit over other approaches, some of the quality concerns outlined below will be alleviated because of this.

It is critical to minimise residual stress and distortions in the WAAM process since they

might lead to early failure, which is especially crucial for big sizes. Induced thermal residual stresses are caused by nonuniform constriction of the material, which leads in nonuniform extension (Ding *et al*., 2015) of the material. Despite the fact that residual stresses may be minimised by post-processing techniques, the bending caused by the loads must be restricted by monitoring and reducing residual stresses throughout the process of metal deposition (Sagar Singh *et al*., 2021).

With the capacity to generate big metal components at high deposition rates, Electric Arc Additive Production (WAAM) has lately gained popularity in industrial manufacturing owing to the rising need for large metal parts produced by WAAM. In the case of big constructions, the use of WAAM may be utilised to replace conventional techniques of construction. Following the review of prior papers, the research showed that no research has utilised the control variable method to tune the characteristics of the stainless steel 316 material through ANSYS WORKBENCH before.

Three variables were used in this study, welding power, welding speed and temperature of base material. The article selects the optimal combination of parameters through the control variable method.

During this simulation, the Goldak Double Ellipsoid Heat Source will be used. Figure 2.13 here are the parameters and exterior of Goldak double ellipsoid heat source.

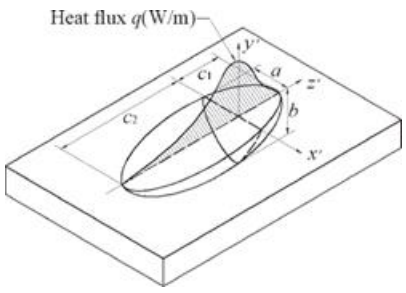

Figure 2.13: Goldak double ellipsoid heat source (Gu *et al*., 2019).

q1=10.392*f1*Q/a/b/c1/5.5655*exp(-3*({X}^2/a^2+({Y}-{TIME}*V)^2/c1^2+{Z}^2/b^2)) (Gu et al., 2019).

q2=10.392*f2*Q/a/b/c2/5.5655*exp(-3*({X}^2/a^2+({Y}-{TIME}*V)^2/c2^2+{Z}^2/b^2)) (Gu *et al*., 2019).

Q: heat input power, 2448w

V: Speed, 10mm/s

a: 2e-3m

b: 5e-3m

c1 and c2: c1=3e-3m, c2=7e-3m. a,b, and c are the size of the heat source, as shown in the figure, a is the half width, b is the height from the top to the middle bottom, c1 is the length of the front half, and c2 is the length of the back half

f1 and f2: f1=2/3, f2=4/3. f1 and f2 are the energy distribution coefficients of the front and rear heat sources, and the sum is 2.

The precision of the simulation is greatly influenced by the quality of the welding heat source model. In order to account for the limited penetration of the Gaussian heat source, the double ellipsoid heat source model described by Goldak provides an excellent solution to this issue (Li Yana & Liu Jiahao, 2021). Such critical parameters are often established based on the geometry of the molten pool, resulting in high costs and poor efficacy in the process. At this time, there is no cost-effective and widely applicable formula that can be calculated in advance.

In order to account for the unequal energy distribution before and after the arc movement, Goldak optimised the Gaussian heat source and presented a double ellipsoid heat source model, according to the results.

$$q(x,y,z) = \frac{6\sqrt{3}f_f q_0}{abc_f\pi\sqrt{\pi}}\exp\left(-\frac{3x^2}{c_f^2}-\frac{3y^2}{a^2}-\frac{3z^2}{b^2}\right) \quad (1)$$

Mathematical expression for the front half of the ellipsoid (Gu *et al*., 2019).

$$q(x,y,z) = \frac{6\sqrt{3}f_r q_0}{abc_r \pi \sqrt{\pi}} \exp\left(-\frac{3x^2}{c_r^2} - \frac{3y^2}{a^2} - \frac{3z^2}{b^2}\right) \quad (2)$$

Mathematical expression for the rear half of the ellipsoid (Gu *et al*., 2019).

A, B, Cf, and Cr are the shape parameters, whereas f1, f2 are the heat input parameters. Double ellipsoid heat source models are defined by their respective width and depth, and their respective lengths are determined by the lengths of the head and back semi-axes of double ellipsoid heat model, respectively. Figure 1 depicts the schematic design and shape parameters of the Goldak‘s model.

In the process of this research, the APDL code in is generated through these two formulas (1) and (2).

Goldak proposed that half of the measured melt pool width be used as a parameter, melt pool depth be used as a parameter of b, half of the measured melt pool width be used as the Cf length parameter of the first half ellipsoid, and twice the measured melt pool width be used as the rear half ellipsoid Cr length parameter(Kang-Hyun. Lee & Gun Jin Yun, 2020). As a result, at this time, the parameters used to define the shape of the double ellipsoid heat source in the software simulation are mostly dictated by the parameters used to establish the shape of the weld pool in the cross-section of the weld that was actually welded(Yue Chen *et al*., 2013). However, because to the limited availability of finances and locations in the real simulation, it is impossible to determine the breadth and depth of penetration of actual welding in the actual simulation. Even if the circumstances are favourable for carrying out the actual measurement, the procedure will be highly hard and time-consuming to complete. Take, for example, the locomotive bogie, which has dozens or hundreds of welds and will need a significant amount of time to pass the real measurement.

CHAPTER 3: METHODOLOGY

3.1 Introduction to control variates

In this study, the control variates method was used. Three variables are considered, power, welding speed and temperature of base material. When doing the simulation, three groups will be done separately. The first group is to keep the power and welding speed unchanged, to change the temperature of base material; the second group is to keep the power and the temperature of base material unchanged, and only change the welding speed; the third group is to keep the welding speed and temperature of base material remains unchanged, only the welding power is changed. By comparing the effects of the three parameters on the thermal field, find optimal solution that can make the welding successful.

Control variates are a technique that is used to decrease variation. By first determining the known values, this strategy helps to decrease the error in predicting unknown numbers. Physicists often utilise the approach of regulating factors (variables) to break down multi-factor issues into several single-factor problems, and then only modify one of the factors in order to examine that element in more detail. The effect of many factors is investigated independently, and the problem is eventually resolved fully. The control variable approach is the name given to this technique. Scientific inquiry relies on it as a critical thinking tool, and it is frequently used in a variety of scientific investigations and experiments, as well as in scientific experimental research.

3.2 Experimental Design

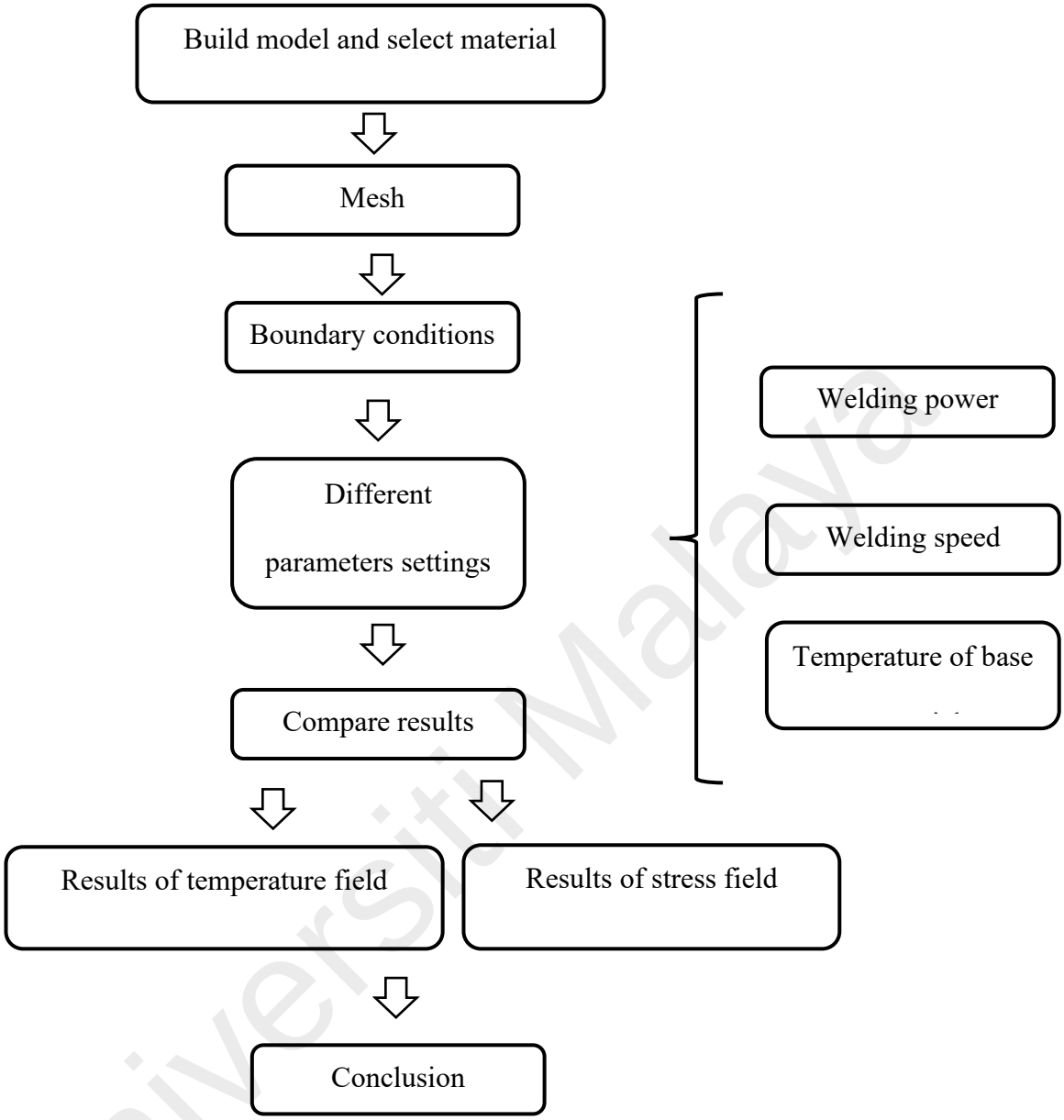

Figure 3.1: The flowchart of the experiment.

3.3 Experimental Procedure

3.3.1 Introduction to ANSYS

In this study, ANSYS WORKBENCH transient thermal is used.

Figure 3.2: ANSYS

In general, the ANSYS is divided into three sections: the pre-processing module, the analysis calculation module, and the postprocessing module.

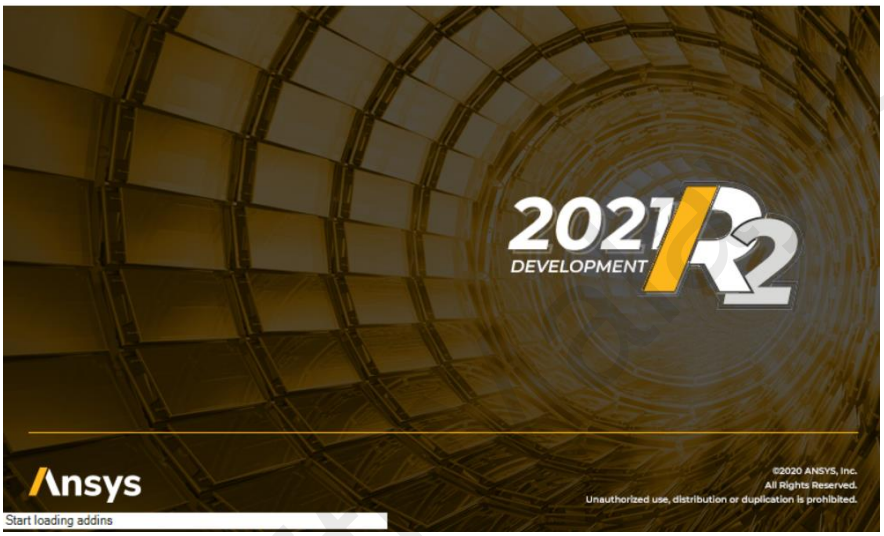

Figure 3.2: Workbench

The assignment of material attributes to the material, including thermal conductivity, density, specific heat capacity, and initial temperature is required in transient thermal analysis, as is solving boundary conditions like time and time increment. When performing a thermal analysis of the assembly.

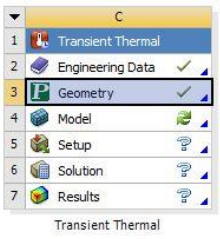

Figure 3.4: Transient thermal

Design modeler is the modelling software for this study.

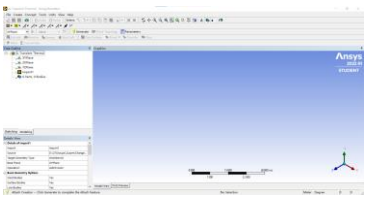

Figure 3.5: Design modeler

3.3.2 Procedures for Gaussian Heat Source.

1. Commands generation of running Gaussian Heat Source

Use Mechanical APDL Product Launcher 2021 R2 to generate commands. It should be noted here that the folder of the working Directory needs to be an all-English path, and it needs to be newly created when needed.

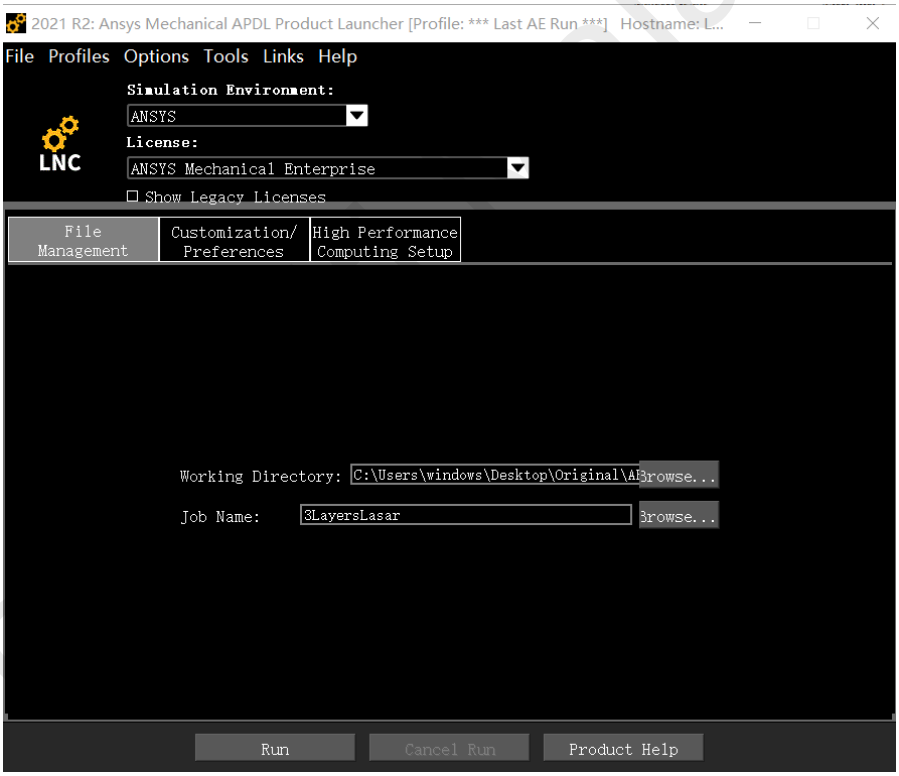

Figure 3.6: Mechanical APDL Product Launcher

It should be noted here that the folder of the working Directory needs to be an all-English path, and it needs to be newly created when needed. In Parameters select Functions, then select Define/Edit. Enter the formula where the picture is marked. After saving the file of this formula, select parameters, then read from file.

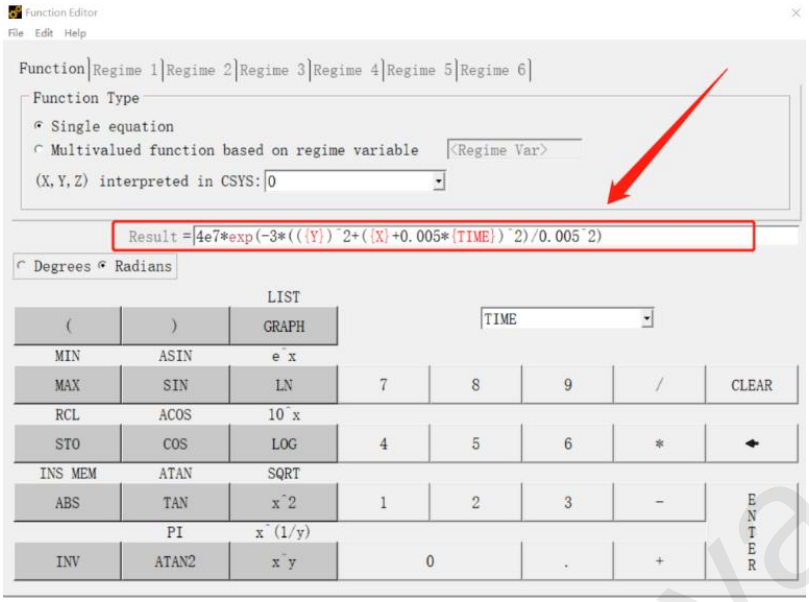

Figure 3.7: Function editor

At this time, the software will automatically generate the code of the movement path of the heat source. The steps to get the code are File-List-Log file. Below is the generated code.

```
*DEL,_FNCNAME
*DEL,_FNCMTID
*DEL,_FNCCSYS
*SET,_FNCNAME,'Gaosi'
*SET,_FNCCSYS,0
! /INPUT,.\Desktop\ABC\SecondSimulation\FUNC.func,,,1
*DIM,%_FNCNAME%,TABLE,6,22,1,,,,%_FNCCSYS%
!
! Begin of equation: 4e7*exp(-3*(({Y})^2+({X}+0.005*{TIME})^2)/0.005^2)
*SET,%_FNCNAME%(0,0,1), 0.0, -999
*SET,%_FNCNAME%(2,0,1), 0.0
*SET,%_FNCNAME%(3,0,1), 0.0
*SET,%_FNCNAME%(4,0,1), 0.0
*SET,%_FNCNAME%(5,0,1), 0.0
*SET,%_FNCNAME%(6,0,1), 0.0
*SET,%_FNCNAME%(0,1,1), 1.0, -1, 0, 0, 0, 0, 0
*SET,%_FNCNAME%(0,2,1), 0.0, -2, 0, 1, 0, 0, -1
*SET,%_FNCNAME%(0,3,1),  0, -3, 0, 1, -1, 2, -2
*SET,%_FNCNAME%(0,4,1), 0.0, -1, 0, 3, 0, 0, -3
*SET,%_FNCNAME%(0,5,1), 0.0, -2, 0, 1, -3, 3, -1
*SET,%_FNCNAME%(0,6,1), 0.0, -1, 0, 2, 0, 0, 3
*SET,%_FNCNAME%(0,7,1), 0.0, -3, 0, 1, 3, 17, -1
*SET,%_FNCNAME%(0,8,1), 0.0, -1, 0, 0.005, 0, 0, 1
*SET,%_FNCNAME%(0,9,1), 0.0, -4, 0, 1, -1, 3, 1
*SET,%_FNCNAME%(0,10,1), 0.0, -1, 0, 1, 2, 1, -4
*SET,%_FNCNAME%(0,11,1), 0.0, -4, 0, 2, 0, 0, -1
*SET,%_FNCNAME%(0,12,1), 0.0, -5, 0, 1, -1, 17, -4
*SET,%_FNCNAME%(0,13,1), 0.0, -1, 0, 1, -3, 1, -5
*SET,%_FNCNAME%(0,14,1), 0.0, -3, 0, 1, -2, 3, -1
*SET,%_FNCNAME%(0,15,1), 0.0, -1, 0, 0.005, 0, 0, 0
*SET,%_FNCNAME%(0,16,1), 0.0, -2, 0, 2, 0, 0, -1
*SET,%_FNCNAME%(0,17,1), 0.0, -4, 0, 1, -1, 17, -2
*SET,%_FNCNAME%(0,18,1), 0.0, -1, 0, 1, -3, 4, -4
*SET,%_FNCNAME%(0,19,1), 0.0, -1, 7, 1, -1, 0, 0
*SET,%_FNCNAME%(0,20,1), 0.0, -2, 0, 4e7, 0, 0, -1
*SET,%_FNCNAME%(0,21,1), 0.0, -3, 0, 1, -2, 3, -1
*SET,%_FNCNAME%(0,22,1), 0.0, 99, 0, 1, -3, 0, 0
! End of equation: 4e7*exp(-3*(({Y})^2+({X}+0.005*{TIME})^2)/0.005^2)
```

Figure 3.8: Example program generated from formula

2. Engineering data setting

When selecting materials, 316 stainless steel was used in this study. The melting point of this material is 1370 degrees Celsius, and its density, Isotropic Thermal Conductivity and Specific Heat Constant Pressure are in three pictures below.

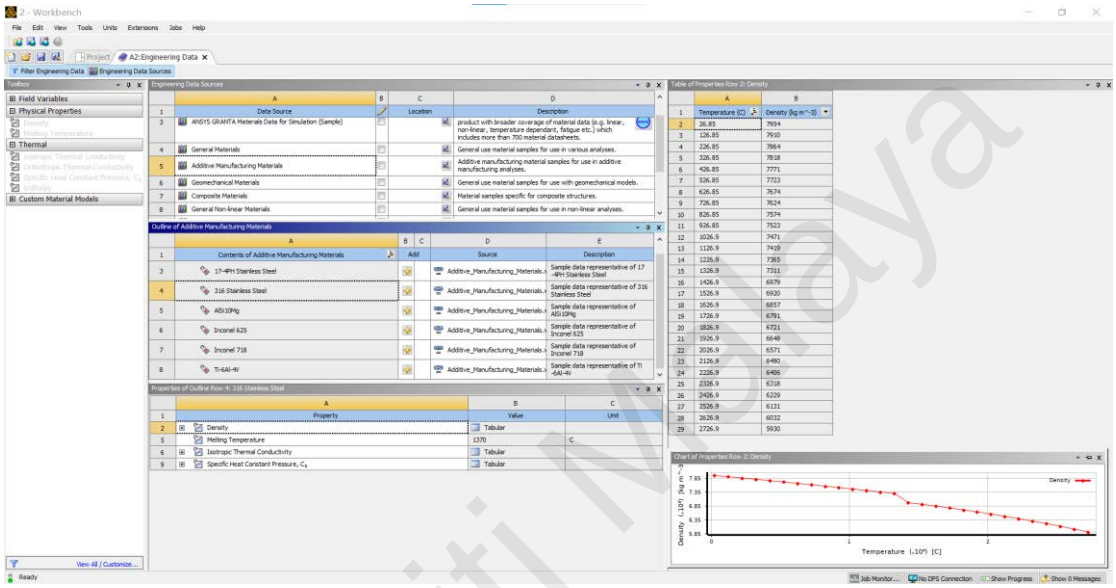

Figure 3.9: Density of 316 stainless steel

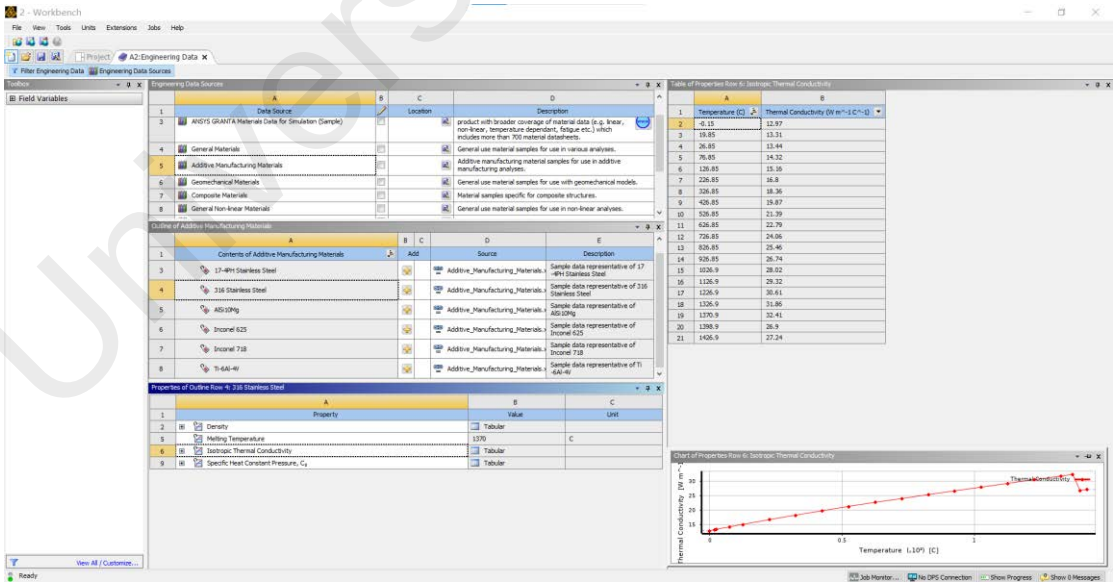

Figure 3.10: Isotropic Thermal Conductivity of 316 stainless steel

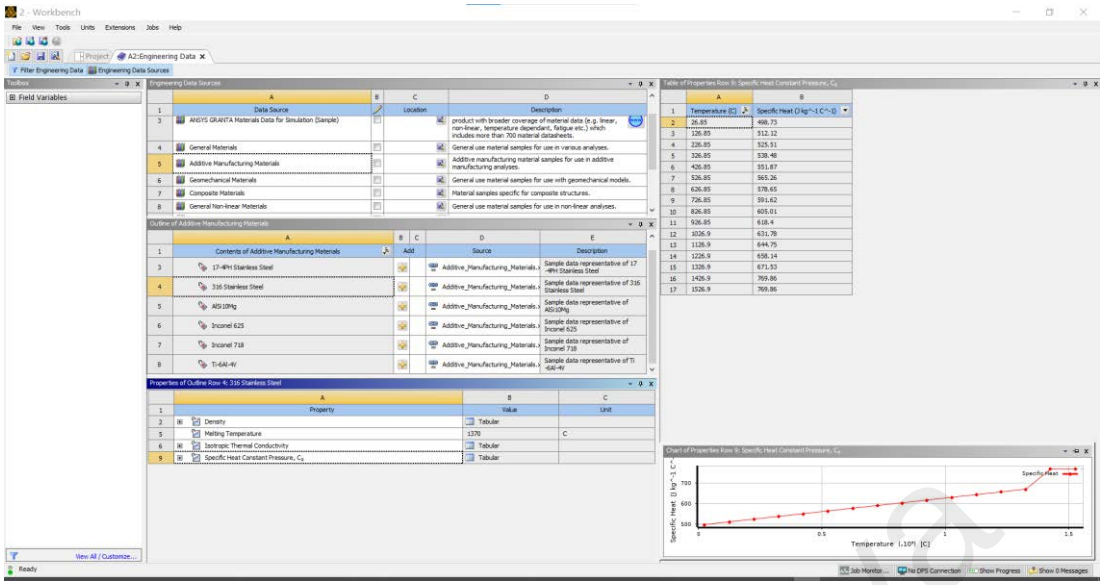

Figure 3.11: Specific Heat Constant Pressure of 316 stainless steel

3. Geometry building

In the modelling process, it is important to note that an entity must correspond to a sketch. First you need to create the weld bead, which is a half cylinder with a diameter of 15mm and a length of 100mm. In the process of establishment, the weld bead can be cut into 15 pieces by setting the plane, which is used for setting the elements birth and death later. The image below shows the weld bead created.

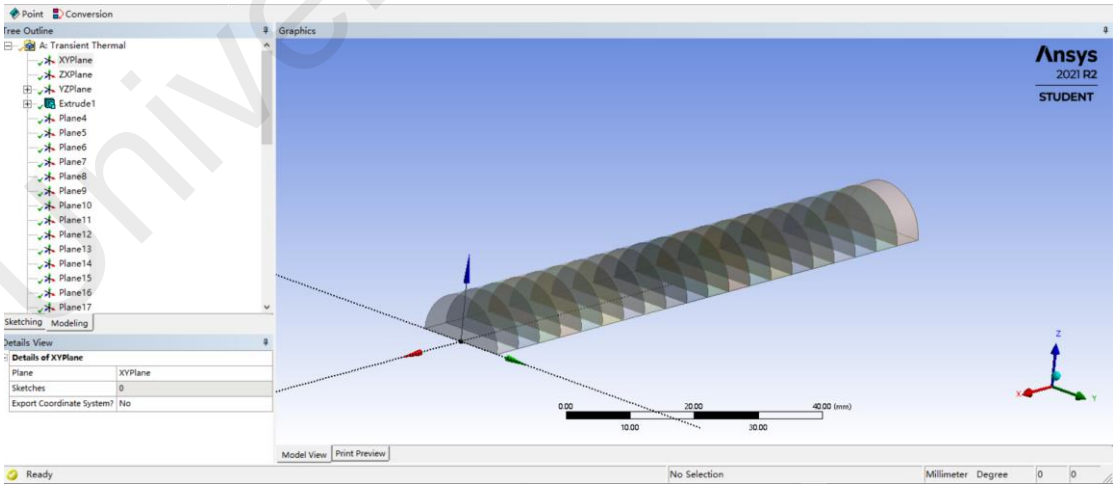

Figure 3.12: Semi-cylindrical bead

The next step is to use the stretch function to build up the bottom sheet. Its width is 50mm, height is 20mm, and length is 100mm. The green part below is a model of the bottom plate.

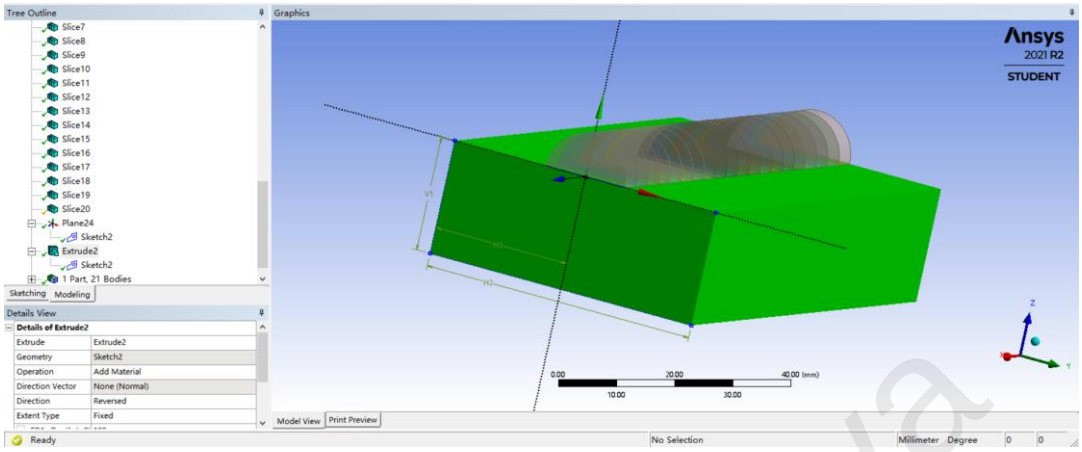

Figure 3.13: Semi-cylindrical bead and base

4. Model design

In this step, the most important thing is to assign the material to the geometry. Stainless steel is used here.

After updating the material in the material database, it needs to be updated in this module before it can be displayed.

This study uses the default coordinate system.

This study uses the default mesh generation 0.05 m.

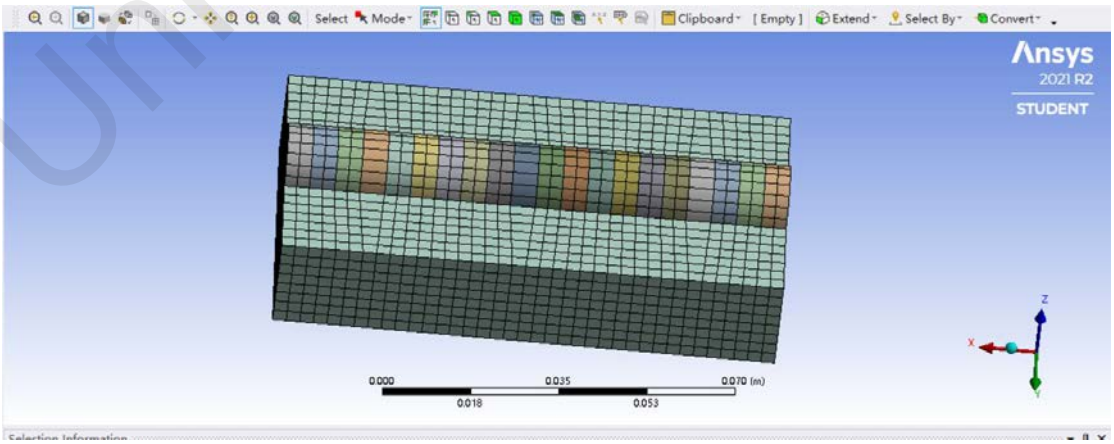

Figure 3.14: Result of meshing

5. Named selection

Naming the upper surface as A1 of the weld bead ensures that the heat source can be applied to this surface in the following commands (T.R. Walker and C.J. Bennett, 2019).

6. Transient thermal settings

In this step, thermal convection, commands from APDL, and elements of birth and death need to be inserted. The movement speed of the birth and death units needs to match the movement speed of the commands. For example, in this case, the movement velocity of Gaussian heat source and speed of elements of birth and death are both 20 mm/s.

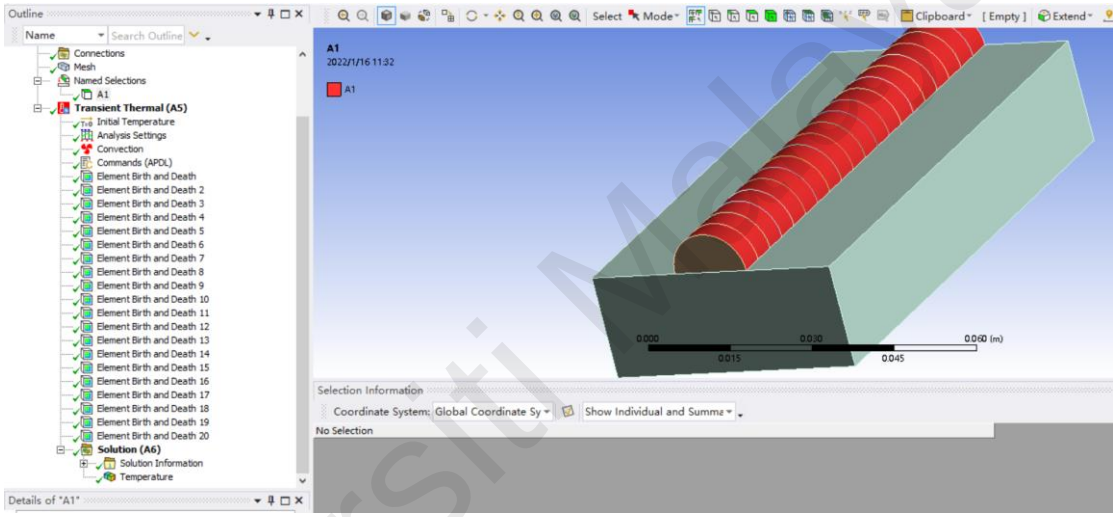

Figure 3.15: Heat source loading surface

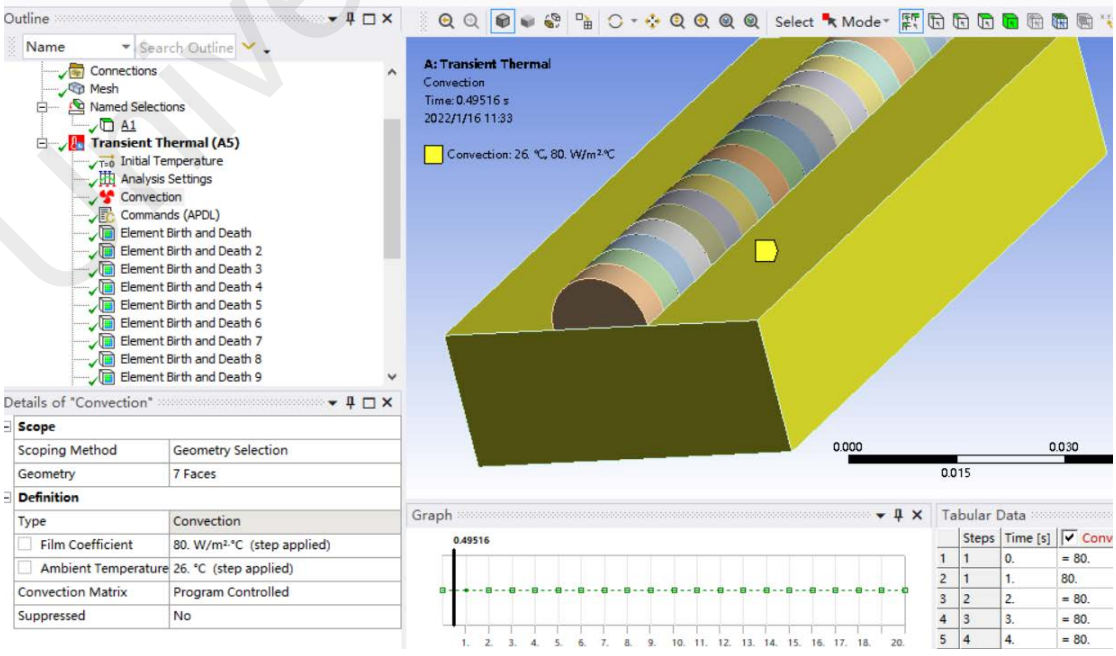

Figure 3.16: Thermal convection loading surface

7. Generation of Solution

In the final solver block, a temperature block needs to be inserted. Then click solve and wait for the result. Isotherms can be displayed, which makes the results of the temperature field easier to observe.

The figure below is the result of the temperature field at 12.5 seconds, the maximum temperature is 2060.5 degrees Celsius.

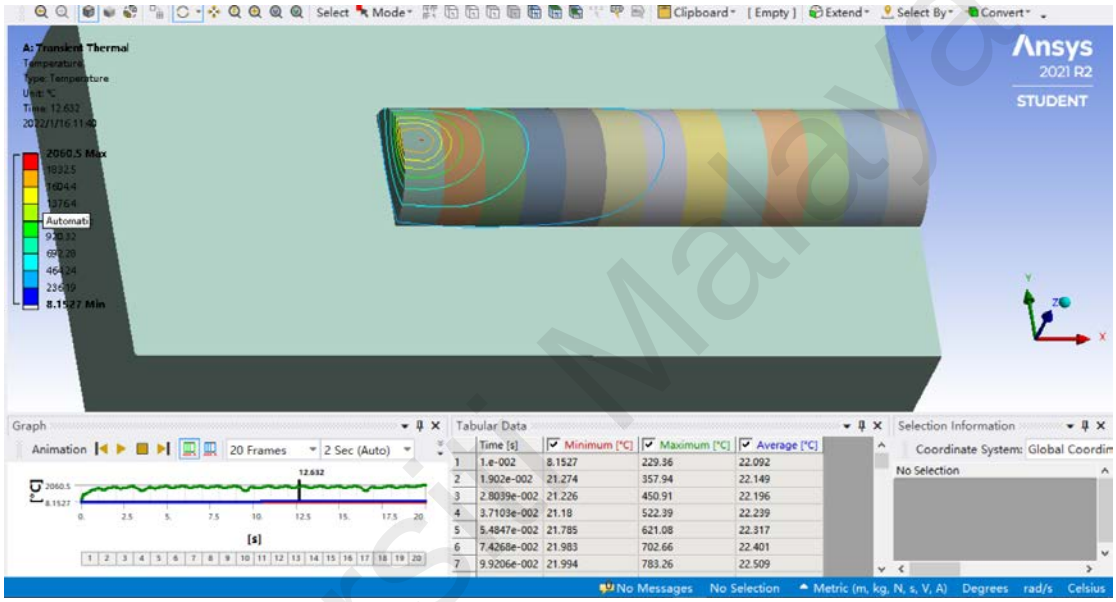

Figure 3.17: Results of the isotherm

3.3.3 Procedures for Goldak Heat Source

The operation process in ANSYS of the Goldak double ellipsoid heat source model is similar to that of the Gaussian heat source, except that the Goldak heat source is a three-dimensional heat source(Zhenkun Lei *et al*., 2020).

This is the model of the cross section of the Goldak double ellipsoid heat source used this time.

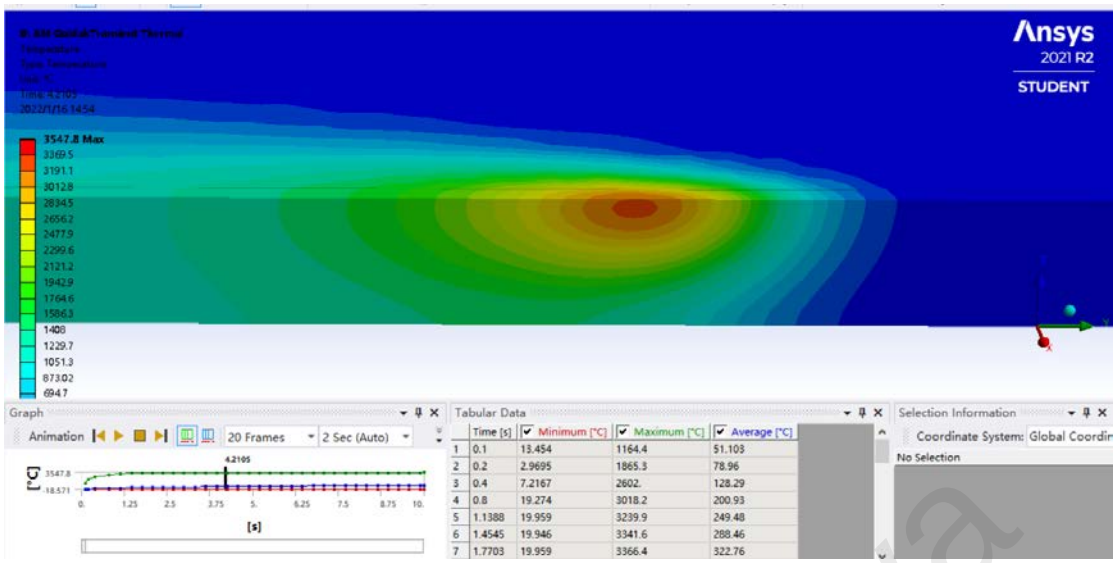

Figure 3.18: Goldak double ellipsoid heat source used

When meshing the mesh, it is necessary to increase the mesh density near the middle bead and reduce the mesh density on both sides. The reason for this is that if the model all had a small mesh, the computer's processor would be heavily taxed. The single-layer and single-channel simulation of the Goldak double ellipsoid model took 23 hours.

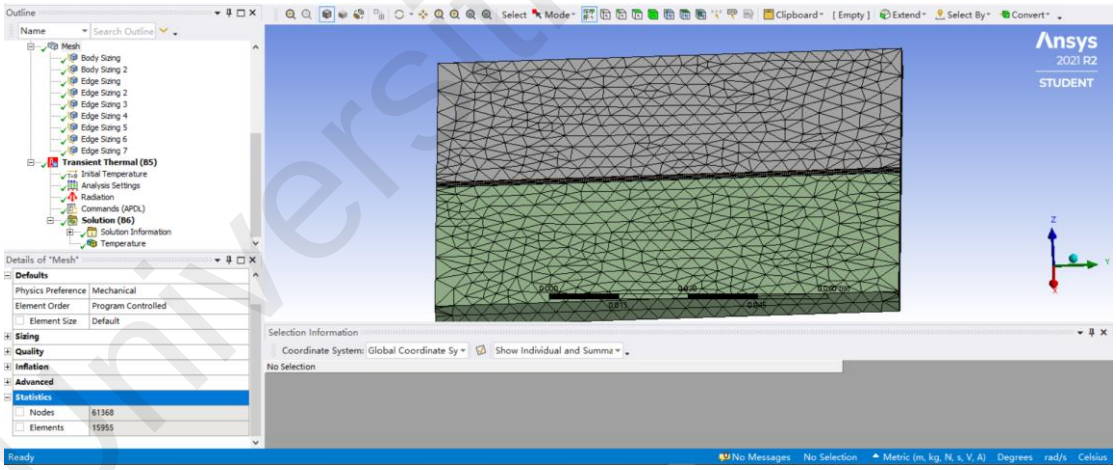

Figure 3.19: Mesh results for the Goldak model

The APDL program is divided into three parts, the most important part is the expression of the formula of the second part. Below is an explanation of the formula.

```
! This is the first part, some commands are predefined.
FINISH ! Predefined commands.
/PREP7
! Below are some parameters of the dual ellipsoid heat source model.
Q=ARG1 ! Heat input power. U is welding voltage, I is welding current, y is welding efficiency, so
Q=y*U*I=60*68*0.6=2448 W.
V=ARG2 ! Velocity. 10mm/s, these two parameters of ARG are set in APDL commands.
a=2e-3 ! The units of a, b, and c are meters.
b=5e-3
c1=3e-3
c2=7e-3 !a, b, c are all heat source dimensions, a is the half width, b is the height from the top to the bottom half,
c1 is the front half length, c2 is the back half length
f1=2/3 ! f1 and f2 are the energy distribution coefficients of the front and rear heat sources, and their sum is 2
f2=4/3
N=100 ! Set the moving heat source into 100 moving steps, calculated once every 1mm, 100*1mm=0.1m.

*DO,I,1,N! is a cycle, note that I is from 1 to 100, run 50 times, at this time assign a new value to the I cycle
BDELE,ALL,ALL ! Deletes all body loads and previous body loads.
T=I*1e-3/V ! Time in seconds.
nsel,s,loc,y,I*1e-3,0.1 ! Select all node positions, from loc, along the y direction, from the current execution step
I*1e-3 to 0.1m. 0.1m is the board length, that is, the movement length.
CM, FRONT, NODE ! Front node.
nsel,s,loc,y,0,I*1e-3 ! Select the node position, from loc, along the y direction, from 0 to I*1e-3m.
CM,BHIND,NODE ! Post node.

!the second part.
!Two formulas. 10.392*f1*Q/a/b/c1/5.5655*exp(-3*({X}^2/a^2+({Y}-{TIME}*V)^2/c1 ^2+{Z}^2/b^2))
!                    10.392*f2*Q/a/b/c2/5.5655*exp(-3*({X}^2/a^2+({Y}-{TIME}*V)^2/c2^2+{ Z}^2/b^2))
!Define the front elliptical heat source. Below are the coordinates of the heat source trace.
*DEL,_FNCNAME

*DEL,_FNCMTID
*DEL,_FNC_C1
*DEL,_FNC_C2
*DEL,_FNC_C3
*DEL,_FNC_C4
*DEL,_FNC_C5
*DEL,_FNC_C6
*DEL,_FNCCSYS
*SET,_FNCNAME,'Front'
*DIM,_FNC_C1,,1
*DIM,_FNC_C2,,1
*DIM,_FNC_C3,,1
*DIM,_FNC_C4,,1
*DIM,_FNC_C5,,1
*DIM,_FNC_C6,,1
*SET,_FNC_C1(1),f1
*SET,_FNC_C2(1),Q
*SET,_FNC_C3(1),a
*SET,_FNC_C4(1),b
*SET,_FNC_C5(1),c1
*SET,_FNC_C6(1),V
*SET,_FNCCSYS,0
!/INPUT,Front.func,,,1
*DIM,%_FNCNAME%,TABLE,8,36,1,,,,%_FNCCSYS%

!Begin of equation: 10.392*f1*Q/a/b/c1/5.5655*exp(-3*({X}^2/a^2+({Y}-{TIME}*V)^2/c1 ^2+{Z}^2/b^2))
*SET,%_FNCNAME%(0,0,1), 0.0, -999
*SET,%_FNCNAME%(2,0,1), 0.0
*SET,%_FNCNAME%(3,0,1), %_FNC_C1(1)%
*SET,%_FNCNAME%(4,0,1), %_FNC_C2(1)%
*SET,%_FNCNAME%(5,0,1), %_FNC_C3(1)%
*SET,%_FNCNAME%(6,0,1), %_FNC_C4(1)%
*SET,%_FNCNAME%(7,0,1), %_FNC_C5(1)%
*SET,%_FNCNAME%(8,0,1), %_FNC_C6(1)%
*SET,%_FNCNAME%(0,1,1), 1.0, -1, 0, 10.392, 0, 0, 17
*SET,%_FNCNAME%(0,2,1), 0.0, -2, 0, 1, -1, 3, 17
```

```
*SET,%_FNCNAME%(0,3,1), 0, -1, 0, 1, -2, 3, 18
*SET,%_FNCNAME%(0,4,1), 0.0, -2, 0, 1, -1, 4, 19
*SET,%_FNCNAME%(0,5,1), 0.0, -1, 0, 1, -2, 4, 20
*SET,%_FNCNAME%(0,6,1), 0.0, -2, 0, 1, -1, 4, 21
*SET,%_FNCNAME%(0,7,1), 0.0, -1, 0, 5.5655, 0, 0, -2
*SET,%_FNCNAME%(0,8,1), 0.0, -3, 0, 1, -2, 4, -1
*SET,%_FNCNAME%(0,9,1), 0.0, -1, 0, 0, 0, 0, 0
*SET,%_FNCNAME%(0,10,1), 0.0, -2, 0, 1, 0, 0, -1
*SET,%_FNCNAME%(0,11,1), 0.0, -4, 0, 1, -1, 2, -2
*SET,%_FNCNAME%(0,12,1), 0.0, -1, 0, 3, 0, 0, -4
*SET,%_FNCNAME%(0,13,1), 0.0, -2, 0, 1, -4, 3, -1
*SET,%_FNCNAME%(0,14,1), 0.0, -1, 0, 2, 0, 0, 2
*SET,%_FNCNAME%(0,15,1), 0.0, -4, 0, 1, 2, 17, -1
*SET,%_FNCNAME%(0,16,1), 0.0, -1, 0, 2, 0, 0, 19
*SET,%_FNCNAME%(0,17,1), 0.0, -5, 0, 1, 19, 17, -1
*SET,%_FNCNAME%(0,18,1), 0.0, -1, 0, 1, -4, 4, -5
*SET,%_FNCNAME%(0,19,1), 0.0, -4, 0, 1, 1, 3, 22
*SET,%_FNCNAME%(0,20,1), 0.0, -5, 0, 1, 3, 2, -4
*SET,%_FNCNAME%(0,21,1), 0.0, -4, 0, 2, 0, 0, -5
*SET,%_FNCNAME%(0,22,1), 0.0, -6, 0, 1, -5, 17, -4
*SET,%_FNCNAME%(0,23,1), 0.0, -4, 0, 2, 0, 0, 21
*SET,%_FNCNAME%(0,24,1), 0.0, -5, 0, 1, 21, 17, -4
*SET,%_FNCNAME%(0,25,1), 0.0, -4, 0, 1, -6, 4, -5
*SET,%_FNCNAME%(0,26,1), 0.0, -5, 0, 1, -1, 1, -4
*SET,%_FNCNAME%(0,27,1), 0.0, -1, 0, 2, 0, 0, 4
*SET,%_FNCNAME%(0,28,1), 0.0, -4, 0, 1, 4, 17, -1
*SET,%_FNCNAME%(0,29,1), 0.0, -1, 0, 2, 0, 0, 20
*SET,%_FNCNAME%(0,30,1), 0.0, -6, 0, 1, 20, 17, -1
*SET,%_FNCNAME%(0,31,1), 0.0, -1, 0, 1, -4, 4, -6
*SET,%_FNCNAME%(0,32,1), 0.0, -4, 0, 1, -5, 1, -1
*SET,%_FNCNAME%(0,33,1), 0.0, -1, 0, 1, -2, 3, -4
*SET,%_FNCNAME%(0,34,1), 0.0, -1, 7, 1, -1, 0, 0
*SET,%_FNCNAME%(0,35,1), 0.0, -2, 0, 1, -3, 3, -1
*SET,%_FNCNAME%(0,36,1), 0.0, 99, 0, 1, -2, 0, 0
!End of equation: 10.392*f1*Q/a/b/c1/5.5655*exp(-3*({X}^2/a^2+({Y}-{TIME}*V)^2
!/c1^2+{Z}^2/b^2))
```

```
!-->

!Defines the power, shape, and motion parameters of the rear elliptical heat source.
*DEL,_FNCNAME
*DEL,_FNCMTID
*DEL,_FNC_C1
*DEL,_FNC_C2
*DEL,_FNC_C3
*DEL,_FNC_C4
*DEL,_FNC_C5
*DEL,_FNC_C6
*DEL,_FNCCSYS
*SET,_FNCNAME,'Bhind'
*DIM,_FNC_C1,,1
*DIM,_FNC_C2,,1
*DIM,_FNC_C3,,1
*DIM,_FNC_C4,,1
*DIM,_FNC_C5,,1
*DIM,_FNC_C6,,1
*SET,_FNC_C1(1),f2
*SET,_FNC_C2(1),Q
*SET,_FNC_C3(1),a
*SET,_FNC_C4(1),b
*SET,_FNC_C5(1),c2
*SET,_FNC_C6(1),V
*SET,_FNCCSYS,0
!/INPUT,Bhind.func,,,1
*DIM,%_FNCNAME%,TABLE,8,36,1,,,,%_FNCCSYS%
!
!Begin of equation: 10.392*f2*Q/a/b/c2/5.5655*exp(-3*({X}^2/a^2+({Y}-{TIME}*V)^2/c2 ^2+{Z}^2/b^2))
*SET,%_FNCNAME%(0,0,1), 0.0, -999
*SET,%_FNCNAME%(2,0,1), 0.0
*SET,%_FNCNAME%(3,0,1), %_FNC_C1(1)%
*SET,%_FNCNAME%(4,0,1), %_FNC_C2(1)%
*SET,%_FNCNAME%(5,0,1), %_FNC_C3(1)%
*SET,%_FNCNAME%(6,0,1), %_FNC_C4(1)%
*SET,%_FNCNAME%(7,0,1), %_FNC_C5(1)%
*SET,%_FNCNAME%(8,0,1), %_FNC_C6(1)%
```

```
*SET,%_FNCNAME%(0,1,1), 1.0, -1, 0, 10.392, 0, 0, 17
*SET,%_FNCNAME%(0,2,1), 0.0, -2, 0, 1, -1, 3, 17
*SET,%_FNCNAME%(0,3,1), 0, -1, 0, 1, -2, 3, 18
*SET,%_FNCNAME%(0,4,1), 0.0, -2, 0, 1, -1, 4, 19
*SET,%_FNCNAME%(0,5,1), 0.0, -1, 0, 1, -2, 4, 20
*SET,%_FNCNAME%(0,6,1), 0.0, -2, 0, 1, -1, 4, 21
*SET,%_FNCNAME%(0,7,1), 0.0, -1, 0, 5.5655, 0, 0, -2
*SET,%_FNCNAME%(0,8,1), 0.0, -3, 0, 1, -2, 4, -1
*SET,%_FNCNAME%(0,9,1), 0.0, -1, 0, 0, 0, 0, 0
*SET,%_FNCNAME%(0,10,1), 0.0, -2, 0, 1, 0, 0, -1
*SET,%_FNCNAME%(0,11,1), 0.0, -4, 0, 1, -1, 2, -2
*SET,%_FNCNAME%(0,12,1), 0.0, -1, 0, 3, 0, 0, -4
*SET,%_FNCNAME%(0,13,1), 0.0, -2, 0, 1, -4, 3, -1
*SET,%_FNCNAME%(0,14,1), 0.0, -1, 0, 2, 0, 0, 2
*SET,%_FNCNAME%(0,15,1), 0.0, -4, 0, 1, 2, 17, -1
*SET,%_FNCNAME%(0,16,1), 0.0, -1, 0, 2, 0, 0, 19
*SET,%_FNCNAME%(0,17,1), 0.0, -5, 0, 1, 19, 17, -1
*SET,%_FNCNAME%(0,18,1), 0.0, -1, 0, 1, -4, 4, -5
*SET,%_FNCNAME%(0,19,1), 0.0, -4, 0, 1, 1, 3, 22
*SET,%_FNCNAME%(0,20,1), 0.0, -5, 0, 1, 3, 2, -4
*SET,%_FNCNAME%(0,21,1), 0.0, -4, 0, 2, 0, 0, -5
*SET,%_FNCNAME%(0,22,1), 0.0, -6, 0, 1, -5, 17, -4
*SET,%_FNCNAME%(0,23,1), 0.0, -4, 0, 2, 0, 0, 21
*SET,%_FNCNAME%(0,24,1), 0.0, -5, 0, 1, 21, 17, -4
*SET,%_FNCNAME%(0,25,1), 0.0, -4, 0, 1, -6, 4, -5
*SET,%_FNCNAME%(0,26,1), 0.0, -5, 0, 1, -1, 1, -4
*SET,%_FNCNAME%(0,27,1), 0.0, -1, 0, 2, 0, 0, 4
*SET,%_FNCNAME%(0,28,1), 0.0, -4, 0, 1, 4, 17, -1
*SET,%_FNCNAME%(0,29,1), 0.0, -1, 0, 2, 0, 0, 20
*SET,%_FNCNAME%(0,30,1), 0.0, -6, 0, 1, 20, 17, -1
*SET,%_FNCNAME%(0,31,1), 0.0, -1, 0, 1, -4, 4, -6
*SET,%_FNCNAME%(0,32,1), 0.0, -4, 0, 1, -5, 1, -1
*SET,%_FNCNAME%(0,33,1), 0.0, -1, 0, 1, -2, 3, -4
*SET,%_FNCNAME%(0,34,1), 0.0, -1, 7, 1, -1, 0, 0
*SET,%_FNCNAME%(0,35,1), 0.0, -2, 0, 1, -3, 3, -1
*SET,%_FNCNAME%(0,36,1), 0.0, 99, 0, 1, -2, 0, 0
!End of equation: 10.392*f2*Q/a/b/c2/5.5655*exp(-3*({X}^2/a^2+({Y}-{TIME}*V)^2/c2 ^2+{Z}^2/b^2))
```

```
!-->

! The third part, predefined.
allsel,all! Select all bodies.
/SOL! solve.
!*
ANTYPE,4 ! Meaning of transient thermal module
!*
TRNOPT, FULL!
TUNIF,20, ! defines the initial temperature as 20 degrees.
BF, FRONT, HGEN, %FRONT%! Load the volumetric heat load through the table in the front part area in front of the
heat source, HGEN is the energy.
BF, BHIND, HGEN, %BHIND% ! Load volumetric heat loads through the table in the rear part of the heat source
area.
CMDELE,FRONT
CMDELE,BHIND ! Remove front and rear nodal body loads.
AUTOTS,1 ! The automatic step size is 1, that is, the increment of N is 1 each time.
KBC,1
TIME,T
allsel,all ! Selects all bodies.
OUTRES,ALL,ALL! Output all results.
SOLVE
*ENDDO ! Ends the loop.
save        !  Program ends.
```

Figure 3.20: The APDL program of Goldak double ellipsoid heat source

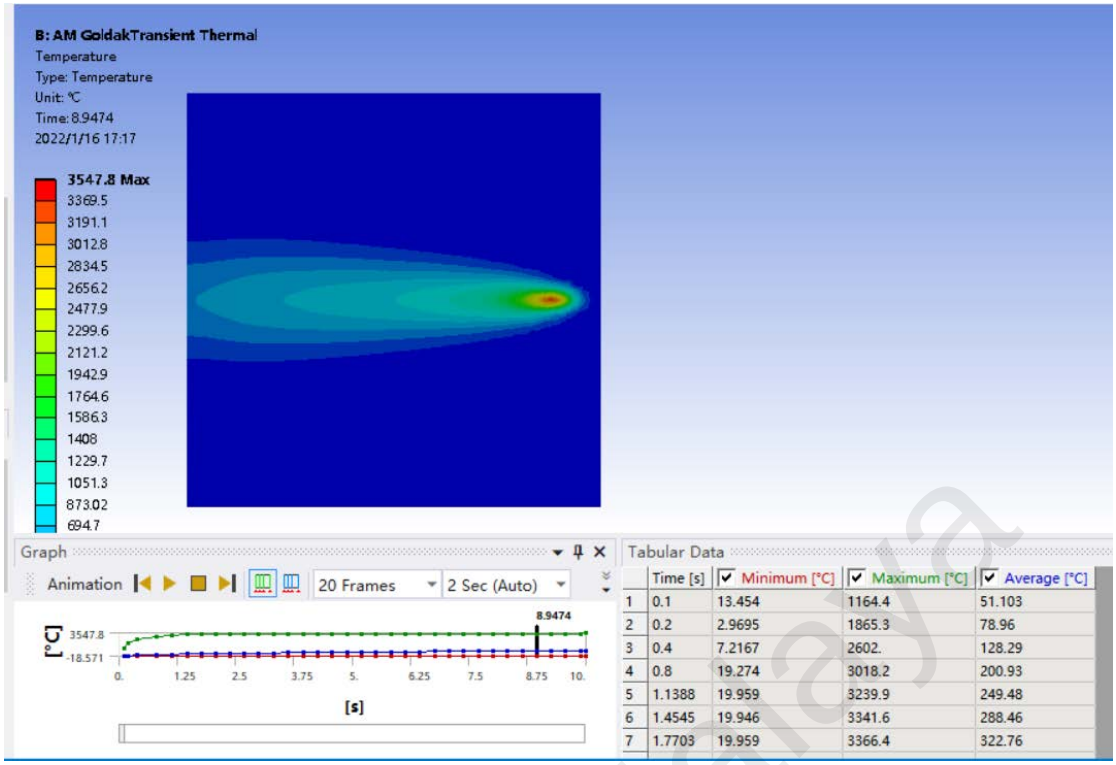

Figure 3.21: Top view of Goldak double ellipsoid heat source

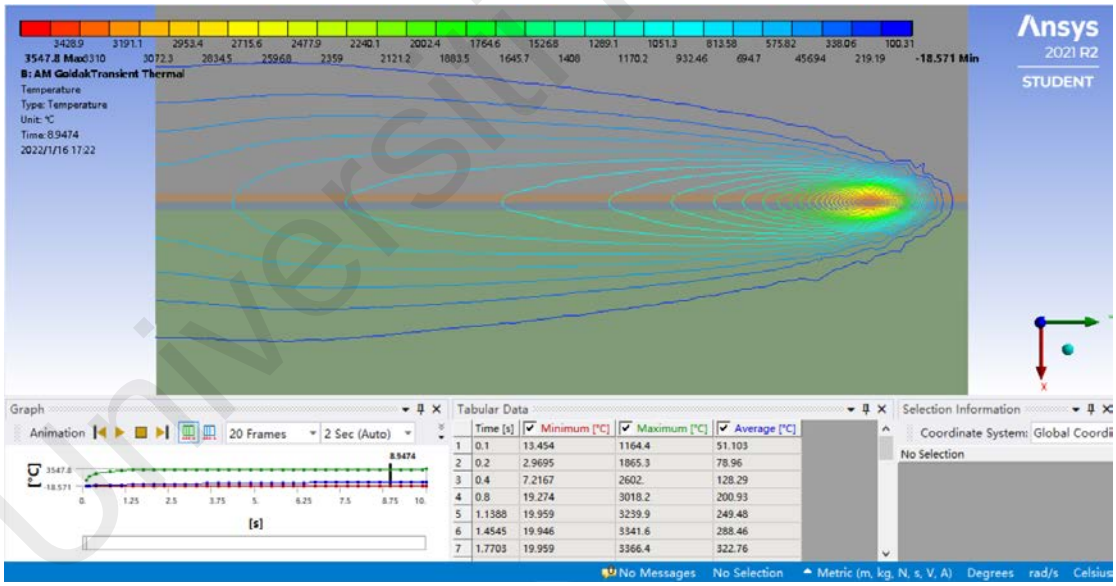

Figure 3.22: The isotherm of Goldak double ellipsoid heat source

This is a graph of the maximum temperature over time, during which time the maximum temperature was 3547.8 degrees Celsius.

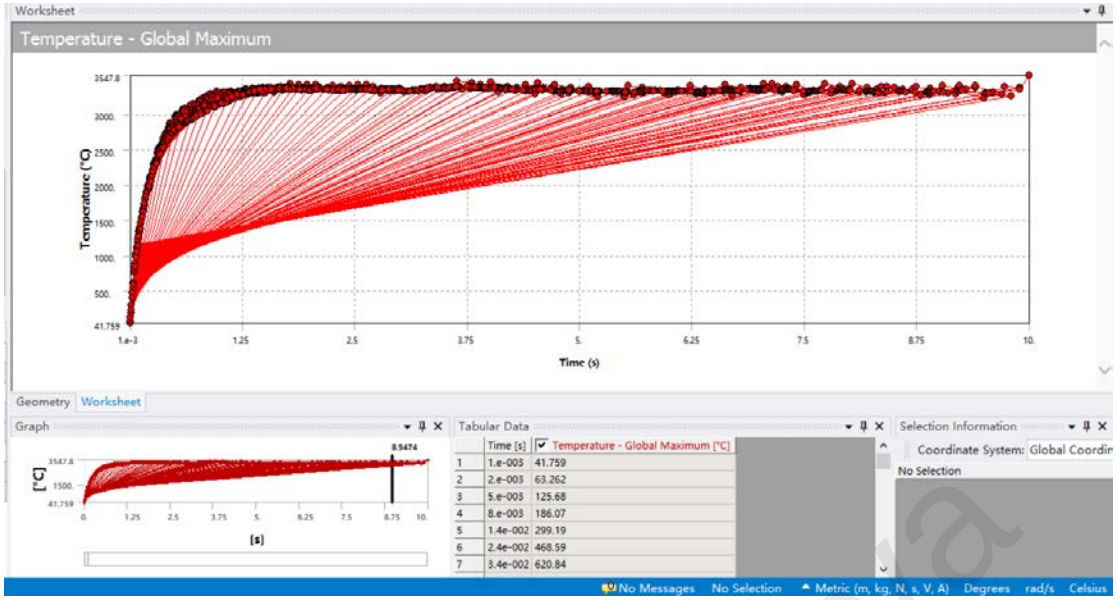

Figure 3.23: Maximum temperature over time of Goldak's model

3.4 Procedures of using ACT Extensions

3.4.1 Introduction to ACT Extensions

Briefly introduce the selection of materials, and the parameters of the simulation, and find similar data to SS316 from the paper. Use sensors, thermocouples. Stress Module. A total of 27 simulations need to be done, but there will actually be several cases with the same parameters.

Using APDL language in Workbench will greatly reduce the operation speed of this simulation. So, the ACT extension is used. The ACT extension is a simplified version of the APDL language, which is easy to use and efficient in operation. For example, under the same conditions, it took 24 hours to simulate a temperature field using APDL in this study, but only one hour using the ACT extension module. This simulation required 27 simulations, so the net simulation time for this study was approximately 27 hours.

The ACT uses a Local Coordinate System (LCS) to define the Goldak Modal heat source. The heat source will move in the positive X-direction of the LCS. X-axis is on the weld line. Y-axis, X-axis, and Z-axis are lies as the picture shows.

Values of af and ar are the size in X-direction. b is value in Y-direction, which equals to half of the width. c is the value in Z-direction, which is depth of the heat source. The starting point is point (0,0,0) of the Local Coordinate System created before. The total time process is the sum of welding time cooling time. Number of steps means that if welding time is 3s and the number of steps is 100, then the time of each sub step is 0.03s.

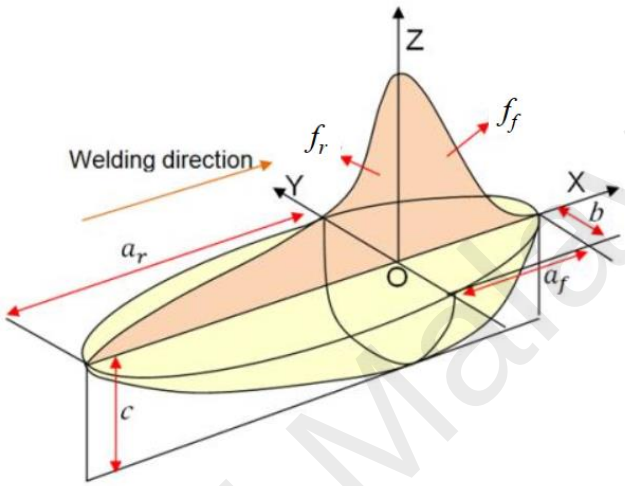

Figure 3.24: Schematic representation of the ACT of the Goldak double ellipsoid heat source

3.4.2 Procedures of using ACT

There is only one example of operation steps, because all 27 groups of operation steps differ only in parameter settings. The welding time multiplied by the welding speed is the total length of the weld bead. Cooling time is not counted into the welding process. The cooling time is the waiting time after the welding is completed and does not alternate between cooling and heating.

The simulation considers three variables, power, welding speed and substrate temperature. During the simulation, three groups of simulation experiments were set up using the control variable method. The first group is to keep the power and welding speed unchanged, and the substrate temperature is changed three times; the second group is to keep the power of the bead and the substrate temperature unchanged, and only the welding speed is changed three times; The third group is to keep the welding speed and substrate

temperature unchanged , and only change the welding power three times.

In order to simplify the calculation and reduce the simulation time, after the calculation of the previous layer is completed, the temperature of the first layer and the temperature of the substrate are set to be equalized respectively. To better simulate a uniform temperature field distribution, the simulation cooling time after each layer was set to 50 seconds. The cooling time between each layer is set to 50 seconds, because in the simulation process, it is found that after 50 seconds of cooling in all cases, the large temperature drop will disappear, and then tend to a normal temperature. Therefore, the efficiency of reducing the temperature by increasing the cooling time after 50 seconds of cooling is very low.

The simulated power is set to half of the rated power because losses will occur in the real production process, whose efficiency is 0.5 in the previous experiment (Saxena *et al*., 2017). The values of all parameters are set only once in the first layer, the parameters of the second and third layers are the same as those of the first layer, because it is convenient to observe the continuous effect on the three layers.

Welding power, speed and initial temperature were referred to Saxena et al. (2017).

For the convenience of comparison, the parameters of the second experiment for each group in the table below are the same. So, in the 27 experiments, 21 different simulations need to be done.

Table 3.1: Table of parameter setting.

Simulation Group	Parameter	Value
Group 1	Power w	200
	Speed mm/s	0.3
	Initial Temperature of base material °C	300
Group 2	Power w	300
	Speed mm/s	0.3
	Initial Temperature of base material °C	300
Group 3	Power w	400
	Speed mm/s	0.3
	Initial Temperature of base material °C	300
Group 4	Power w	300
	Speed mm/s	0.2
	Initial Temperature of base material °C	300
Group 5	Power w	300
	Speed mm/s	0.3
	Initial Temperature of base material °C	300
Group 6	Power w	300
	Speed mm/s	0.4
	Initial Temperature of base material °C	300
Group 7	Power w	300
	Speed mm/s	0.3
	Initial Temperature of base material °C	200
Group 8	Power w	300
	Speed mm/s	0.3
	Initial Temperature of base material °C	300
Group 9	Power w	300
	Speed mm/s	0.3
	Initial Temperature of base material °C	400

The following is an example of Layer 1 of Group1(200w, 0.3mm/s, 300w) to demonstrate the operation process.

Also using ANSYS workbench, but before simulating, an extension needs to be installed.

It is then set to be turned on by default.

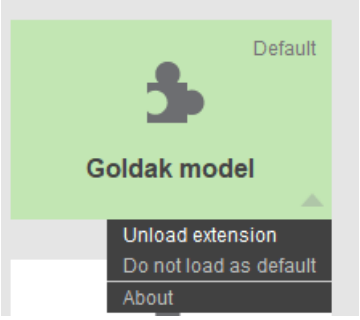

Figure 3.25: ACT

Similar to the creation process of Gaussian heat source, create a transient thermal module. Select SS 316 material in engineering data. Just in building the model, the Goldak double ellipsoid model requires three different models, a model for one-layer weld bead, a model for two-layer weld bead, and a model for three-layer weld bead.

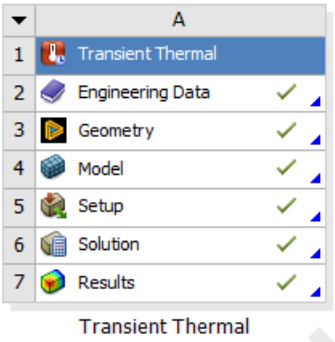

Figure 3.26: Transient thermal

The size of the substrate is 150mm*150mm*3mm. The weld bead is on the middle surface, each layer is 7mm wide, 2mm high and 150mm long. Set 7mm because it fits the width of the heat source model, and 2mm because the heat source model is 2.3mm deep, which transfers heat well to the layers below.

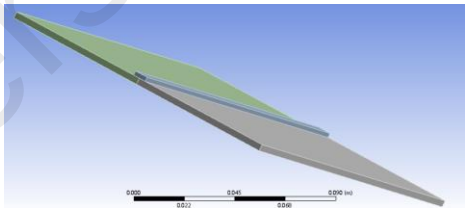

Figure 3.27: First layer

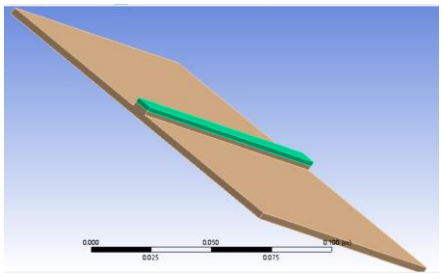

Figure 3.28: Second layer

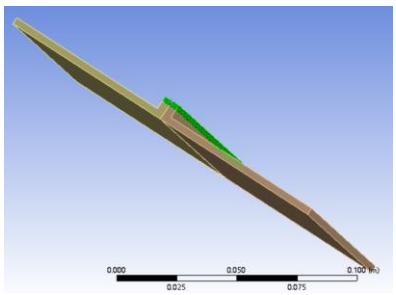

Figure 3.29: Third layer

In the process of building the model, it should be noted that the coordinate system needs to be set in a suitable position. Because the next heat source is to start from the origin and weld along the X-axis direction, the negative direction of the Z-axis is the depth direction of the heat source, and the Y-axis is the width direction of the heat source.

Next is the model settings. In this step, the most important thing is to create a new coordinate system, which is exactly the same as the original one. Since this ACT model cannot select the original coordinate system, a new coordinate system must be selected.

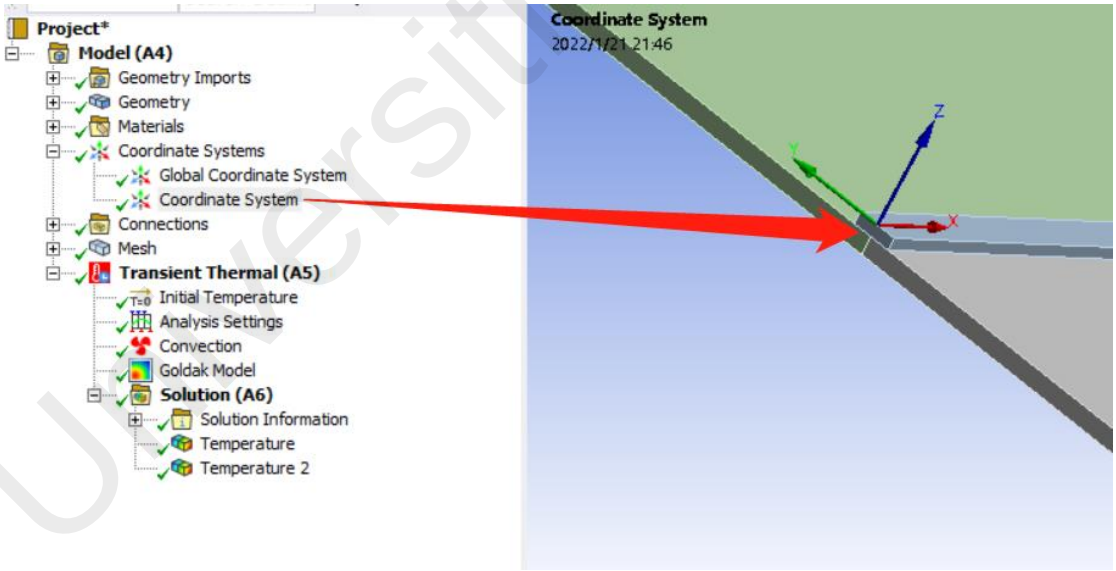

Figure 3.30: New coordinate system

The next step is meshing, and the results of this step affect the speed and quality of the computer's solution. In order to make good use of the computer's CPU, the grid near the weld bead is divided very finely, and the surrounding area of the weld bead is divided very coarsely. The reason for this is to focus the calculation on the vicinity of the weld bead, and the less important surrounding areas will not consume too much computational

resources.

Because there are three layers of weld bead, three times of mesh are required. Tetrahedrons are used as mesh types, and the grids near the weld bead are set to be smaller.

For the three models of base-1st layer bead, base-1st, 2nd layer bead, base-1st, 2nd, and 3rd bead, the corresponding number of nodes are 74758, 51152, and 61484, respectively.

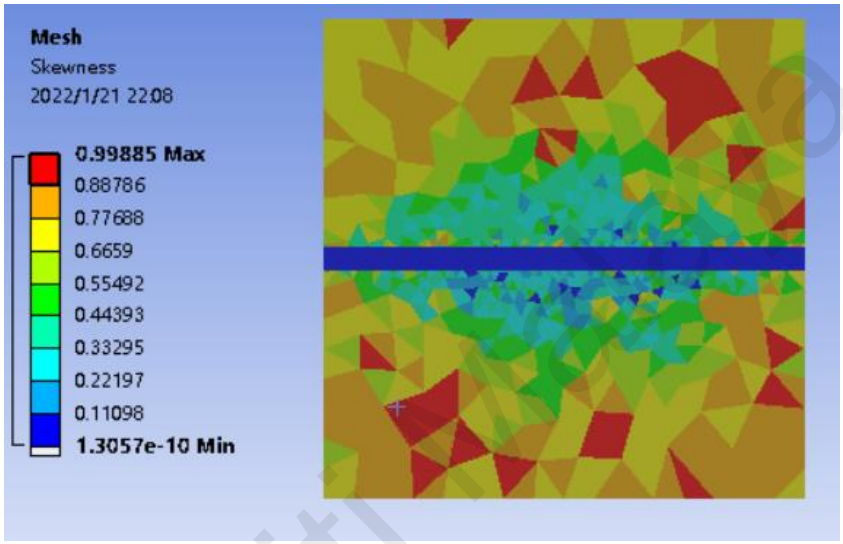

Figure 3.31: Grid quality

The next step is to set the initial temperature and ambient temperature.

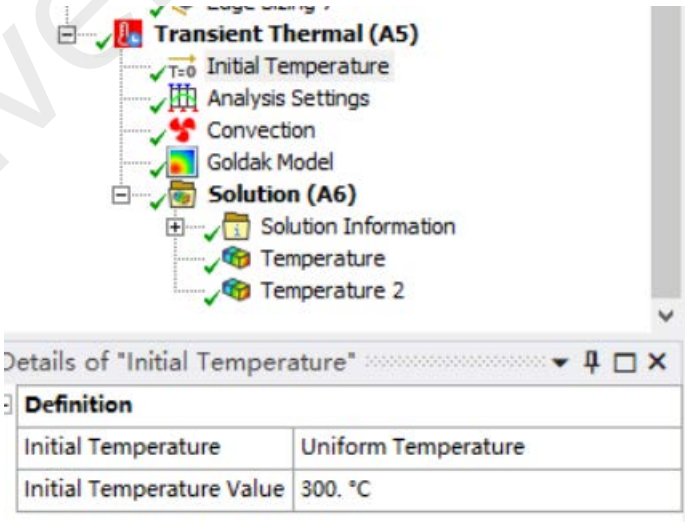

Figure 3.32: Initial temperature setting

In the convective heat transfer stage, the film coefficient is set to Stagnant Air - Horizontal Cyl. Its convective heat transfer coefficient varies with temperature as shown in the figure

below.

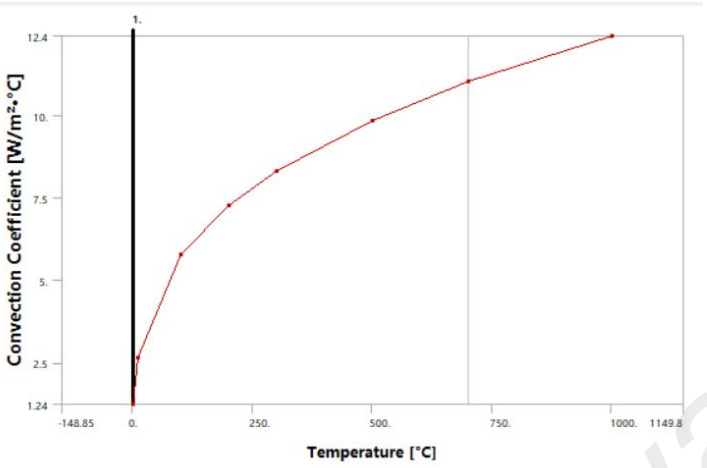

Figure 3.33: Convective heat transfer coefficient-temperature

The next step is to set the parameters of the Goldak heat source. Where the heat source is applied is the body of the weld bead. The unit of power is watts. A_Front is the size of the front half of the heat source along the X-axis direction, and A_Rear is the size of the rear half of the heat source along the X-axis direction. B is the width of the heat source and C is the depth of the heat source. F_front and F_rear are the distribution coefficients of the energy of the heat source in the front and rear halves. Usually, the sum of these two coefficients is 2(Daniela Fátima Giarollo *et al*., 2021). In the start point, select the newly created coordinate system. The unit of welding speed is meters per second. The unit of welding time is seconds. The unit of cooling time after welding is seconds. It is very important that the cooling time does not alternate with the welding time. The number of steps is an indicator to measure the degree of time refinement. The larger the number, the clearer the time refinement, and the more convenient it is to process later, but the disadvantage is that it takes more computing time for the computer.

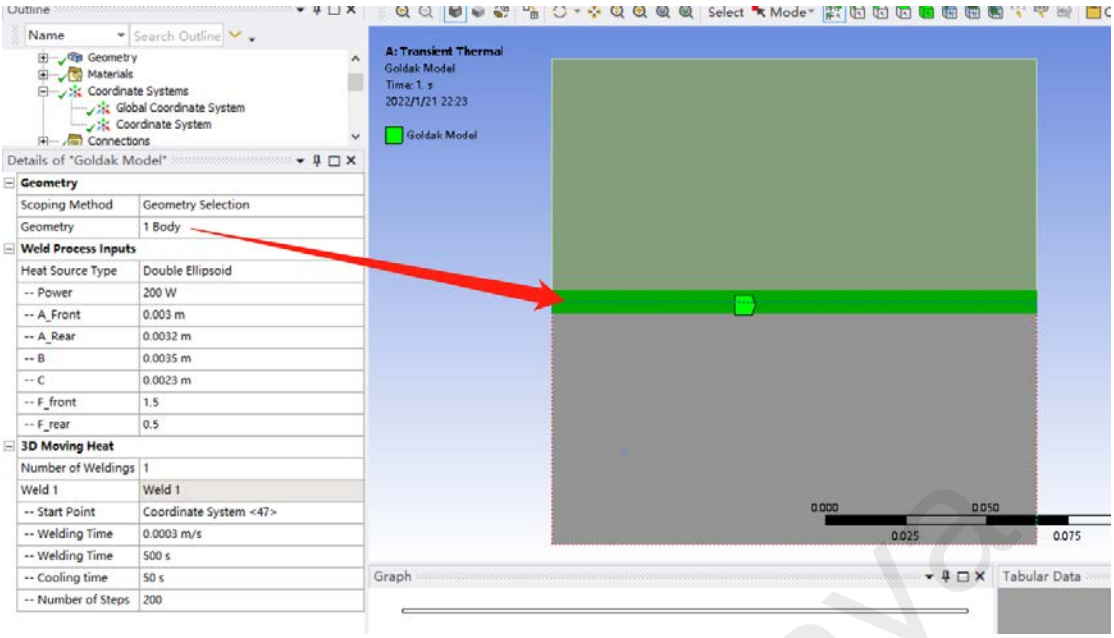

Figure 3.34: Load the heat source on the weld bead

In the solution stage, do not add the temperature field or thermal couple in the calculation, because the calculation will become very slow after adding. Usually, it takes less than a minute to display the added items, such as the overall temperature field change, after the calculation is completed and then added.

When analysing the internal stress, because the computer configuration is not enough, only the steady-state structural stress at the first second of the first layer of Group 1 to Group 9 is calculated. This simulation can only produce relative data, but not absolute data. Because the temperature field is verified, but the stress field is not. Although it has not been verified, the comparison of the results of the 9 groups can also explain the effect of the three factors on the stress.

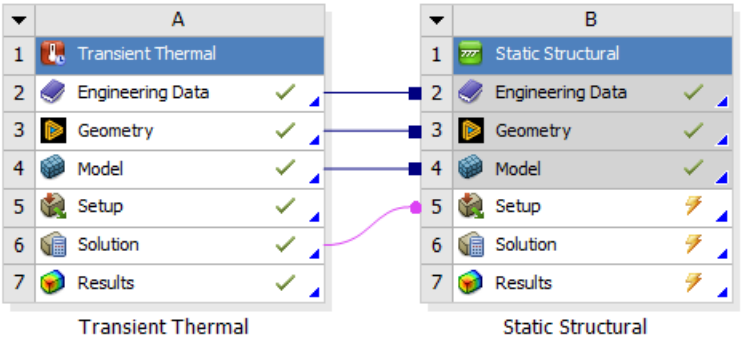

Figure 3.35: Link static structural and transient thermal

Next is to insert a fixed face. The reason for choosing this face is to reduce the influence of the internal stress on the fixed face, so the face farthest from the weld bead was selected. Because if it is two faces, the two faces will produce some serious tensile stress or compressive stress on the object.

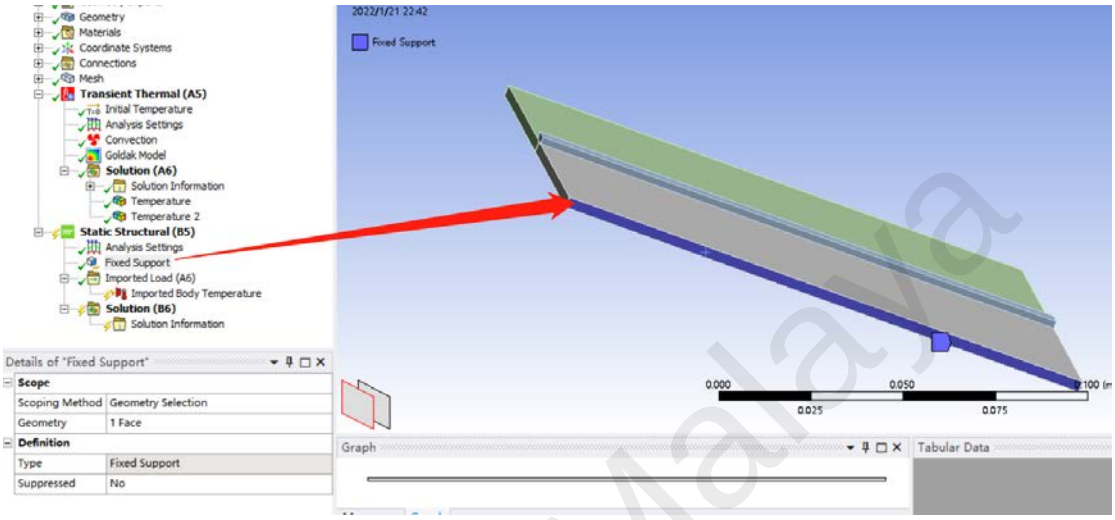

Figure 3.36: Fixed face

Then click solve. The equivalent stress is added after the calculation result. Results of equivalent stress are available within about a minute of loading.

CHAPTER 4: RESULTS AND DISCUSSIONS

4.1 Average temperature of every layer after being cooled for 50 seconds.

Table 4.1: Table of Average temperature of each layer

Simulation Group	Parameter	Variable	First layer	Second layer	Third layer
1	Power w	200	200	200	200
	Speed mm/s		0.3	0.3	0.3
	Temperature after cooling °C		589.74	853.36	1107
2	Power w	300	300	300	300
	Speed mm/s		0.3	0.3	0.3
	Temperature after cooling °C		715.34	1089	1462.5
3	Power w	400	400	400	400
	Speed mm/s		0.3	0.3	0.3
	Temperature after cooling °C		836.45	1320.2	1811.8
4	Power w		300	300	300
	Speed mm/s	0.2	0.2	0.2	0.2
	Temperature after cooling °C		788.33	1226.7	1676.4
5	Power w		300	300	300
	Speed mm/s	0.3	0.3	0.3	0.3
	Temperature after cooling °C		715.34	1089	1462.5
6	Power w		300	300	300
	Speed mm/s	0.4	0.4	0.4	0.4
	Temperature after cooling °C		593.49	928.75	1252.1
7	Power w	Initial temperature of substrate 200 °C	300	300	300
	Speed mm/s		0.3	0.3	0.3
	Temperature after cooling °C		635.25	1016	1390
8	Power w	Initial temperature of substrate 300 °C	300	300	300
	Speed mm/s		0.3	0.3	0.3
	Temperature after cooling °C		715.34	1089	1462.5
9	Power w	Initial temperature of substrate 400 °C	300	300	300
	Speed mm/s		0.3	0.3	0.3
	Temperature after cooling °C		801.1	1168.3	1542.5

In the discussion section, use the control variable method to explore the conclusions. Parameters cause the uneven distribution of the temperature field and the change in the stress field will be discussed by changing only the welding power, welding speed and initial welding temperature.

By comparing Groups 1, 2, and 3, it can be known that the higher the power, the higher the temperature after cooling; Groups 4, 5, and 6 indicate that the increase in speed will lead to a decrease in the speed after cooling; For Group 7-8-9, the variable is the initial temperature of the cuboid-shaped substrate. Groups 7, 8, and 9 show that, the higher the initial temperature of the environment and the substrate, the higher the overall temperature will be.

Groups 1, 2, and 3 show the average temperature field distribution of the workpiece under different welding powers. When the welding power increases, the heat input of the arc will also increase, and the concave degree of the molten pool will increase. As the welding power increases, the temperature on the substrate increases, the distribution of the isotherm expands, and the length and depth of the weld pool increase. After the welding power increases, the high temperature distribution area on the substrate increases significantly, so the length and depth of the weld pool also increase significantly. As the welding power increases, the arc current and voltage increase, the heat input increases, the heat transfer effect is more obvious, and the amount of molten metal increases. When the welding power is 200w and 300w, the average temperature of the workpiece after cooling is 589.74°C and 715.34°C, respectively. As the welding power of the first layer of Group 1 increases, the heat concentration is difficult to dissipate because the substrate is too small, so the temperature of the second layer still rises rapidly to 1089°C under the same welding power.

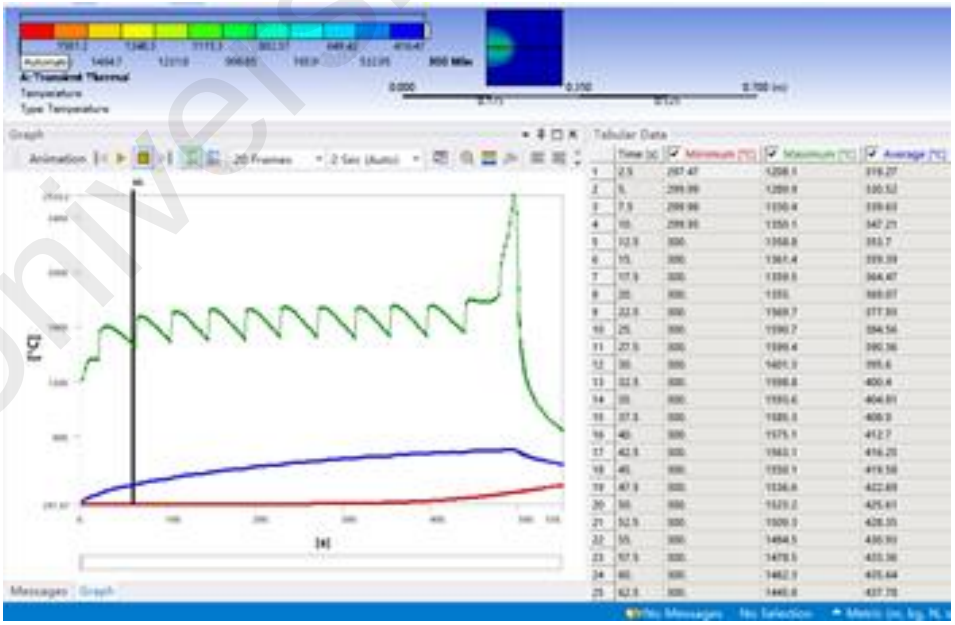

Figure 4.1: Maximum temperature and minimum temperature, average temperature change curve

It can be seen from Group 1 Layer 1 that in the later stage of the arc additive manufacturing process, the maximum temperature rises rapidly, and the maximum temperature in the centre of the formed part reaches 2559.2 °C, which is higher than the melting point of the material (1370 °C), forming a molten pool area, but The heat-affected zone of the molten pool is very small, and the temperature of most areas of the surrounding substrate is still below 1000 °C, and the formed part experiences a process of instantaneous high temperature and then rapid cooling. But with the increase of cooling time, the temperature field distribution of the formed parts is gradually uniform.

4.2 The distribution characteristics of the temperature field.

1. The central temperature of the heat source is high and the surrounding temperature is low.

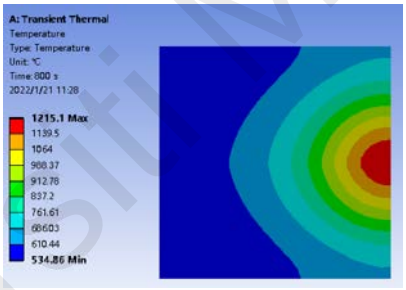

Figure 4.2: Heat source with high core temperature

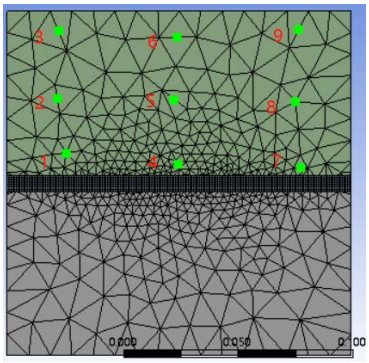

Figure 4.3: Points of thermocouples

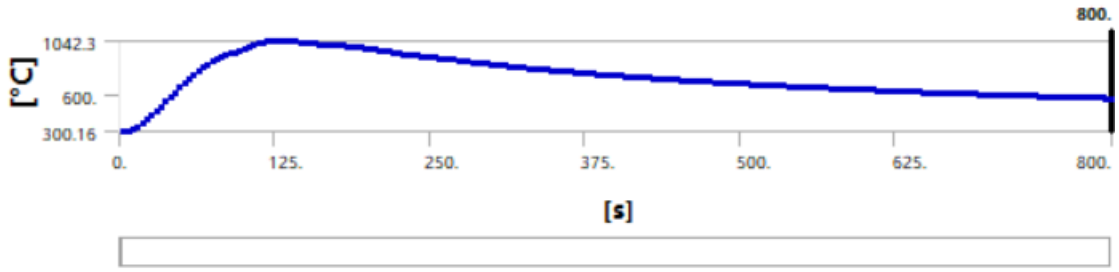

Figure 4.4: Temperature change curve at Point 1

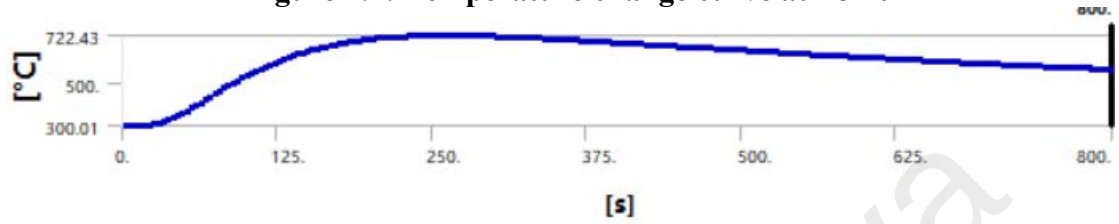

Figure 4.5: Temperature change curve at Point 2

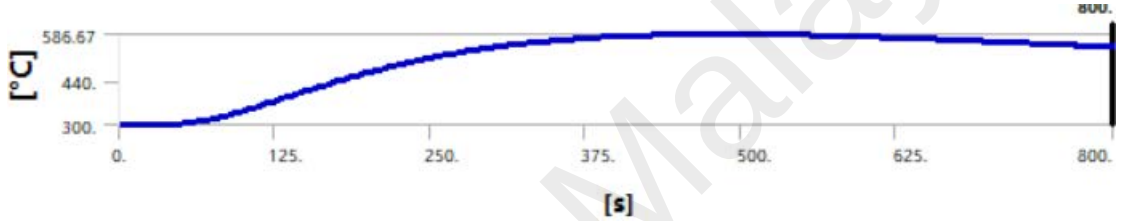

Figure 4.6: Temperature change curve at Point 3

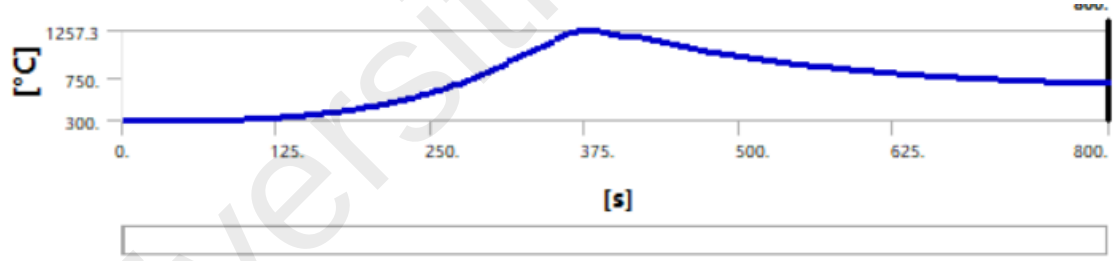

Figure 4.7: Temperature change curve at Point 4

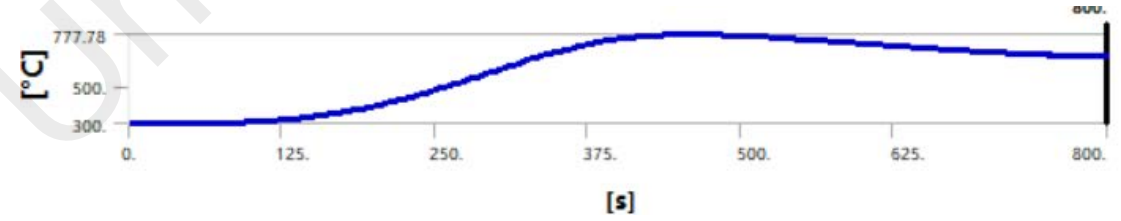

Figure 4.8: Temperature change curve at Point 5

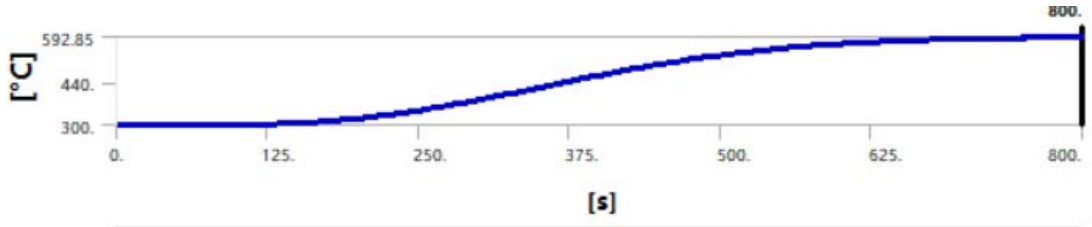

Figure 4.9: Temperature change curve at Point 6

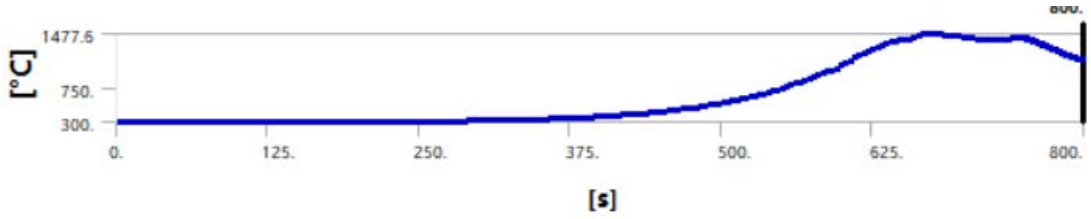

Figure 4.10: Temperature change curve at Point 7

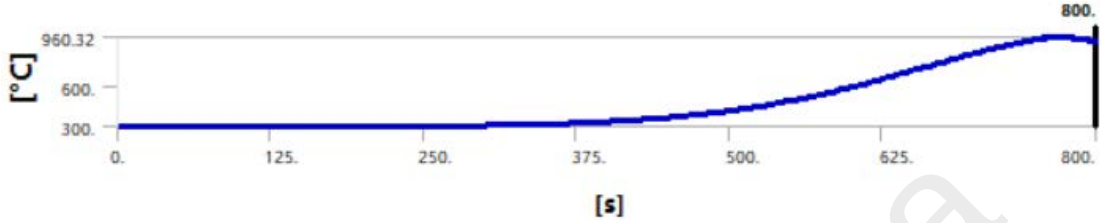

Figure 4.11: Temperature change curve at Point 8

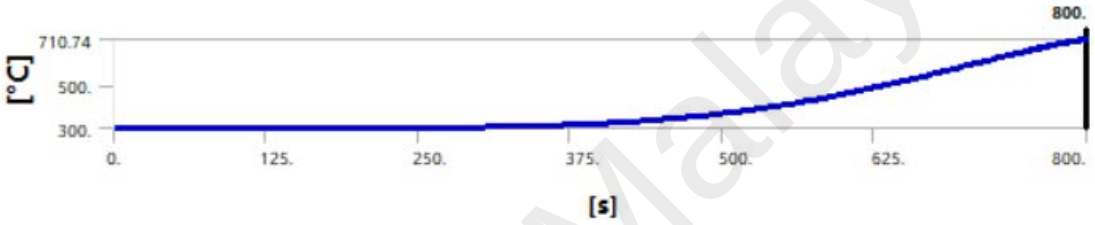

Figure 4.12: Temperature change curve at Point 9

2. The area of high temperature that the heat source passes through during the movement will gradually expand over time, and this will affect the internal stress. After the heat source passes the same black line in the figure below, the thermal field will gradually expand over time.

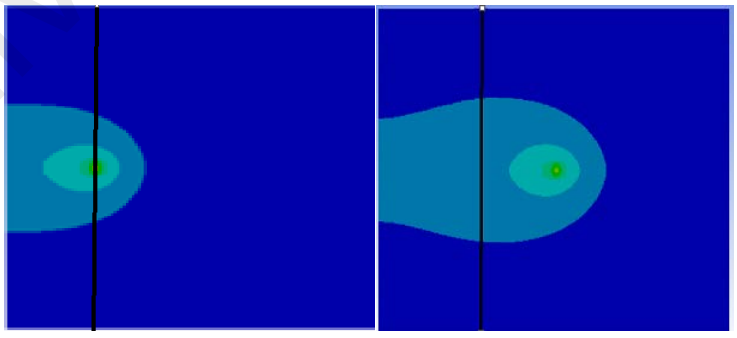

Figure 4.13: The effect of the heat source passing through the same location at different times

(a)168.42s (b) 378.95s

4.3 The maximum temperature of the thermocouples at the green geometric midpoint of the contact surface between bead and substrate, whether it reaches the melting point (1370 °C):

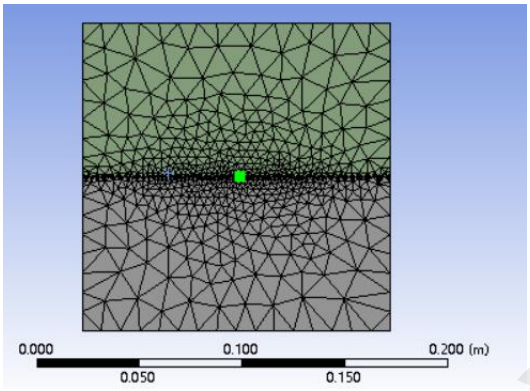

Figure 4.14: Midpoint of the contact surface

Group 1 200w 0.3mm/s 300 °C

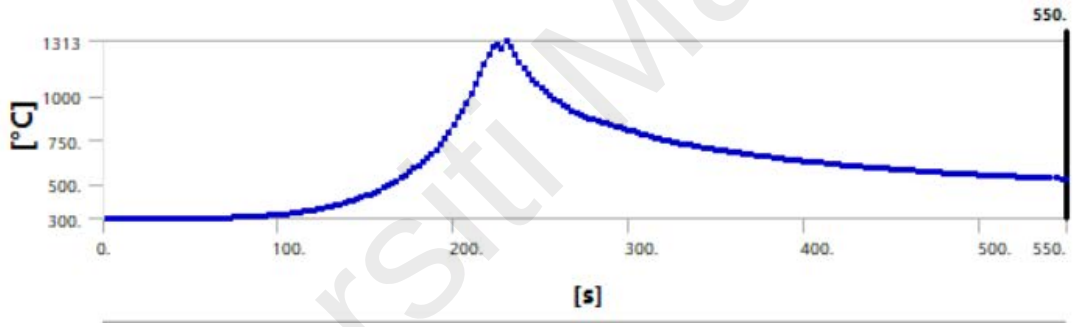

Figure 4.15: Layer 1 of group 1 1313 ° C

1313 °C is less than 1370 °C, so Group 1 is not accepted.

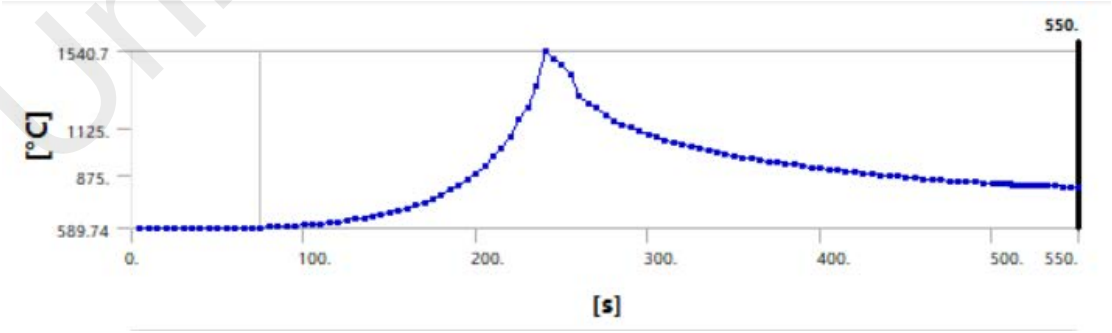

Figure 4.16: Layer 2 of group 1 1540.7 ° C

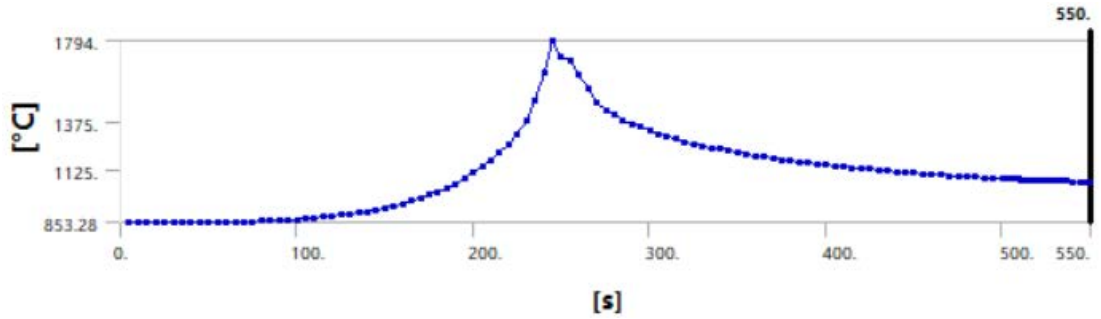

Figure 4.17: Layer 3 of group 1 1794 ° C

Group 2 300w 0.3mm/s 300 °C

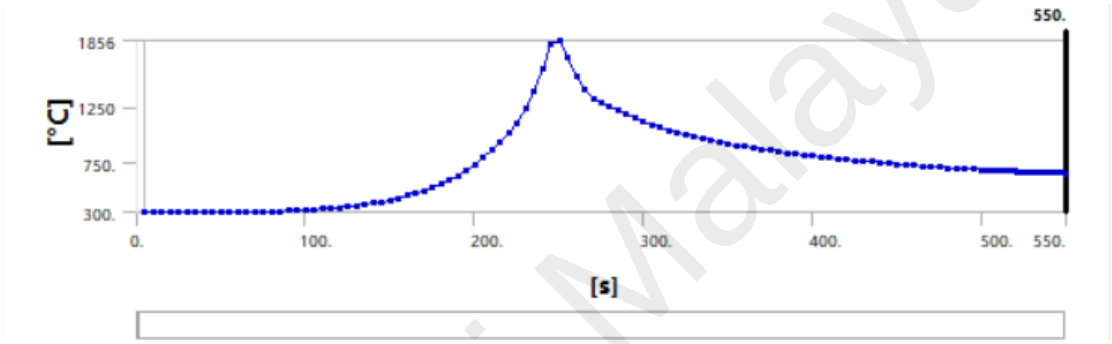

Figure 4.18: Layer 1 of group 2 1856 ° C

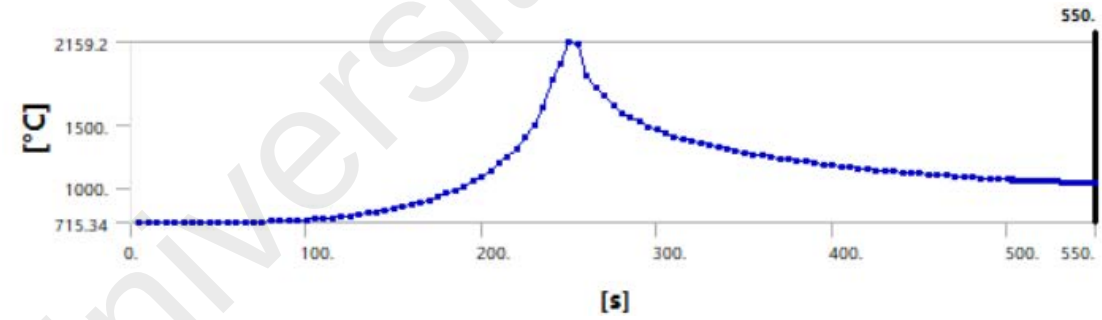

Figure 4.19: Layer 2 of group1 2159.2 ° C

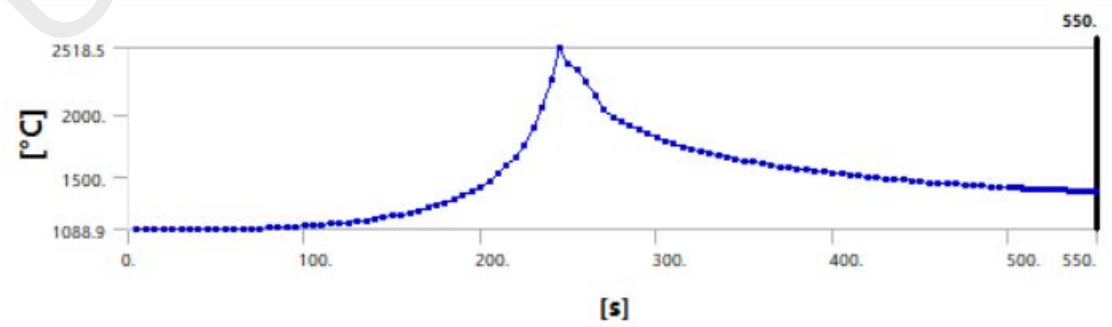

Figure 4.20: Layer 3 of group 2 2518.5 ° C

Group 3 400w 0.3mm/s 300 °C

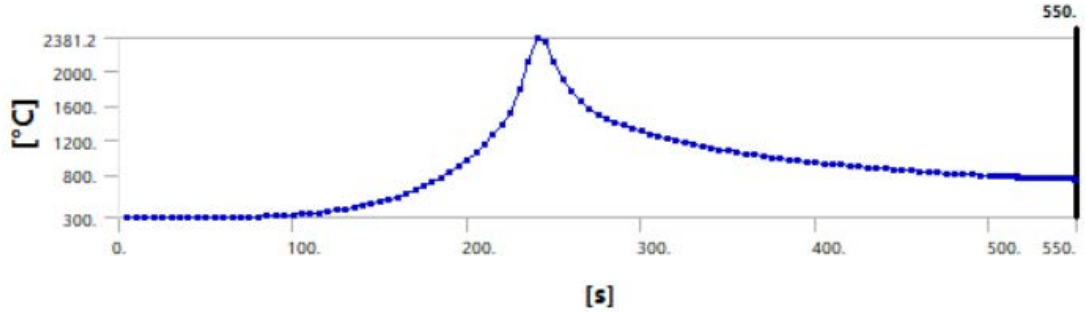

Figure 4.21: Layer 1 of group 3 2381.2 ° C

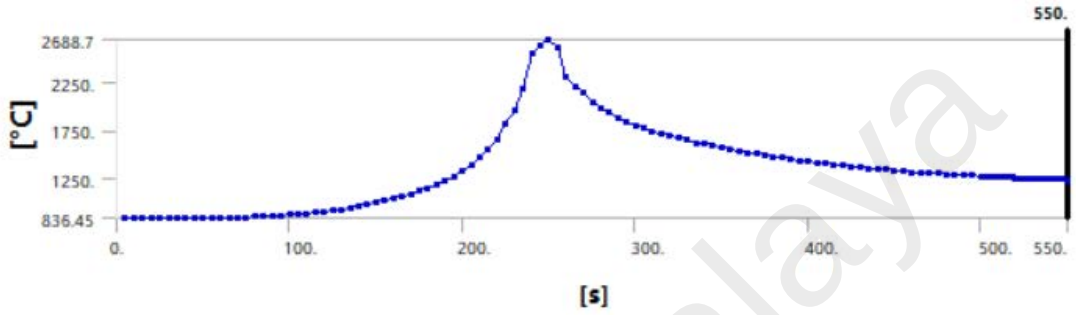

Figure 4.22: Layer 2 of group 3 2688.7 ° C

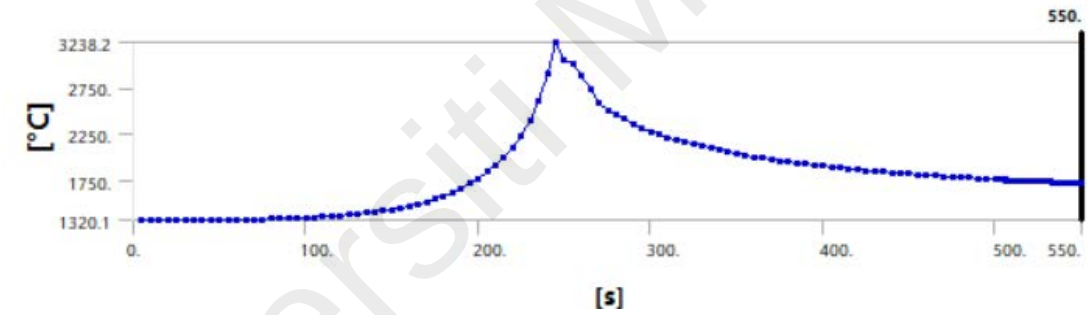

Figure 4.23: Layer 3 of group 3 3238.2 ° C

Group 4 300w 0.2mm/s 300 °C

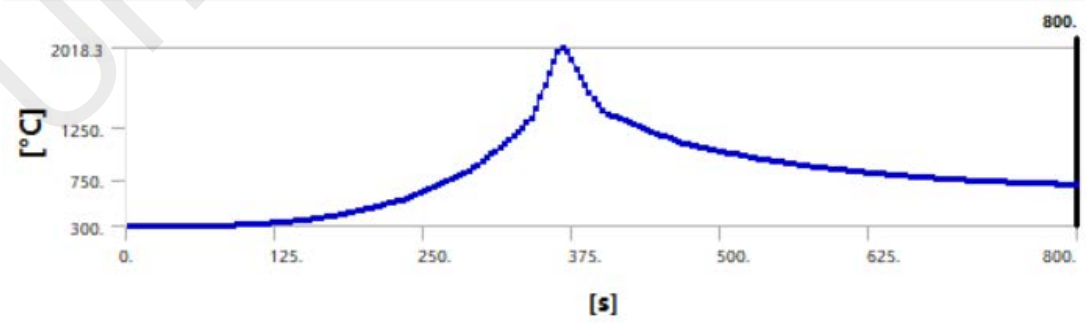

Figure 4.24: Layer 1 of group 4 2017.3 ° C

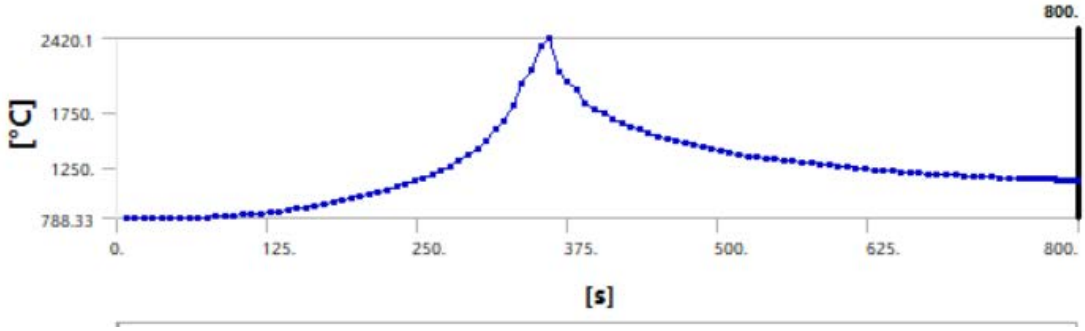

Figure 4.25: Layer 2 of group 4 2420.1 ° C

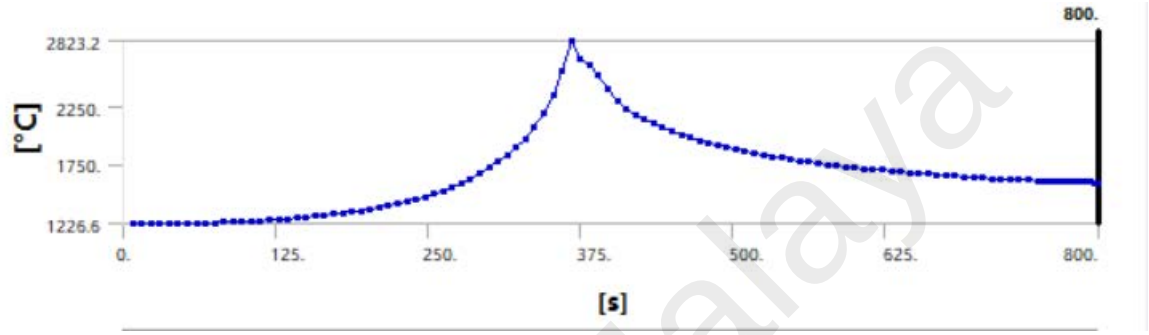

Figure 4.26: Layer 3 2823.2 ° C

Group 5 300w 0.3mm/s 300°C

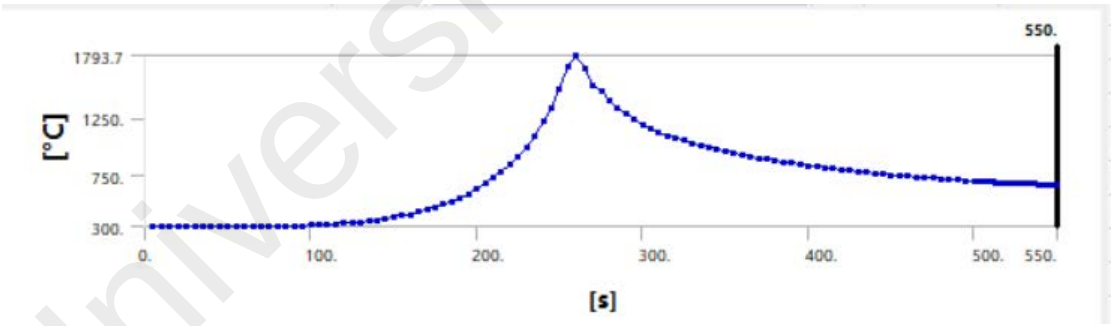

Figure 4.27: Layer 1 of group 5 1793.7 ° C

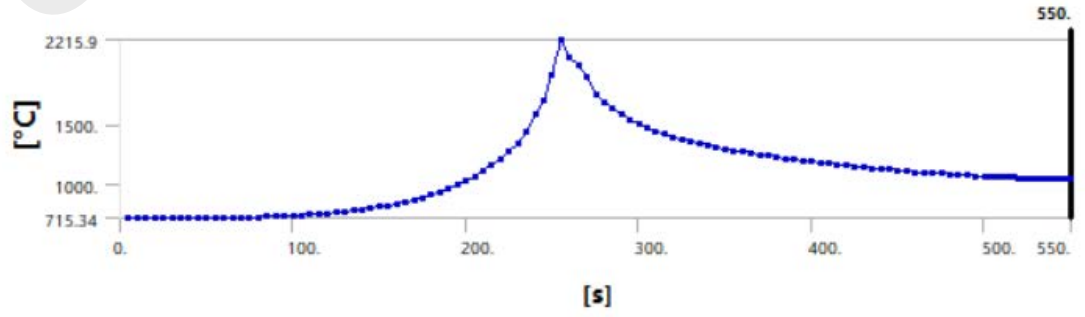

Figure 4.28: Layer 2 of group 5 2215.9 ° C

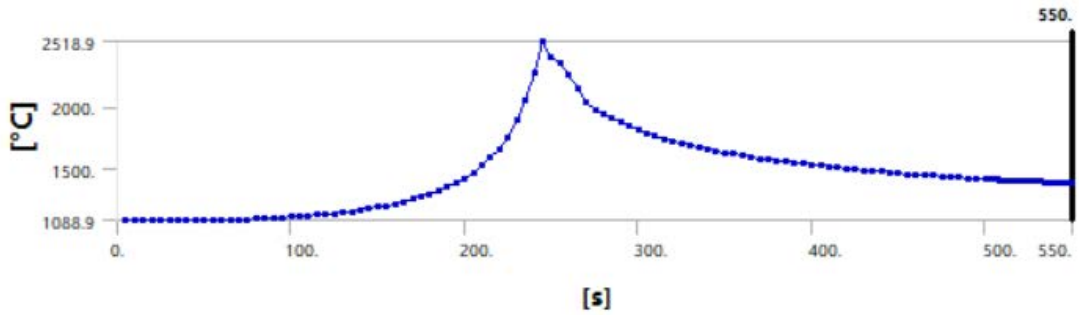

Figure 4.29: Layer 3 of group 5　2518.9 ° C

Group 6　300w 0.4mm/s 300°C

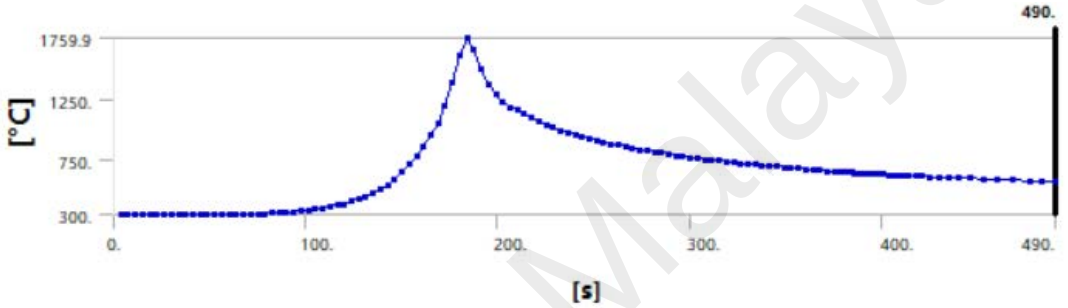

Figure 4.30: Layer 1 of group 6　1759.9 ° C

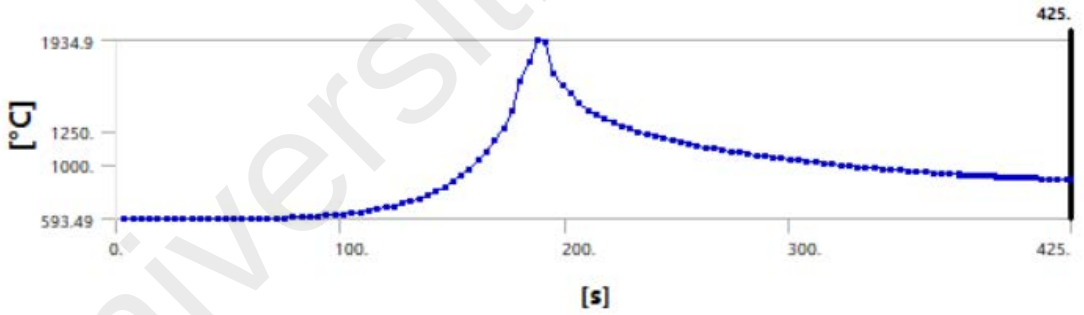

Figure 4.31: Layer 2 of group 6　1934.9 ° C

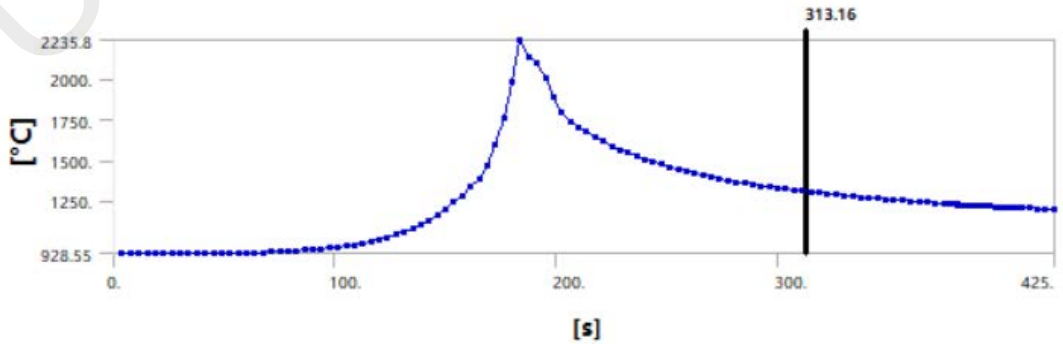

Figure 4.32: Layer 3 of group 6　2235.8 ° C

Group 7 300w 0.3mm/s 200°C

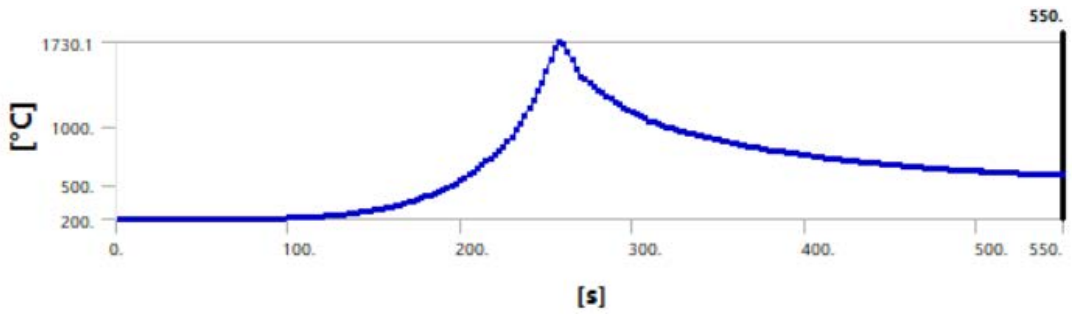

Figure 4.33: Layer 1 of group 7 1730.1 ° C

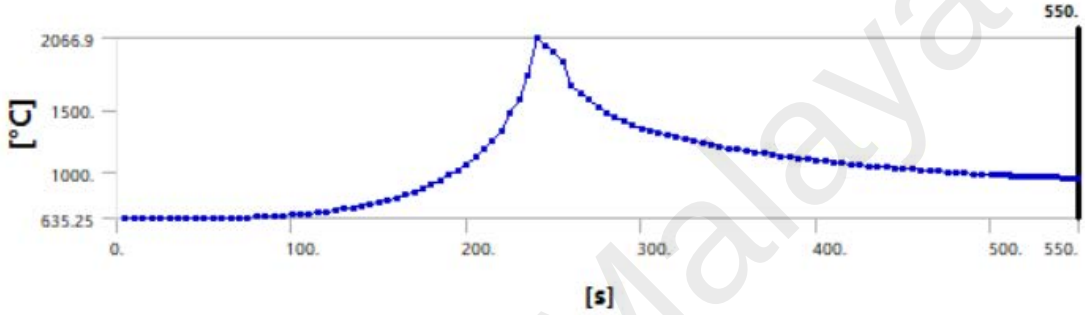

Figure 4.34: Layer 2 of group 7 2066.9 ° C

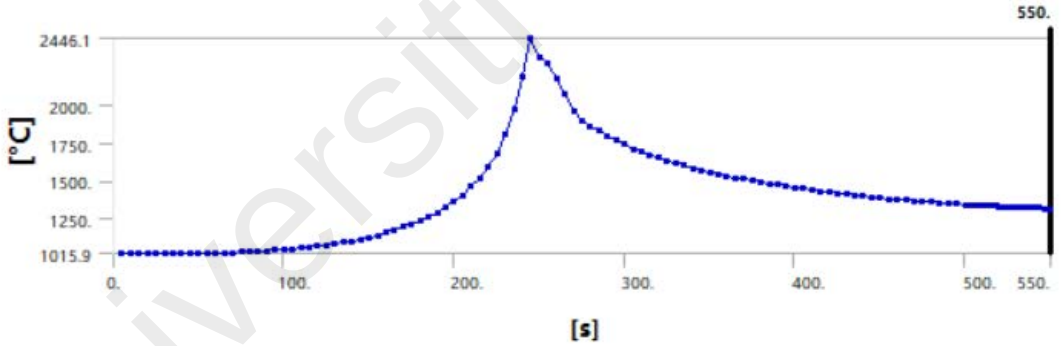

Figure 4.35: Layer 3 of group 7 2446.1 ° C

Group 8 300w 0.3mm/s 300°C

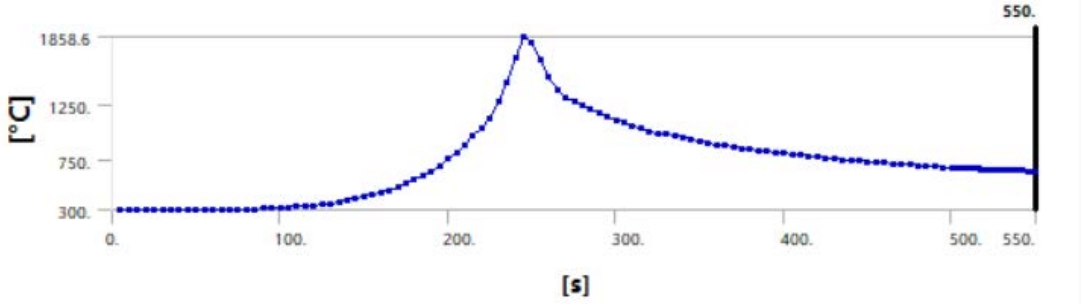

Figure 4.36: Layer 1 of group 8 1858.6 ° C

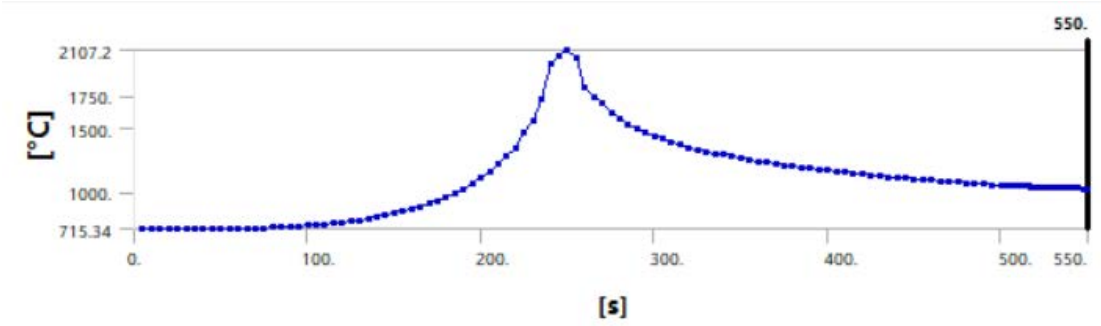

Figure 4.37: Layer 2 of group 8 2107.2 ° C

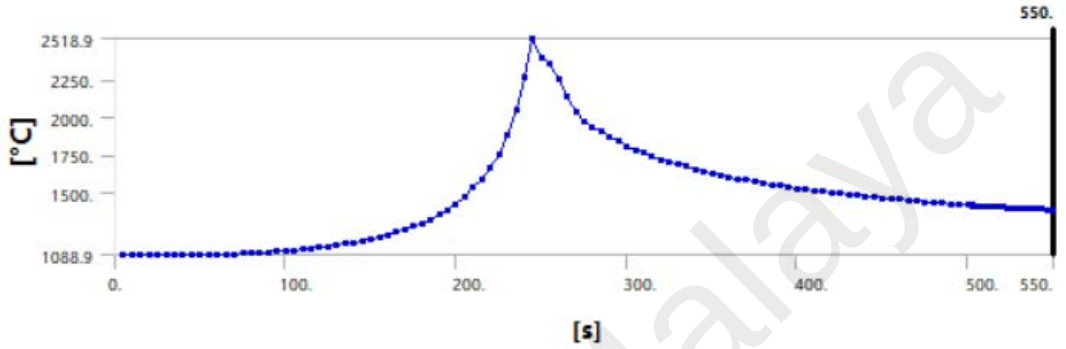

Figure 4.38: Layer 3 of group 8 2518.9 ° C

Group 9 300w 0.3mm/s 400°C

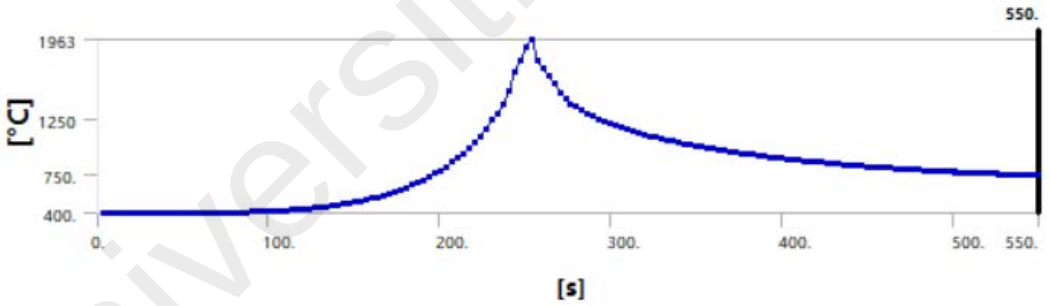

Figure 4.39: Layer 1 of group 9 1963 ° C

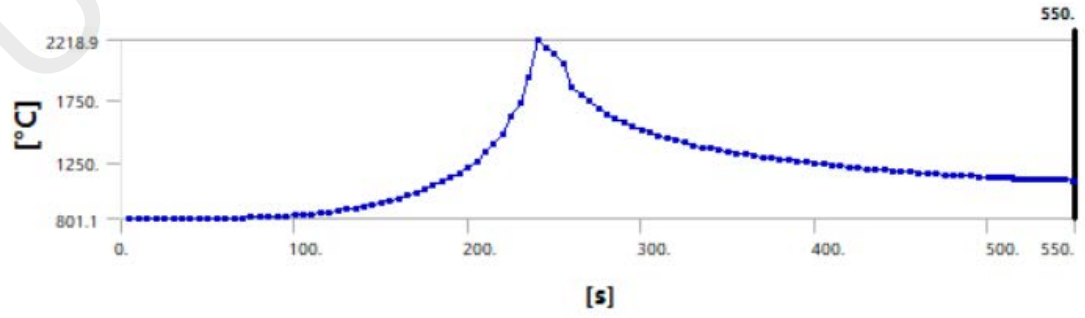

Figure 4.40: Layer 2 of group 9 2218.9 ° C

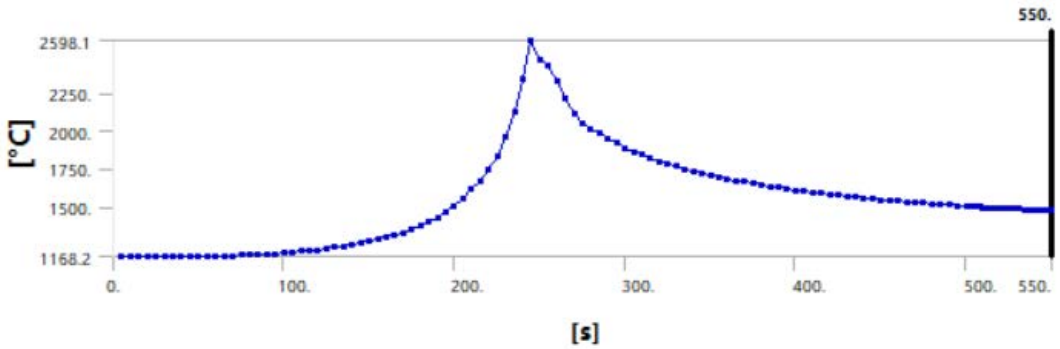

Figure 4.41: Layer 3 of group 9 2598.1 ° C

The temperature of the point at the geometric centre of the contact surface needs to be above the melting point because failure to reach the melting point indicates that the welding fails. Under the condition that the melting point of the welding contact surface is satisfied, the group that does not meet the melting point temperature of the welding is excluded, and the group with the lowest temperature obtained after cooling in each group is the optimal solution.

The midpoint position of the first layer was selected to explore the change rule of its thermal cycle. As could be showed from the figure, the midpoint of the 1st layer has experienced a total of three peaks and valleys. As the heat source leaves, the temperature at this point drops rapidly. Before the heat source returns to the midpoint of the second layer, the temperature at the midpoint of the first layer keeps dropping. As the heat source passes near the midpoint of the weld bead of the second layer, the The temperature of the midpoint of the layer rises rapidly, which is also higher than the melting point of the material, which meets the requirements for fusion between layers. After that, with the movement of the heat source, the temperature at this point continued to decrease. As the heat source came to the vicinity of the midpoint of the third layer, the temperature at the midpoint of the first layer increased again, but the temperature peak was lower than the melting point of the material. Currently, the third layer is equivalent to a high temperature tempering effect on the first layer. The accumulation process of the second layer to the third layer will affect the thermal cycle of the first

layer. The recovery of the peak temperature at the midpoint of a layer gradually decreases. The overall minimum temperature gradually increased, and the thermal cycle curve also flattened.

The distribution patterns of the temperature field under the three walking speeds are similar. The temperature gradient in the substrate area in front of the heat source is large, and the isotherm distribution is dense, and the temperature gradient in the substrate area behind the heat source is small, and the isotherm distribution is relatively loose.

During the moving of the heat source, the temperature of a certain point on the formed part first changes from low to high and then from high to low over time. This process is called the thermal cycle of welding. Different thermal cycle characteristics will affect the internal temperature of the formed part. Microstructure and properties are mainly concerned with the four parameters of heating rate, maximum temperature, residence time above the material phase transition temperature, and cooling time in the thermal cycle characteristics. The above figure explores the thermal cycle curve at the centre of the smaller exterior of the weld bead.

It can be seen from the figure that when the heat source passes by, the center of the intersection of the weld bead and the substrate instantly reaches a temperature above the melting point, which meets the requirements of metallurgical fusion, and as the heat source continues to move, the temperature at this point drops rapidly. After about 50s the temperature gradually levelled off.

It could be showed from temperature distribution of longitudinal section of the workpiece that when the walking speed increases, the temperature on the substrate decreases, and the length and depth of the molten pool decrease. The gradient is the largest and the isotherm distribution is the densest. In the first layer of Group 4, 5, 6,

when the walking speed is 0.002 m/s, 0.0003 m/s and 0.0004 m/s, the maximum temperature of the contact surface is 2017.3 °C, 1793.7 °C and Layer 1 1759.9 °, respectively C. Due to the serious heat accumulation under continuous accumulation, the temperature of the substrate under the three walking speeds increased significantly, but the temperature field distribution was similar to that of the first layer. The temperature gradient in front of the heat source was large, the isotherm was dense, and the temperature gradient behind the heat source was affected. Small, the isotherm distribution is loose. Comparing the temperature distribution of the workpiece cross-section at the three travel speeds, it can be found that the slower the travel speed, the more heat the metal in front of the accumulation path receives, and the easier it is to store more energy, which in turn leads to a widening of the molten pool and an increase in the temperature of the substrate. However, since the traveling speed is too high, the melting amount of metal will be reduced and the heat accumulation will be reduced, so the effect of welding needs to be considered when choosing to reduce the speed. Comparing the temperature distribution of the same layer at different walking speeds, with the increase of the walking speed, the temperature gradient on the substrate decreases, the isotherm distribution is sparse, and the width and depth of the molten pool decrease. This is because the welding time increases after the speed is reduced, the corresponding heat input and the amount of molten metal increase, the width and depth of the molten pool increase, and the temperature field distribution range also expands.

The temperature at the geometric centre of the contact surface increases with the number of layers. The reason is that after the weld bead of the first layer is completed, the temperature below the weld bead has already risen during the process of welding the second layer. After the accumulation of energy layer by layer, the temperature finally increases layer by layer.

The above nine groups of simulation experiments, only the welding surface of Group 1 did not meet the requirements, and the rest of the groups reached the melting point.

Because of the characteristics of thermal expansion and contraction of stainless steel, the lowest temperature 1730.1 °C of Group 7(300w, 0.3mm/s, 200°C) meeting the melting point requirements of the welding surface is selected. The temperature of the first layer of Group 5 is 1793.7°C, and the temperature of the first layer of Group 6 is 1759.9°C.

4.4 Equivalent stress

The position of the red line is the detected position. The result of the detection is a process from 0 seconds to 1 second.

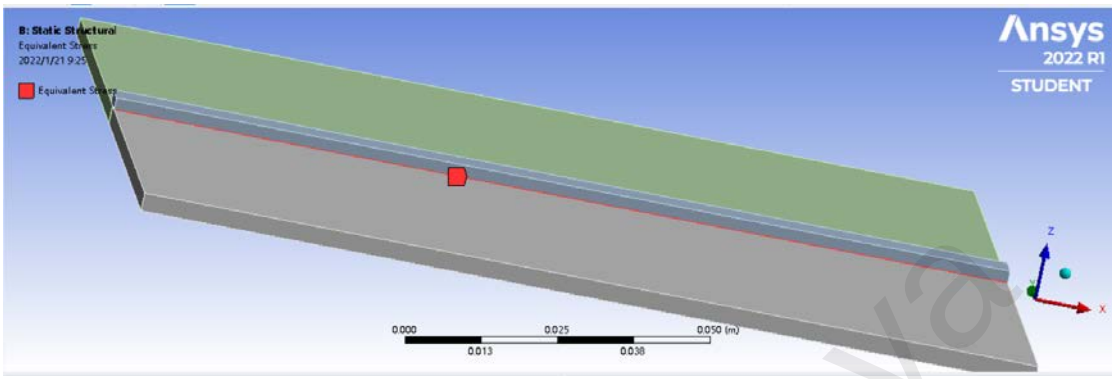

Figure 4.42: The detected position of equivalent stress

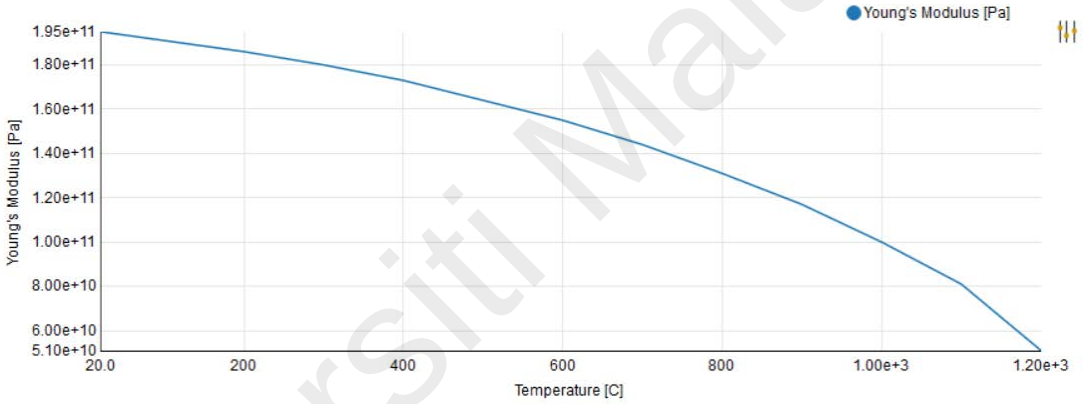

Figure 4.43: Young's modulus-Temperature of 316 Stainless Steel

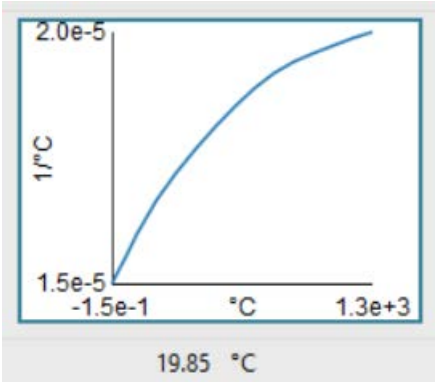

Figure 4.44: Coefficient of Thermal Expansion of 316 Stainless Steel

Zero-Thermal-Strain Reference Temperature is 19.85 °C. Because of the low configuration of the computer, only the stress value of the edge of the weld bead in contact with the substrate of first layer is measured.

Tabular Data

	Time [s]	Minimum [Pa]	Maximum [Pa]	Average [Pa]
1	1.	5.8403e+006	1.5286e+008	2.0178e+007

Figure 4.45: Group 1 1.53*10^8 Pa

Tabular Data

	Time [s]	Minimum [Pa]	Maximum [Pa]	Average [Pa]
1	0.2	2.0271e+006	1.2287e+008	9.4118e+006
2	0.4	5.203e+006	1.7663e+008	1.7354e+007
3	0.535	7.5406e+006	1.5114e+008	2.1024e+007
4	0.67	8.892e+006	1.6431e+008	2.4229e+007
5	0.71101	9.2731e+006	1.4999e+008	2.38e+007
6	0.75201	9.6355e+006	1.4892e+008	2.4897e+007
7	0.75453	9.6583e+006	1.4927e+008	2.5166e+007
8	0.75706	9.6803e+006	1.4968e+008	2.4616e+007
9	1.	9.6803e+006	1.4968e+008	2.4616e+007

Figure 4.46: Group 2 1.7663*10^8 Pa

Tabular Data

	Time [s]	Minimum [Pa]	Maximum [Pa]	Average [Pa]
1	0.1	6.4242e+005	7.3661e+007	5.2666e+006
2	0.2	1.3893e+006	1.759e+008	1.1365e+007
3	0.35	2.8279e+006	1.7678e+008	1.6434e+007
4	0.45125	3.9193e+006	1.547e+008	1.8748e+007
5	0.5525	4.8957e+006	1.5402e+008	2.0782e+007
6	0.58325	5.2038e+006	1.5236e+008	2.1048e+007
7	0.61401	5.5252e+006	1.5142e+008	2.1414e+007
8	0.63477	5.7337e+006	1.5264e+008	2.1857e+007
9	0.63666	5.7522e+006	1.524e+008	2.2344e+007
10	1.	5.7522e+006	1.524e+008	2.2344e+007

Figure 4.47: Group 3 1.7678*10^8 Pa

Tabular Data

	Time [s]	Minimum [Pa]	Maximum [Pa]	Average [Pa]
1	0.2	1.0966e+006	1.5935e+008	9.077e+006
2	0.4	2.5612e+006	1.6942e+008	1.4811e+007
3	0.7	4.9025e+006	1.5533e+008	2.0032e+007
4	0.72734	5.1114e+006	1.5371e+008	2.0458e+007
5	0.75468	5.3198e+006	1.5698e+008	2.0759e+007
6	0.79568	5.5709e+006	1.5699e+008	2.0999e+007
7	0.7982	5.5888e+006	1.5793e+008	2.104e+007
8	0.80073	5.6041e+006	1.5889e+008	2.0986e+007
9	1.	5.6041e+006	1.5889e+008	2.0986e+007

Figure 4.48: Group 4 1.69*10^8 Pa

Tabular Data

	Time [s]	Minimum [Pa]	Maximum [Pa]	Average [Pa]
1	0.2	1.1509e+006	1.2373e+008	9.5744e+006
2	0.4	2.9116e+006	1.7703e+008	1.5987e+007
3	0.535	4.2075e+006	1.5094e+008	1.8897e+007
4	0.67	5.3332e+006	1.5822e+008	2.1707e+007
5	0.71101	5.6468e+006	1.5937e+008	2.1257e+007
6	0.75201	5.9536e+006	1.6097e+008	2.227e+007
7	0.75453	5.9728e+006	1.5745e+008	2.2533e+007
8	0.75706	5.9898e+006	1.5514e+008	2.1872e+007
9	1.	5.9898e+006	1.5514e+008	2.1872e+007

Figure 4.49: Group 5 1.77*10^8 Pa

Tabular Data

	Time [s]	Minimum [Pa]	Maximum [Pa]	Average [Pa]
1	0.2	1.0853e+006	1.2618e+008	9.625e+006
2	0.4	2.5632e+006	1.8371e+008	1.5828e+007
3	0.535	3.8199e+006	1.5789e+008	1.8416e+007
4	0.67	4.8746e+006	1.6692e+008	2.1082e+007
5	0.76112	5.5263e+006	1.8481e+008	2.2001e+007
6	0.85225	6.0783e+006	1.8966e+008	2.24e+007
7	0.85898	6.1184e+006	1.9001e+008	2.2834e+007
8	0.86201	6.1338e+006	1.9557e+008	2.2839e+007
9	1.	6.1338e+006	1.9557e+008	2.2839e+007

Figure 4.50: Group 6 1.96*10^8 Pa

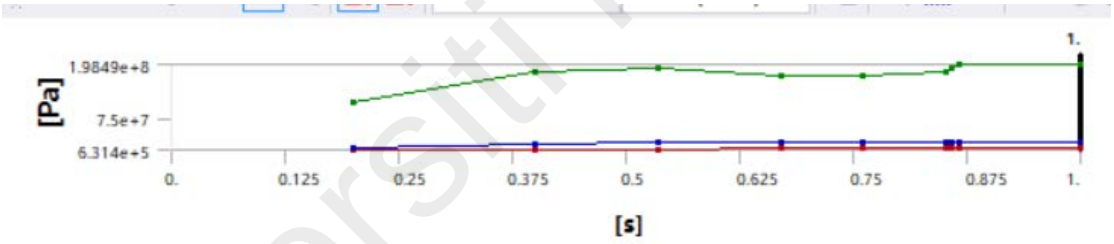

Figure 4.51: Group 7 1.98*10^8 Pa

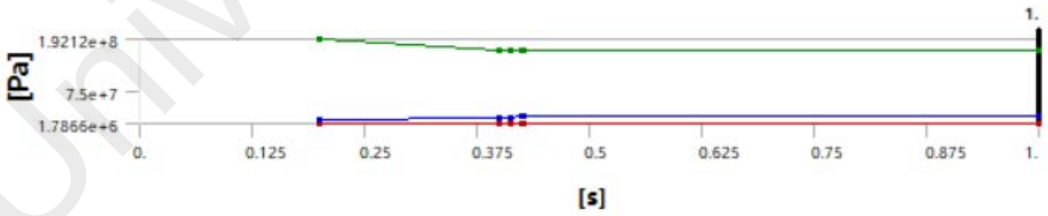

Figure 4.52: Group 8 1.92*10^8 Pa

Tabular Data

	Time [s]	Minimum [Pa]	Maximum [Pa]	Average [Pa]
1	0.2	2.0271e+006	1.2287e+008	9.4118e+006
2	0.4	5.203e+006	1.7663e+008	1.7354e+007
3	0.535	7.5406e+006	1.5114e+008	2.1024e+007
4	0.67	8.892e+006	1.6431e+008	2.4229e+007
5	0.71101	9.2731e+006	1.4999e+008	2.38e+007
6	0.75201	9.6355e+006	1.4892e+008	2.4897e+007
7	0.75453	9.6583e+006	1.4927e+008	2.5166e+007
8	0.75706	9.6803e+006	1.4968e+008	2.4616e+007
9	1.	9.6803e+006	1.4968e+008	2.4616e+007

Figure 4.53: Group 9 1.77*10^8 Pa

During the analysis of the temperature field, Group 1 was eliminated because it did not meet the melting point requirement, leaving Group 5, 6, and 7.

During the analysis of the stress field, although Group 1 has the smallest stress, it does not meet the melting point requirement. Group 4 has the least stress 1.69*10^8 Pa and has a temperature of 2017.3 °C after cooling.

Analysis in Group 4, 5, 6 shows that as the welding speed increases, the stress also increases. Groups 1, 2, and 3 show that as power increases, so does the stress. From Group 7 to Group 9, the stress becomes smaller as the temperature of the initial material increases.

Because the result of optimization can only be one, the result is chosen between group 4 and group 6. The percent change in stress and temperature between the two groups can be compared. Temperature change rate: (1676.4-1251.1)/1251.1=34.0%; Stress change rate: (1.96-1.69)/1.69=16.0%. The temperature difference between group 4 and group 6 is relatively large, while the stress difference smaller. Therefore, the temperature should be used as the selection criterion, that is, the 6 groups with lower temperature should be selected (300 w, 0.4 mm/s, 300 °C).

Among the 21 different parameter setting methods, the stress is concentrated in the welded bead fusion area, which is often the location where microcracks are likely to

occur. Therefore, the junction between the weld bead and the substrate is the fragile area of the entire specimen.

During the WAAM process, the specimen experienced a process of instantaneous high temperature and rapid cooling, and the temperature field distribution was extremely uneven. As the number of stacked layers increases, the remelting effect of the latter layer on the former layer will cover the weld bead layer outside the adjacent layer. Since the material is in a flowing state in the high temperature region, the morphology and size of the weld bead at this time It is difficult to control and will seriously affect the forming quality. Therefore, in the multi-layer stacking process, the interlayer cooling time should be appropriately increased to avoid interlayer remelting other than adjacent layers.

The conclusion is that the smaller the power, the smaller the whole temperature and maximum temperature after cooling, and the resulting stress will also decrease; the higher the speed, the lower the overall temperature and the maximum temperature, but the greater the lower the initial temperature, the lower the overall temperature and the maximum temperature, and the lower the stress will be. Moreover, within the parameters of the same setting, as the layer increase to more, both the average temperature and the maximum temperature increase.

The evolution process of residual stress in WAAM formed parts is studied, and the simulation results show that in the process of WAAM, the residual stress generated in the surfacing area of the test piece mainly comes from the tensile stress generated by the welding bead metal due to cooling shrinkage during the cooling process, because the stress values are all positive. During the cooling process, the equivalent stress value It rises again quickly, and finally a stable residual stress is formed.

CHAPTER 5: CONCLUSION

5.1 Summary of Results

This research project finished two goals,

1. To determine the temperature distribution in the WAAM process.

2. To propose the suitable parameters in the WAAM process based on

temperature distribution.

For the first target, a total of 27 simulation processes for the three layers of Group 1 to Group 9 simulate the temperature distribution of the entire weld bead and substrate over time.

For the second target, the optimal choice Group 7(300w, 0.3mm/s, 200°C) has been selected based on the temperature field. Furthermore, the most reasonable parameter setting based on the stress field is Group 4(300w, 0.2 mm/s, 300 °C).5.2 Future recommendation

This research project uses the controlled variable method to draw the conclusion that as the power of the welding arc increases, the maximum temperature of the interface between the weld bead and the substrate and the overall average temperature increase gradually, and the internal stress increases gradually; As the welding speed decreases, the maximum temperature and average temperature of the contact surface will decrease, while the internal stress will increase; with the decrease of the initial temperature, the maximum temperature of the welding contact surface and the overall average temperature will decrease, but the internal stress will gradually increase reduce.

5.2 Limitation of Research

In the process of arriving at the results of this study, a number of limitations occurred.

First, the computer used in this study was configured with only 2.5Ghz, which caused stuttering when running this software. Computer problems can lead to extended simulation time. For example, when I ran a simulation process, it took a full 23 hours. However, this problem has been solved by using the school's laboratory.

In addition, at the welding power, it is felt that the scanning speed and the initial temperature of the substrate are difficult to control in a real situation. Especially the effective welding power, because the welding process of arc welding is very unstable, the effective power will not be as stable as the simulated process, and it will lead to simulation errors.

In addition, due to the pandemic, the laboratories that can simulate the temperature field of the WAAM are closed, so corresponding real results cannot be obtained that are consistent with the set parameters of the simulated results. However, as an alternative verification scheme, this study followed a similar case and obtained similar temperature field results. Therefore, this study cannot carry out further analysis on the real results of the temperature field and stress field.

5.3 Future Recommendations

Because of the limited time, this study proposes an approximate method to simulate the Goldak double ellipsoid heat source.

A method of using multiple Gaussian monolayers to replace the Goldak double ellipsoid heat source. Because of the problem of computer configuration, it takes a lot of time to simulate the Goldak method with 4 cores and 8 threads, and the most time is close to a day. In this case, if the result is not ideal, you need to reset the code, re-run and wait another day. After some thought, this study proposes an approximate simulation, the Multiple-Gaussian method. The heat source of the weld bead is replaced by the three-dimensional body of the Goldak heat source with multiple horizontal planes. Different

planes are given different power coefficients and different heat source areas, but the total power remains unchanged.

Advantages:

1. When using the same size, the same speed, and the same power, after modifying the parameters, the verification results are similar to the results of the Goldak double ellipsoid heat source, but the operation time is greatly reduced. Because the calculation of body heat sources is much more complicated than surface heat sources.

2. The adjustment of parameters is more diverse. In addition to the fixed elliptical shape in the horizontal section, others such as the heat source area, power of each layer, and the volume shape of the entire heat source can be modified, and can even be made into a vertical gourd-shaped model.

An iterative optimization method is also proposed, because speed and temperature are negatively correlated, power and temperature are positively correlated, and initial temperature and temperature are positively correlated, so a method of exploring paths is proposed. For example, set a set of values, Speed1, Power1, Temperature1, and decrease or increase the three in turn according to the simulation results. Loop a certain number of times, if the three parameters converge to a set of values after multiple calculations, that is the optimal solution of the value.

REFERENCE LISTS

A N Jinoop, C P Paul, J Ganesh Kumar, V Anilkumar, R Singh, S Rao, K S Bindra. Influence of Heat Treatment on the Microstructure Evolution and Elevated Temperature Mechanical Properties of Hastelloy-X Processed by Laser Directed Energy Deposition, Journal of Alloys and Compounds, 2021

A R Kohandehghan. Effects of different heat flux schemes in modelling of transport phenomena during gas tungsten arc welding of AA1050, Proceedings of the Institution of Mechanical Engineers Part B Journal of Engineering Manufacture, 01/01/2010

Chen Yuhua,Tian Fuyang,Yan Yinfa,Song Zhanhua,Li Fade,Zhang Zhongliang. Design and Modal Analysis of Film Cutting and Baling Machine[J].Agricultural Mechanization Research,2019,41(04):101-106.DOI: 10.13427/j.cnki.njyi.2019.04.019.

Chunming Xu, Qiang Yin, Bowen Luo, Chao Xu. Modal analysis of flying shear crankshaft system architecture, International Journal of Wireless and Mobile Computing, 2019

Dang Xiaoling, Wang Jing.Research status and prospect of additive manufacturing technology at home and abroad[J].Aviation Precision Manufacturing Technology,2020,56(02):35-38.

Daniela Fátima Giarollo, Cíntia Cristiane Petry Mazzaferro, José Antônio Esmério Mazzaferro. Comparison between two heat source models for wire-arc additive manufacturing using GMAW process, Journal of the Brazilian Society of MechanicalSciences and Engineering, 2021

DEREKAR K. A review of wire arc additive manufacturing and advances in wire arc additive manufacturing of aluminium [J]. Materials Science and Technology, 2018，34（9）：1743-2847.

Ding, D., Pan, Z., Cuiuri, D., & Li, H. (2015). Wire-feed additive manufacturing of metal components: technologies, developments and future interests. The International Journal of Advanced Manufacturing Technology, 81(1), 465-481.

Dong-Gyu Ahn. "Directed Energy Deposition (DED) Process: State of the Art", International Journal of Precision Engineering and Manufacturing-Green Technology, 2021

Ermakova, A., Mehmanparast, A., & Ganguly, S. (2019). A review of present status and challenges of using additive manufacturing technology for offshore wind applications. Procedia Structural Integrity, 17, 29-36.

G. Posch, V. Holtsinger, S.L. Bychkovskii. Welding of railway wagons: tasks in the area of materials, processes and automation, Welding International, 2014

Gu, Y., Li, Y. D., Yong, Y., Xu, F. L., & Su, L. F. (2019). Determination of parameters of double-ellipsoidal heat source model based on optimization method. Welding in the World, 63(2), 365-376.

Hao Lv, Xudong Li, Zhijie Li, Wenxiao Wang, Kun Yang, Fei Li, Hualong Xie. Investigation on the columnar-to-equiaxed transition

J.T. Hofman, D.F. de Lange, B. Pathiraj, J. Meijer. FEM modeling and experimental verification for dilution control in laser cladding, Journal of Materials Processing Technology, 2011

Jiajing Pan, Lijun Yang, Shengsun Hu, Shuo Chai. Numerical analysis of thermal cycle characteristics and prediction of microstructure in multi-pass UWW, The International Journal of Advanced Manufacturing Technology, 2015

Junzhou Huo, Dong Zhu, Weizheng Wang, Wei Sun, Liping Wang, Jianghui Dong. Theoretical crack growth prediction model for thick plate butt welding joints based on stress/strain transitions, The International Journal of Advanced Manufacturing Technology, 2017

Kang-Hyun. Lee, Gun Jin Yun. A novel heat source model for analysis of melt Pool evolution in selective laser melting process, Additive Manufacturing, 2020

Li Chao, Zhu Sheng, Shen Canduo, et al. Research status and development trend of arc additive manufacturing technology [J]. China Surface Engineering, 2009, 22(3): 7-12.

Li Yana, Liu Jiahao. Simplified model of shape parameters of double ellipsoid heat source based on welding quality [J]. Welding, 2021(08):7-11+62.

Liuping Qiao.(2013). Integrated deposition and machining of aluminium alloy using WAAM.

Liang Tian, Shouhang Xing, Guojun Liu, Yu Luo. Numerical Simulation of Hardfacing Remanufacturing for Large-Scale Damaged Grinding Roller, Research Square, 2021

Michaleris, P., & DeBiccari, A. (1997). Prediction of welding distortion. Welding Journal-Including Welding Research Supplement, 76(4), 172s.

Rachel Gordon.(2016). Opportunities in 3 d printing of metals 2016 2026. https://www.slideshare.net/RMEvents/opportunities-in-3-d-printing-of-metals-2016-2026

Rodrigues, T. A., Duarte, V., Miranda, R. M., Santos, T. G., & Oliveira, J. P. (2019). Current status and perspectives on wire and arc additive manufacturing (WAAM). Materials, 12(7), 1121.

Sagar Singh, Satish kumar Sharma, Dinesh W. Rathod. A review on process planning strategies and challenges of WAAM, Materials Today: Proceedings, 2021

Saxena, R., Karnewar, A. K., & Puntambekar, V. P. T. (2017). FEM simulation of weld pool of SS316–SS316 butt joint and its comparison with experimental results. Indian Conference on Applied Mechanics (INCAM) 2017

T.R. Walker, C.J. Bennett. An automated inverse method to calibrate thermal finite element models for numerical welding applications, Journal of Manufacturing Processes, 2019

Tan, C., Zhou, K., Tong, X., Huang, Y., Li, J., Ma, W., ... & Kuang, T. (2017, July). Microstructure and mechanical properties of 18Ni-300 maraging steel fabricated by selective laser melting. In 2016 6th International Conference on Advanced Design and Manufacturing Engineering (ICADME 2016) (pp. 404-410). Atlantis Press.

Xiong Jun, Xue Yonggang, Chen Hui, et al. Research status and prospect of forming control technology for arc additive manufacturing [J]. Electric Welding Machine, 2015(09):51-56.

Xia Ranfei. (2016). Research on the optimization of forming dimensions and process parameters of arc additive manufacturing (Master's thesis, Huazhong University of Science and Technology). https://kns.cnki.net/KCMS/detail/detail.aspx?dbname=CMFD201801&filename=1016744423.nh

Xing Tianhang.(2018). NUMERICAL SIMULATION ON THE TEMPERATURE AND STRESS FIELDS OF WIRE ARC ADDITIVE MANUFACTURE FOR DUPLEX STAINLESS STEEL AND PROCESS OPTIMIZATION (Master's thesis, Yanshan University).http://www.syhmjs.com/degree/55bf3004c5f81c1b6a0b8a35e87b4d0c.html

Xushan Zhao, Yuanxun Wang, Guilan Wang, Runsheng Li, Haiou Zhang. Effect of process parameters on stress and strain of hybrid deposition and micro-rolling, Rapid Prototyping Journal, 2021Yu Lu.(2017). Research on Arc Additive Manufacturing Process of High Strength Aluminum Alloy (Master's Thesis, Beijing Institute of Technology). https://kns.cnki.net/KCMS/detail/detail.aspx?dbname=CMFD202001&filename=1020607147. Nh

Yue Chen, Jianmin Han, Zhiqiang Li, Lingqin Xia, Zhiyong Yang. An inverse method for searching parameters of combined welding heat source model, Inverse Problems in Science and Engineering, 2013

Yap, Y. L., & Yeong, W. Y. (2014). Additive manufacture of fashion and jewellery products: a mini review: This paper provides an insight into the future of 3D printing industries for fashion and jewellery products. Virtual and Physical Prototyping, 9(3), 195-201.

Yue Chen, Jianmin Han, Zhiqiang Li, Lingqin Xia, Zhiyong Yang. An inverse method for searching parameters of combined welding heat source model, Inverse Problems in Science and Engineering, 2013

Yan, Chun Yan, Xin Zhao, Song Ya Tian, Sheng Xun Xu, Bai Qing Ma, and Hai Yang Jiang. Effect of Welding Parameters on Temperature Field during Twin-Wire Submerged Arc Welding of X80 Pipeline Steel, Advanced Materials Research, 2013.

Yeye Cheng, Hehui Wang. Finite Element Analysis of Welding Residual Stress in Longdistance Gas Pipeline, IOP Conference Series: Earth and Environmental Science, 2021

Zhong Wen Yang, Hong Bin Li, Jing Li Wang, Zong Yue Bi. "Development of Domestic CT80S Sulfur Resistance Coiled Tubing, Materials Science Forum, 2018

Zhenkun Lei, Jianchao Zou, Dawei Wang, Zhenfei Guo, Ruixiang Bai, Hao Jiang, Cheng Yan. Finite-element inverse analysis of residual stress for laser welding based on a contour method, Optics & Laser Technology, 2020